Sapphire scintillation tests for cryogenic detectors in the EDELWEISS dark matter search

M. Luca

N° d'ordre 114-2007
LYCEN – T 2007-12

Thèse

présentée devant

l'Université Claude Bernard Lyon-I

pour l'obtention du

DIPLOME de DOCTORAT
Spécialité : Physique des Particules

(arrêté du 7 août 2006)

par

Melisa LUCA

Sapphire scintilation tests for cryogenic detectors in the EDELWEISS dark matter search

Soutenue le 20 juillet 2007
devant la Commission d'Examen

Jury :	M.	P.	DI Stefano	
	M.	C.	Dujardin	Président du jury
	M	J.	Jochum	Rapporteur
	M.	J.	Rich	Rapporteur
	Mme	M.	Stern	Directeur de thèse
	Mme	C.	Tao	

CENTRE NATIONAL DE LA RECHERCHE SCIENTIFIQUE

IN2P3
INSTITUT NATIONAL DE PHYSIQUE NUCLÉAIRE ET DE PHYSIQUE DES PARTICULES

No ordre : 114-2007 anne 2007

THÈSE

présentée

devant l'UNIVERSITÉ CLAUDE BERNARD - LYON 1

pour l'obtention

du DIPLÔME DE DOCTORAT

Spécialité: Physique des Particules

par

Melisa LUCA

Sapphire Scintillation Tests for Cryogenic Detectors in the EDELWEISS Dark Matter Search

Soutenue le 20 Juillet 2007
devant la Commission d'Examen

Jury :	M.	DI STEFANO	Philippe	
	M.	DUJARDIN	Christophe	Prsident du jury
	M.	JOCHUM	Josef	Rapporteur
	M.	RICH	James	Rapporteur
	Mme.	STERN	Martine	Directeur de thèse
	Mme.	TAO	Charling	

Contents

Remerciements

Je tiens tout d'abord à remercier l'ensemble du groupe MANOIR pour leur acceuil et pour tout ce qu'ils m'ont appris tout au long de cette thèse.

Merci à Philippe Di Stefano et Martine Stern pour avoir co-dirigé mon travail. Jules Gascon a su être toujours disponible, surtout pendant la période la plus difficile d'une thèse, la troisième année. Je le remercie également pour la lecture intégrale de mon manuscrit de thèse.

Maryvonne De Jesus, Daniel Drain et Véronique Sanglard ont fait preuve de gentillesse et de disponibilité pendant toute la durée de mon travail. Je remercie les stagiaires et doctorants qui ont partagé mon bureau et surtout Silvia Scorza pour sa bonne humeur et pour m'avoir supporté pendant les moments délicats de la troisième année de thèse. Je souhaite bonne chance à Marc-Antoine Verdier pour sa thèse et pour la suite du projet SciCryo.

Je suis très reconnaissante envers James Rich et Josef Jochum d'avoir accépté d'être rapporteurs de ma thèse, ainsi qu'envers Christophe Dujardin pour avoir bien voulu présider mon jury. Je remercie également Charling Tao d'avoir accepté d'en faire partie.

Ce travail s'est fait au sein de la collaboration EDELWEISS et je tiens à en remercier chaque membre pour leur soutient. J'ai passé une période agréable et enrichissante au Laboratoire Souterrain de Modane lors des premiers tests d'EDELWEISS II et je remercie Alex Juillard, Stefanos Marnieros, Xavier-François Navick et tous les autres pour les très bons moments liés au montage des détecteurs et aux premières impulsions. Je remercie aussi l'ensemble du personnel du LSM et tout particulièrement Benoît Branlard pour leur disponibilité lors de mes fréquents déplacements à Modane. J'ai beaucoup appris sur la cryogénie grâce à Alain Benoit et Maurice Chapellier. Merci aussi à Bernard Paul pour toutes les informations fournies sur les boites bolo.

Une partie de mon travail s'est déroulé dans le cadre du projet SciCryo. Je remercie Christophe Dujardin pour ses conseils sur la scintillation et pour m'avoir permis d'effectuer des nombreux tests au LPCML. Je suis également reconnaissante envers Gilles Ledoux et Philippe Anfré pour leur soutien technique. Je remercie Franz Proebst

et Federica Petricca pour mes deux séjours très formateurs à l'Institut Max Planck de Munich. J'ai appris beaucoup sur la scintillation cryogénique grâce aux longues discussion téléphoniques avec Noël Coron et aux échanges avec Pierre de Marcillac. Merci à Vitalii Mikhailik et Hans Kraus pour les tests de scintillation réalisés à Oxford. Je remercie Sylvain Vanzetto pour son implication dans la réalisation des différents plans des pièces expérimentales. L'ensemble de l'atelier mécanique a toujours fait preuve de rapidité, tout en réalisant un travail de très bonne qualité.

Je souhaiterais remercier aussi tous les doctorants de l'IPNL avec qui j'ai partagé les joies mais aussi les moments très difficiles inhérents à une thèse.

Je fais partie des doctorants qui ont préféré l'enseignement à la recherche. Je remercie les responsables de modules qui m'ont fait confiance même quand j'étais juste une monitrice débutante, ainsi que les étudiants qui m'ont tous beaucoup appris. C'est grâce à eux que j'ai compris comment il faut gérer un groupe ou comment communiquer efficacement.

Pendant une thèse on vit souvent des moments délicats, quand c'est difficile de se rappeler les raisons qui nous ont poussé à s'engager pour trois ans de recherche. Je remercie Thibaut d'avoir été à mes cotés pour partager les moments bons et mauvais des trois dernières années. Je suis également reconnaissante envers nos deux familles qui ont toujours fait preuve d'un soutient sans failles.

Introduction

Understanding the nature of dark matter in the universe is a major challenge for modern cosmology and astrophysics. Mysterious particles, invisible to traditional detection methods, but interacting gravitationally with ordinary matter could explain 90% of the whole mass of the universe. A large fraction of this mass is thought to be made of non-baryonic particles. One of the dark matter well-motivated candidates is the WIMP, a massive particle interacting weakly with the ordinary matter.

The first chapter briefly presents some of the cosmological experimental observations which lead to the idea that an important part of the whole mass of the universe is made of dark matter. Several candidates for dark matter are presented, one of them being the WIMP. Within the theoretical framework of supersymmetry, a natural WIMP candidate is the neutralino, the lightest supersymmetric particle. Several research teams are involved in the quest for dark matter using different detection techniques. The indirect detection experiments look for products of annihilation between WIMPs and their antiparticles, while direct detection searches try to see the elastic scattering of WIMPs off nuclei of chosen targets. Some of the main experiments are presented as well as their current sensitivities.

The second chapter presents the EDELWEISS direct dark matter search situated in the Modane Underground Laboratory in the French Alps. EDELWEISS uses cryogenic germanium detectors capable of simultaneously measuring the heat and ionisation recoil energy induced by particles interacting with the target. The results and challenges of the first phase of the experiment, EDELWEISS I, are presented, as well as the improvements achieved for EDELWEISS II.

The sensitivity of EDELWEISS I has been limited by the radioactive background. One of the background sources are neutrons, that can mimic a WIMP signal. The third

chapter explains the origin of neutrons in the Modane Underground Laboratory and shows the difference in the neutron event rate if different targets are used within the same experiment. The WIMP event rate is also calculated for different crystals that can be used as cryogenic detectors. It is shown that sapphire can be an interesting material for building heat-scintillation bolometers complementary to the existing germanium detectors.

Sapphire is known to be very efficient as low temperature heat detector. In the fourth chapter it is shown how crystals can be characterized in order to distinguish between good and inefficient scintillators. It is demonstrated that titanium doped sapphire can be a very useful low temperature scintillator. Several tests are presented both at room temperature and down to 30 K, achieved in order to find the titanium concentration which is best suited for dark matter detectors .

The fifth chapter presents the cryogenic tests of a sapphire crystal mounted as heat-scintillation detector performed at the Max Planck Institute in Munich. The experiment proves the feasibility of these tests and the possibility to integrate a sapphire detector in an experimental setup similar to the one used by the CRESST dark matter search.

The final chapter shows the tests performed in order to check the compatibility of a sapphire detector with the EDELWEISS II experimental setup. The first preliminary results prove that the detector, even though conceived for a different experiment, can be compatible with the EDELWEISS electronics and acquisition system with minor alterations. This conclusion is encouraging for future use of sapphire crystals as in-situ neutron detectors.

Chapter 1

Introduction to the Problem of Dark Matter

Abstract

La recherche de la matière sombre est l'un des défis les plus importants de l'astrophysique et de la cosmologie actuelle. Les observations indiquent que cette matière constitue une fraction importante de la masse totale de l'univers, mais la nature de cette masse reste mystérieuse. Un des candidats pour la matière noire est le WIMP, particule massive qui interagit faiblement avec la matière ordinaire. La détection des WIMPs est un défi expérimental important relevé par plusieurs équipes à travers le monde. Les principales expériences de détection de matière noire sont brièvement présentées, ainsi que leur sensibilité actuelle.

1.1 Introduction

When searching the phrase 'dark matter' on the world wide web we obtain today about 70,000,000 answers. This is only a small amount of all that has ever been written on this topic. Therefore, this chapter is only a very brief introduction to a complex problem of modern cosmology and particle physics.

1.2 First experimental observations

The story of the quest for dark matter begins in 1933, when the astronomer Fritz Zwicky realises that the velocities of galaxies in clusters are too high to be explained by ordinary matter. In order to keep the clusters gravitationally bound, 400 times more visible mass is needed, so he suggests the existence of a mysterious 'dark matter' (Zwicky 1933). His idea has not been taken seriously until the 1970s, when, thanks to improved observational techniques, it has been confirmed that there was a problem when trying to explain the rotational curves of galaxies (Ostriker 1974). If there were only visible matter in the galaxy, for large radii the velocity should decrease, instead it remains roughly constant. The shape of the rotational curves can be explained when adding a spherical halo of invisible matter to the model (Fig. 1.1).

Different theories have been developped in order to explain the rotational curves without using any form of exotic matter. One of the recent ones attempts to use modified

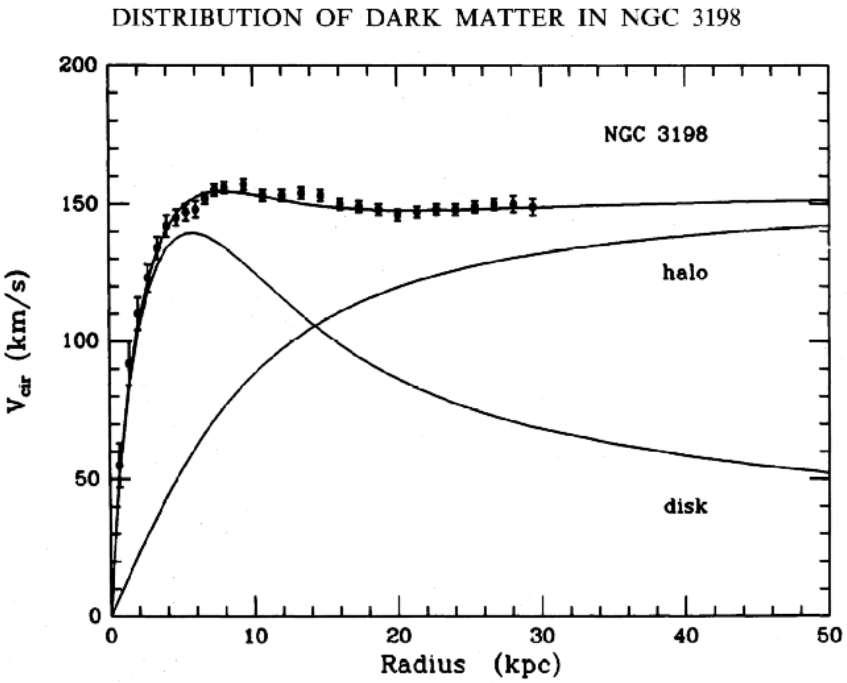

Figure 1.1: *The rotation curve of the NGC3198 galaxy. The disk of visible matter cannot explain the evolution of the velocity, so a halo of exotic matter is added in order to correctely fit the experimental data (Van Albada et al. 1985).*

acceleration laws obtained from Einstein gravity in order to avoid dark matter (Brownstein and Moffat 2006). These theories remain controversial (Iorio 2006). Furthermore, additional evidence for the existence of dark matter is still being found. It has been discovered recently that the collision between two clusters of galaxies splits dark matter and normal matter apart, rendering the gravitational presence of the dark matter observable (Clowe 2006).

1.3 A model for the dark matter halo

In order to find a rotational curve that fits the experimental data let us consider a halo of dark matter surrounding every galaxy, including our own. We can consider a maxwellien velocity distribution:

$$f(v)d^3v = \frac{e^{-v^2/v_0^2}}{\pi^{3/2}v_0^3}d^3v \tag{1.1}$$

This model will be used in the following chapters in order to predict the event rate

of dark matter in different targets. In practice, when applying the model to our galaxy, we consider $\bar{v}$ = 270 km/s, with $\bar{v} = \sqrt{\frac{3}{2}}v_0$. When looking for possible dark matter signatures, another interesting feature concerns the modulation of the speed. When a dark matter particle interacts with a nucleus from a target, this target moves with the Earth around the Sun, while the Sun moves in the galaxy. The Earth velocity is the result of three different velocities: the rotation velocity of the galaxy, the velocity of the Sun and the velocity of the Earth turning around the Sun. We can write it as (Morales 2002):

$$v_{earth} = v_{sun} + 15cos\Big(2\pi\frac{t-152.5}{365.25}\Big)(km/s) \tag{1.2}$$

where t is the time expressed in days from January the 1st. For v_{sun} = 230 km/s, this function has an amplitude of modulation of $\pm$ 6%, that will result in an amplitude of modulation of the event rate of $\pm$ 3%. The event rate will have a minimum value on the 3rd and 4th of December and a maximum value on the 1st and the 2nd of Juin. This can be used as a dark matter signature, provided that the statistics are high enough to detect such small changes in the event rate.

1.4 Dark matter candidates

We have seen arguments in favour of the existence of an exotic type of matter in the universe and some of the general characteristics, but this doesn't give any information on what hides behind the name of dark matter. Ever since the first observational evidence in favour of dark matter has been found, several candidates have been considered.

The most natural solution was to consider that there existed some kind of baryonic matter that we couldn't see because it emitted no light. An example of such matter are the clouds of gas, easy to look for with telescopes like Hubble. The answer is that these clouds can explain less than 10% of the existing dark matter (Weinberg 1997). Another famous candidate was the MACHO, acronym for MAssive Compact Halo Objects. In order to see it, experiments looked at the deflection of the light emitted by distant stars by a massive object. Several experiments have looked for MACHOs, the best known ones being MACHO (Alcock 2000) and EROS (Tisserand 2007). Although they have found dozens of such dark objects, only 25% of the dark matter in the universe could be explained that way.

Since baryonic particles cannot make up the whole mass of dark matter, something more exotic had to be found. An obvious suspect was the neutrino, light particle known to exist, have mass and interact weakly with ordinary matter. Nevertheless, several theoretical arguments and experimental observations showed that it was unlikely that neutrinos be a major part of the dark matter (Tremaine and Gunn 1979), (Fukuda 1998).

The particles that are known to exist have been shown as unsuitable dark matter candidates since none can explain the whole missing mass. Naturally, something more exotic seemed necessary. A theoretical particle that qualifies as a serious possibility is the axion, a Goldstone boson introduced by Peccei and Quinn in order to solve the strong CP problem of QCD (Peccei and Quinn 1977). Axions would be very light, at most 10^{-4} eV, cold (non-relativistic) and stable, with a very small interaction cross-section with ordinary matter of the order of 10^{-20} pb. Several experiments are looking for axions, but only one positive result has been reported so far by the PVLAS collaboration (PVLAS collaboration 2006). The experiment uses the desintegration of an axion into two photons. Their positive signal remains controversial and needs to be confirmed by further experiments.

Another candidate for dark matter is called Weakly Interacting Massive Particle (WIMP). The WIMP is the theoretical motivation behind the work presented in this thesis. Within the Supersymmetric extensions of the Standard Model, a WIMP candidate is the Lightest Supersymmetric Particle (LSP).

1.5 Supersymmetry in a nutshell

Supersymmetry is a theoretical framework that has been created in order to address some of the problems occuring within the Standard Model. One of them appears when calculating the radiative corrections to particle masses. For fermions the corrections are small, while for bosons they diverge quadratically. This is called the problem of fine tuning. The solution provided by supersymmetry is to introduce a super-partner for each particle in the Standard Model. For each particle with a spin S there is a super-particle with a spin equal to S - 1/2. Hence, there is a supersymmetric fermion partner (sfermion) for every boson and a supersymmetric boson (bosino) for every fermion.

Another argument in favour of superymmetric theories is the unification of the strong and electroweak interactions. There is a coupling constant associated to each type of interaction, which depends on the energy scale. Up to the energies attained so far, the coupling constants associated to the strong, weak and electromagnetical interactions are different, but it is possible that for certain energies these constants have the same value. This effect is possible by taking into account the existence of supersymmetric particles (Yao 2006). An important effort has been made in order to build accelerators capable to obtain the high energies necessary for the creation of supersymmetric particles. Great expectations concern the Large Hadron Collider (**LHC**), that will start commissioning runs in 2007. Therefore, if dark matter is made of supersymmetric particles, two steps are intimately tied together: demonstrate that galaxies are made of a new form of matter (particle astrophysics community) and study the properties of this

new matter (collider physics community) (Baltz et al. 2006).

In the minimal extension of the Standard Model, the sparticles are:

- 6 squarks and 6 sleptons with a spin S = 0;
- 8 gluinos with S = 1/2;
- 4 charginos with S = 1/2;
- 4 neutralinos with S = 1/2;

Theories differ on how these four neutralinos will mix. The exact nature of mixing defines the particle mass and cross section. The LSP is thought to be a mixing of the four. A new quantum number associated to each particle within supersymmetry is the R-parity $R = (-1)^{L+2S+3B}$, where S is the spin, B the baryonic number and L the leptonic number. The R-parity is 1 for Standard Model particles and -1 for sparticles. If the R-parity is conserved, the LSP cannot decay and is therefore stable.

The fact that the effects of neutralino interactions have not yet been seen shows that this particle interacts weakly with ordinary matter. An electromagnetic or a strong interaction would have already had important effects on baryonic matter.

To sum up, the neutralino is a massive, neutral, stable particle interacting weakly with ordinary matter. These characteristics make it a perfect WIMP. Supersymmetric models define a range of values for the neutralino mass and scattering cross section on nucleons that need to be confirmed by experimental data.

Within certain supersymmetric models, other dark matter candidates exist: axinos, gravitinos, etc. These candidates appear less naturally and are more difficult to detect than axions or WIMPs which are already a genuine experimental challenge. In this thesis, we will only focus on the detection of WIMPs.

1.6 Looking for WIMPs

There are two experimental approaches in the search for dark matter: trying to detect the products of WIMP-WIMP annihilation in cosmic rays (indirect detection) or trying to see directly the interaction between WIMPs from the galactic halo and a chosen target (direct detection).

1.6.1 Indirect detection

The annihilation between a WIMP (ω) and its antiparticle ($\bar{\omega}$) can be written:

$$\omega + \bar{\omega} \rightarrow l + \bar{l} \tag{1.3}$$

where l is either a lepton, a boson or a quark. If the flux of decay products detected is higher than the value expected coming from conventional sources, this can be the signature of a WIMP annihilation. Most of the possible annihilation products are already produced in very large quantities by usual sources, which means that the excess is difficult to detect. Possible exceptions are neutrinos, antiprotons, positrons and high energy gamma rays, which can supply valuable information on neutralino dark matter.

Many experimental efforts concentrate on neutrinos. Those expected from WIMP annihilation should have several tens of GeV, energies much higher than those produced by conventional sources. Experiments like **MACRO**, **AMANDA**, **Super-Kamiokande** set upper limits on neutrino fluxes coming from the center of the earth and the sun, places where WIMPs would be concentrated because of the gravitational attraction. Neutrinos are detected via the associated muons which produce a Cerenkov effect when interacting with the target. **ANTARES** and **IceCube** experiments, that use sea water and ice as targets, aim to a final detection volume of the order of km^3 that will increase the sensitivity to WIMP annihilation neutrinos. The KM3 experiment will be a collaboration between the ANTARES, NEMO and NESTOR experiments.

Positrons are another possible annihilation product. Several experiments like the balloon-borne **BESS** or the High Energy Antimatter Teloescope (**HEAT**) have looked for a positron excess. The main difficulty of this type of experiment is to establish precisely the contribution of standard sources. For instance, the HEAT experiment has demonstrated an excess of high energy positrons (Beach 2001) that could be explained by WIMP annihilation but only in a highly optimistic scenario, with a WIMP density 30 times higher than the usual value. It is therefore difficult to draw any conclusion on the reported signal.

High energy gamma rays from the galactic center are another possible signature for WIMPs. The **EGRET** experiment has reported a gamma ray excess of energies above 1 GeV (Hunter 1997). This data could be explained under certain assumptions by a 50-100 GeV neutralino annihilation (de Boer 2005). Another positive signal has been seen by the **HESS** collaboration that could be explained by an unusually heavy dark matter candidate with a minimum mass of 12 TeV (Horns 2005). The **CACTUS** collaboration also reported a gamma-ray excess from de Draco dwarf spheroidal galaxy, one of the most dark matter dominated galaxies known (Marleau 2005). All these experimental observations remain inconclusive for now and need more thorough investigation. Some answers may come from the Gamma-ray Large Area Space Telescope (**GLAST**) that will be launched in 2007 and will be able to search for dark matter signals from a few MeV up to a few hundreds GeV.

1.6.2 Direct Detection

Started about 20 years ago, direct dark matter searches continue increasing in sensitivity and target mass. These experiments look for the elastic scattering of WIMPs off target nuclei. They are very challenging since in order to detect an extremely low event rate (less than 1 evt/kg/week) and small recoil energies (of the order of a few dozens keV), they demand low thresholds, low radioactive background and large target mass.

Each experiment uses one or more experimental WIMP signatures which enables the discrimination between searched particles and radioactive background. One interesting aspect is that WIMPs produce *nuclear recoils*, like neutrons but unlike gammas or electrons which produce electron recoils. Some experiments use this information in their search for dark matter. It is also known that the WIMP event rate is modulated, with a maximum value in June and a minimum value in December. The *annual modulation* is another strategy used to look for WIMPs. Besides the annual modulation, there is also a *diurnal modulation*, proof of the galactic origin of the signal. As WIMPs interact weakly with ordinary matter, *no multiple interactions* are expected, information that can be used in order to identify neutrons which also produce nuclear recoils. The energy recoil spectrum depends on the target nucleus, once a signal detected with one type of detector, the *consistency between targets of different nuclei* will need to be checked. We shall now see how some of the main experiments use these pieces of information in order to look for dark matter.

The only dark matter search having reported a WIMP signal so far is the **DAMA** collaboration. When a particle interacts with a scintillating crystal, light is being emitted. DAMA used nine 9.7 kg NaI crystals, each viewed by two photomultipliers, that amplify the light and convert it into electric signal. There are several advantages to this method: NaI scintillation detection with photomultipliers is a well known technology, the detection mass is important, the event rate depends on the atomic mass of the target nucleus and ^{127}I has a high atomic mass. DAMA was located in the Gran Sasso Underground Laboratory and used a photon and neutron shielding. However, there was no event by event discrimination between WIMP signal and radioactive background. In 1998, DAMA announced an annual modulation after two years of data taking (Bernabei 1998). The modulation was confirmed in 2000 (Bernabei 2000) and interpreted by the collaboration as a dark matter signal, corresponding to a WIMP mass of about 50 GeV and a cross section on proton of the order of 10^{-6} pb. This WIMP mass and cross section have been excluded by first EDELWEISS (Sanglard 2005) and then CDMS (CDMS collaboration 2006). Nevertheless, for non-standard WIMP models (Bottino 2005), the observations of both DAMA and current most sensitive experiments can be reconciled, so even though it seems unlikely that DAMA detected a genuine WIMP signal, this hypothesis cannot be completely ruled out for the time being.

Further information may come one day from LIBRA, a 250 kg NaI experiment that has been operated since 2003.

KIMS, located in an underground laboratory in Korea, uses a similar experimental setup, with CsI as scintillating target. Their most recent result is based on one crystal of 6.6 kg (Lee 2006). KIMS is starting to explore the DAMA parameter space and since the targets are similar it could in future confirm or deny the claimed signal.

DRIFT, situated in the Boulby underground laboratory in the U.K., uses an original approach in order to identify a potential WIMP signal (Kudryavtsev 2004). This is due to its ability to determine the direction of the recoiling nucleus. Since the Earth is rotating in the WIMP halo, there will be a diurnal modulation of the signal that can be detected as the interaction takes place in a time projection chamber filled with low pressure CS_2. Drift I has been running a cubic meter detector since 2001. The long term objective is to increase the detection mass up to 100 kg (DRIFT III).

The **PICASSO** experiment is situated in the Sudbury mine in Canada. With superheated C_4F_{10} droplets as active material, the experiment is looking for spin-dependent interactions between WIMPs and ^{19}F nuclei (Barnabé-Heider 2005).

The best upper limits on WIMP dark matter and cross section are currently established by experiments using **cryogenic detectors**. The interaction between a particle and a target can have three effects: scintillation, ionisation or heat. The detectors, working at very low temperature (of the order of 20 mK), can discriminate nuclear recoils by simultaneously measuring two of the three signals: phonon and ionisation or phonon and scintillation. As this thesis has been done within the EDELWEISS experiment and some of the tests within CRESST, both heat-scintillation and heat-ionisation detectors will be presented in more detail in the following chapters.

CRESST, situated in the Gran Sasso underground laboratory, is a dark matter search using $CaWO_4$ heat-scintillation detectors. The event by event discrimination is ensured by the fact that nuclear recoils have much smaller light yield than electron recoils. Another interesting feature is that WIMPs will predominantly be scattered by tungsten nuclei, while neutrons mainly by oxygen. By now, CRESST succesfully operated two 300 g $CaWO_4$ prototypes (Angloher 2005), without a neutron shield and a muon veto. The shielding is now complete and the experiment, upgraded to 10 kg of crystals, has started commissioning runs.

ROSEBUD, situated in the Canfranc underground laboratory in Spain is an experiment using different light-scintillation detectors (Cebrian 1999). The experiment is low-scale, its originality consisting in the multitude of targets that have already been tested as heat-scintillation detectors, such as Al_2O_3 , $CaWO_4$, BGO, LiF, CaF_2, SrF_2, GSO. Right now, the experiment is running at Canfranc with three detectors: Al_2O_3 , LiF and BGO.

Both **EDELWEISS** and **CDMS** are dark matter searches using heat-ionisation detectors. CDMS detectors are mainly Ge and some Si, while EDELWEISS uses Ge as

standard target.

The future of dark matter european searches with cryogenic detectors is the project **EURECA** (European Underground Rare Event Calorimeter Array) (Kraus 2006). EURECA will be based on CRESST and EDELWEISS expertise, with additional groups joining the project (ROSEBUD and CERN). The aim is to diversify targets (Ge, $CaWO_4$, etc) and to increase the target mass up to one ton.

After having spent long time on the development stages, **liquid experiments** start publishing competitive results. These experiments have the potential to challenge cryogenic detectors as targets usually have high atomic numbers which means high cross sections in the WIMP-nucleon interaction, they are easy to scale up to large volumes without major alterations and can be highly purified. The working temperature is much higher than the one of cryogenic detectors (87 K for Argon, 165 K for Xenon, 27 K for Neon), so much easier to achieve.

Located in Boulby underground laboratory, **ZEPLIN** is an experiment using liquid xenon as target. The only signal measured is scintillation. The detector is made out of liquid xenon with a layer of xenon gas at the top and an electric field through the detector. A particle interacting with the detector creates primary scintillation and ionisation. Thanks to the electric field, the electrons are drifted into the gas and create secondary scintillation. Photomultipliers on top of the detector are sensitive to the two signals, that can be compared in order to determine the nature of the interacting particle and discriminate nuclear recoils. The first stage of the experiment, ZEPLIN I used a total target mass of 3.2 kg (Alner 2005). The first preliminary results of the second stage using 31 kg of fiducial volume have recently been published (Alner 2007).

The **WARP** experiment, operated in the Gran Sasso laboratory, uses liquid Ar for dark matter detection. The experimental setup is similar to the one used for Xe experiments: Ar in both liquid and gaseous phase are viewed by photomultipliers. WARP has recently published competitive results, using a small prototype chamber filled with 2.3 natural Ar (Benetti 2007). The main background of the detector is the presence of radioactive isotopes ^{39}Ar and ^{42}Ar that will be reduced in future stages of the experiment by isotopic purification.

I have presented here the major dark matter experiments running now as well as the main detection techniques. The limits established so far are shown in Fig. 1.2. Experiments are now increasing the detection mass and plan to expand up to the ton-scale, reserving interesting prospects for the future (Fig. 1.3).

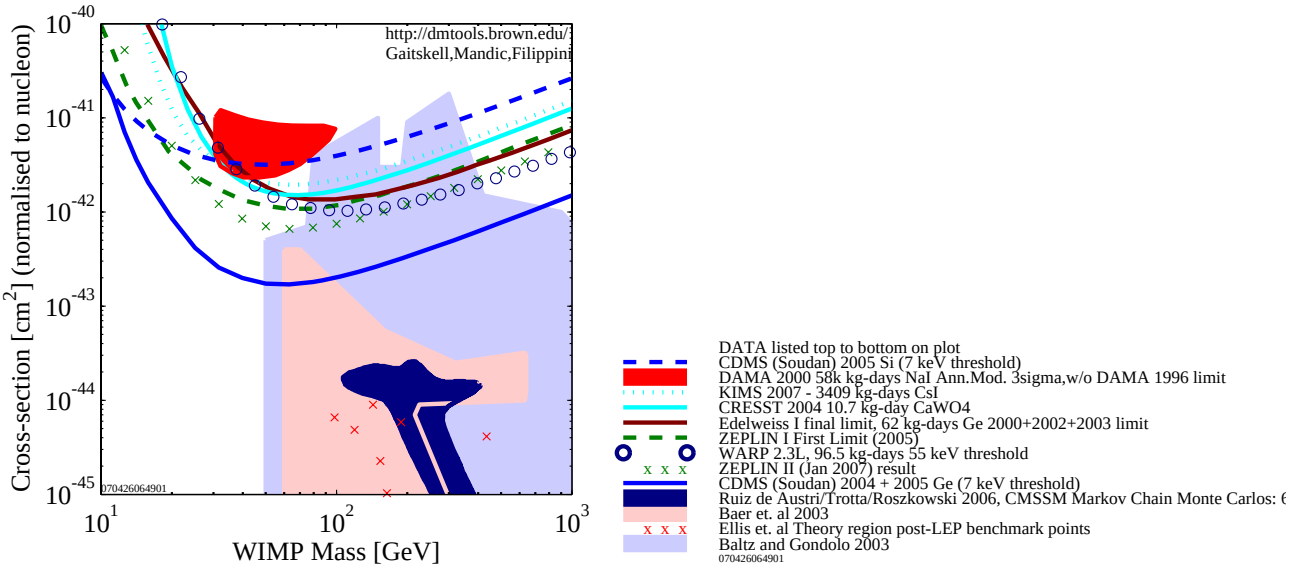

Figure 1.2: *Limits for the WIMP mass and cross section of the present most sensitive dark matter searches compared to a few theoretical predictions (Gaitskell n.d.).*

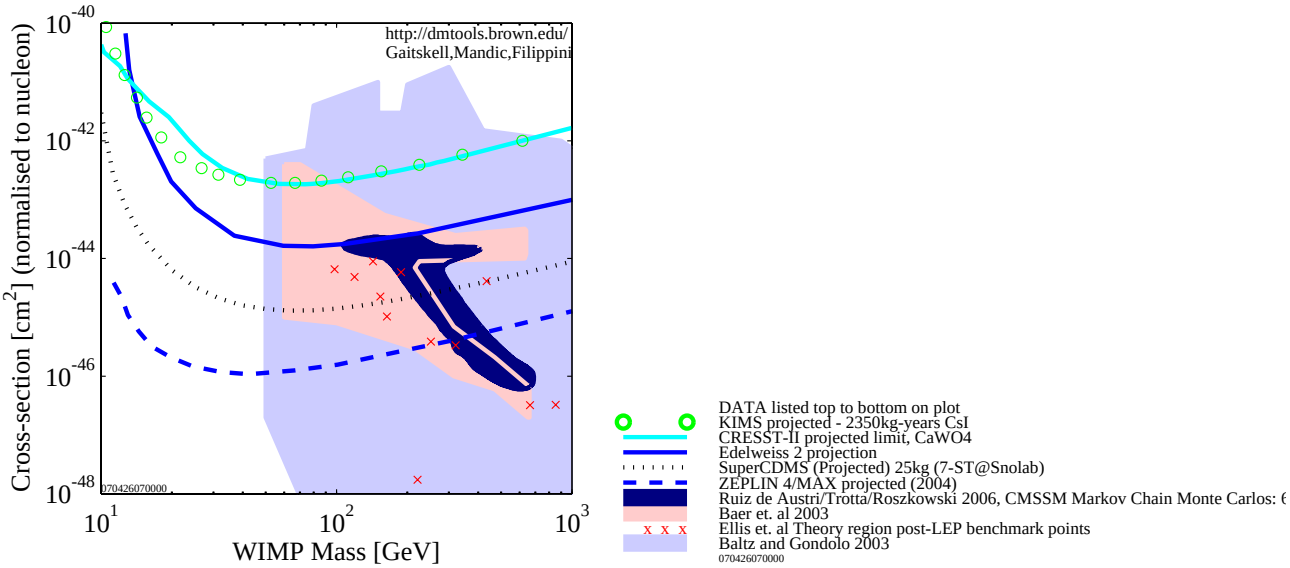

Figure 1.3: *Predicted sensitivities of future dark matter searches compared to some supersymmetry theoretical models (Gaitskell n.d.).*

Chapter 2

The EDELWEISS Experiment

Abstract

EDELWEISS est une expérience de recherche directe de matière noire, située dans le Laboratoire Souterrain de Modane. EDELWEISS utilise des détecteurs cryogéniques en germanium qui mesurent simultanément les signaux chaleur et ionisation créés par l'interaction d'une particule avec la cible. Après une première phase où trois détecteurs de 320 g ont été utilisés, pour EDELWEISS II la masse de détection a été augmentée et le fond radioactif diminué afin de gagner deux ordres de grandeur en sensibilité.

2.1 Historical introduction

EDELWEISS (Expérience pour Détecter les WIMPs en Site Souterrain) is an international collaboration between several institutes from France, Germany and Russia. EDELWEISS looks for WIMPs, which, as explained in the previous chapter, interact very weakly with ordinary matter. Therefore, the experiment needs to reduce the radioactive background. In order to be protected from the muon flux, EDELWEISS is situated in the Modane Underground Laboratory (Laboratoire Souterrain de Modane - LSM), in the Fréjus tunnel between France and Italy. An overburden of 1700 m of rock, equivalent to 4800 m of water, reduces the muon flux down to 4.5 $\mu/m^2/day$, that is about 10^6 times less than at the surface.

EDELWEISS started tests in underground laboratory in 1994. The first goal was to develop a detector capable of simultaneously measuring heat and ionisation signals created by the interaction of a particle with a Ge crystal. In 1998, the first Ge 70 g detector has been succesfully operated (Di Stefano 2001). During the first stage of the experiment, EDELWEISS I, up to three 320 g Ge detectors have been operated simultaneously (Sanglard 2005). EDELWEISS I has been stopped in March 2004, being replaced by EDELWEISS II. With a larger detection mass and lower background radioactivity, EDELWEISS II aims at gaining two orders of magnitude in sensitivity.

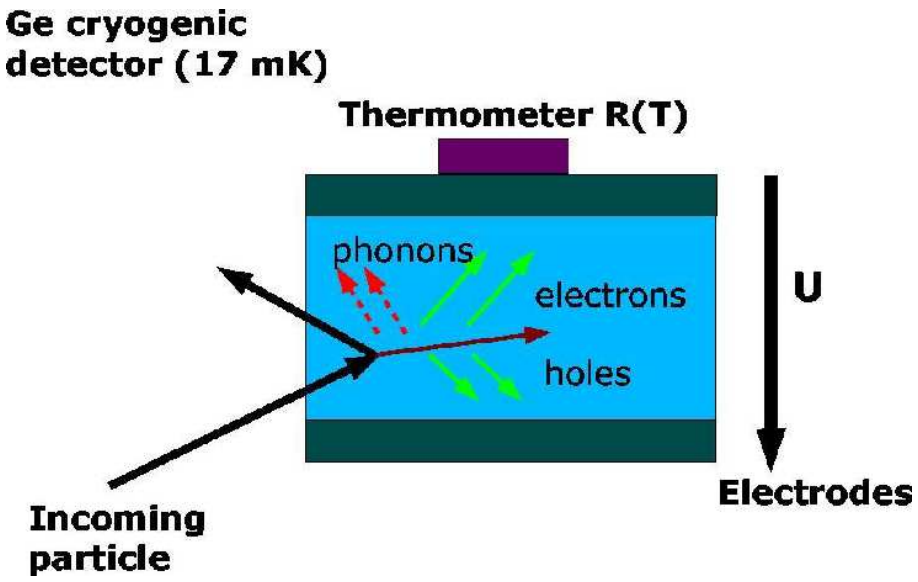

Figure 2.1: *Each EDELWEISS Ge detector has a NTD-Ge thermistor that measures the heat signal and two Al electrodes for the ionisation.*

2.2 Principle of detection

In order to detect low recoil energies, EDELWEISS uses very sensitive cryogenic detectors (Fig. 2.1) working at temperatures of the order of 20 mK, that measure simultaneously the heat and ionisation signal (Navick 2006).

The detectors are high-purity Ge crystals (70 mm in diameter, 20 mm in thickness, with 4 mm thick beveled edges), i.e. they have less than 10^{10} residual impurities per cm^3. The electrodes for ionisation measurement are made of 100 nm Al layers sputtered on the upper and lower side of the crystal. The top electrode is divided in a central part and a guard ring, electrically decoupled for radial localization of the charge deposition. The bottom electrode is the common reference. The heat signal is measured with a 7 mm^3 NTD-Ge (Neutron Transmutation Doped Germanium) glued on a sputtered gold pad near the edge of the bottom Al electrode. Thus, the residual radioactivity of the NTD sensor is mostly rejected by the guard electrode. The simultaneous measurement of two signals allows an event by event discrimination between the two possible kinds of recoils in the detector: electronic (induced by photons or electrons) and nuclear (induced by neutrons or WIMPs), as shown in Fig. 2.2. In a Ge crystal, for the same recoil energy, the ionisation is 3-4 times higher for an electronic recoil than for a nuclear one (Benoit 2006). Therefore, there is a good separation between electronic and nuclear recoils down to an energy of about 15 keV.

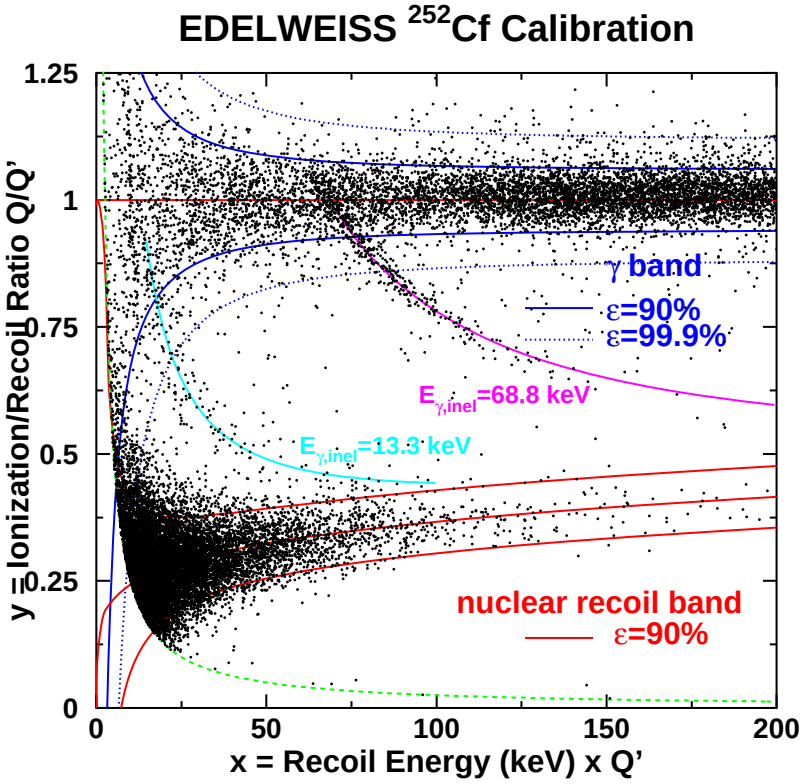

Figure 2.2: *Ratio between the ionisation and the recoil energy versus the recoil energy. The separation between the electronic and the nuclear recoil band is excellent down to an energy of about 15 keV.*

2.3 EDELWEISS I

EDELWEISS I used 320 g Ge detectors during several campaigns. Between 2002 and 2003, three 320 g detectors have been operated simultaneously in a cryostat shielded by 10 cm of Cu, 15 cm of Pb, 7 cm of internal roman Pb and 30 cm of paraffin. After a total fiducial exposure of 62 kg·day with an effective threshold of 15 keV, 59 events have been observed in the nuclear-recoil band. As shown in Fig. 2.3, most of these events are at low energy, between 10 and 30 keV. Only three nuclear recoil events have been seen in the relevant energy range 30-100 keV. The simulated spectra of WIMPs having a scattering cross section on nucleons of 10^{-5} pb and masses of 20, 40, 100 and 500 GeV/c^2 show that the events in the nuclear recoil band can not be explained by a single WIMP mass, a part of the spectrum has to be attributed to a non-WIMP background.

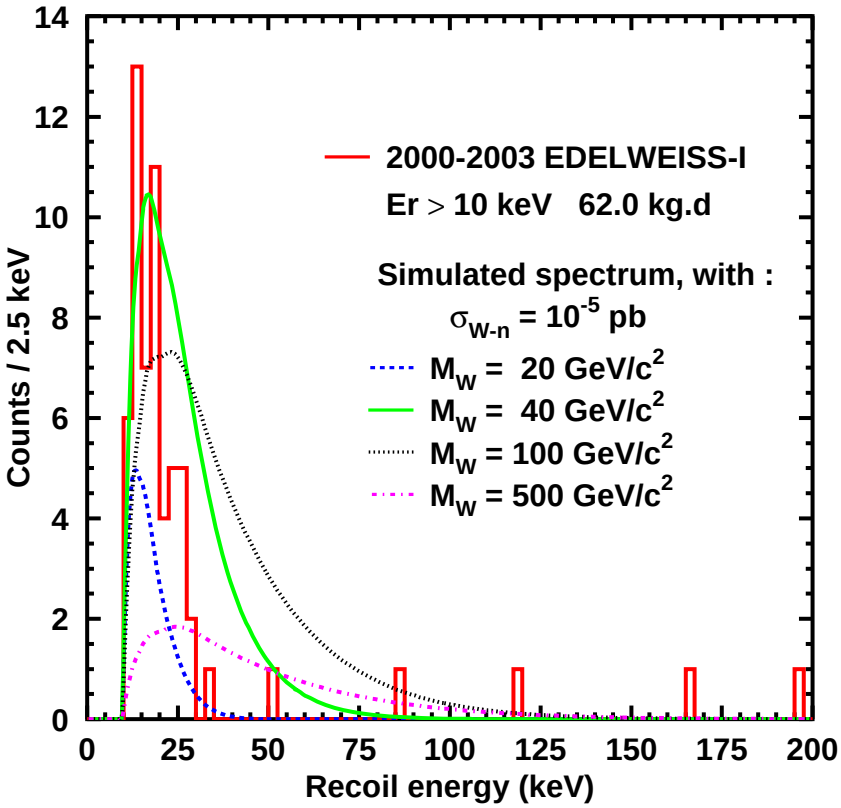

Figure 2.3: *Energy spectrum of the EDELWEISS I experimental data compared to simulated spectra for different WIMP masses in the range of interest.*

After having been the most sensitive direct dark matter search, EDELWEISS I became limited mainly because of the radioactive background and the detection mass. Therefore, the experiment has been stopped in 2004 and replaced by EDELWEISS II.

2.4 Radioactive background

The main limiting factor for EDELWEISS I was the radioactive background.

In a Ge detector, charges coming from particles that interact very close to the surface (like alphas or electrons) can be mis–collected, hence the resulting events appearing in the nuclear recoil band. One way of dealing with this problem is by depositing a 60 nm Ge or Si amorphous layer on the crystal surface which diminishes the number of surface events (Shutt 2000). All detectors used for EDELWEISS I 2002–2003 runs had such layers. Concentric electrodes provide a radial sensitivity allowing to select events

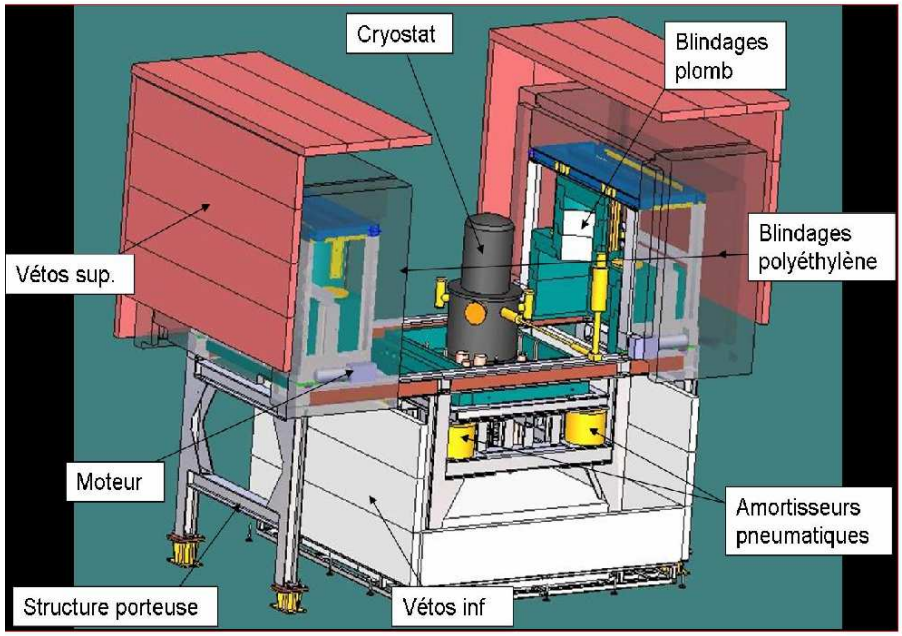

Figure 2.4: *Experimental setup of EDELWEISS II. The cryostat is in the middle, shielded by Pb, paraffin and a muon veto.*

occuring in the central part of the detector (Martineau 2004) where the electric field is more homogeneous and the detector better shielded from its environement.

Another method which is used for some of the EDELWEISS II detectors is to replace the NTD thermistors by two NbSi Anderson insulator thermometric layers on the upper and lower central parts of the detector. These layers are sensitive to athermal phonons. When the event occurs near the surface, the athermal signal is much higher in the closest thermometer than the bulk events and can be eliminated during analysis (Juillard 2006).

High energy neutrons are hard to moderate and can penetrate the shielding. When interacting with the detector, neutrons can mimic WIMP events, therefore they are an important issue for EDELWEISS II. Some of the ways of dealing with this problem in EDELWEISS II are a better shielding, a muon veto and the increase in the number of neutron coincident events by an increase in the number of detectors. The problem of the neutron radioactive background will be further described in the next chapters.

2.5 EDELWEISS II

The second stage of the experiment is EDELWEISS II. The new experimental setup is shown in Fig. 2.4.

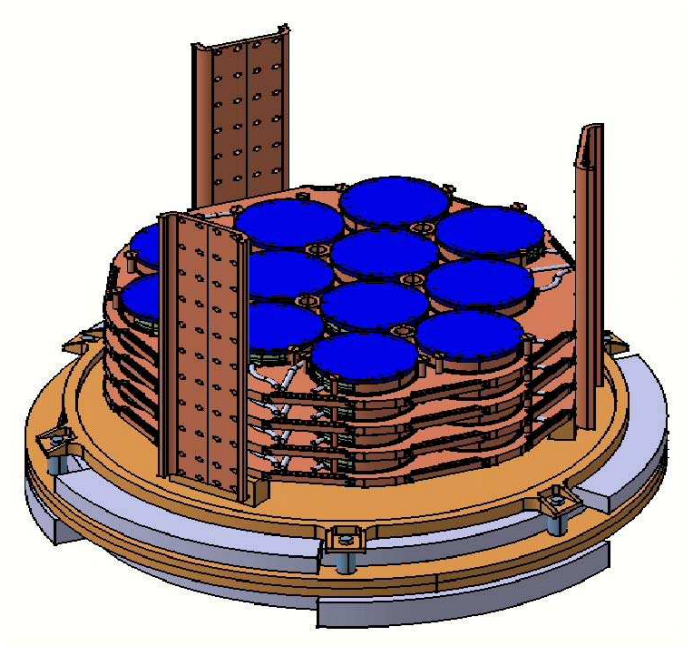

Figure 2.5: *Compact hexagonal arrangement of detectors within the EDELWEISS II cryostat.*

The experiment is shielded by 50 cm of paraffin, 20 cm of Pb and a 99% coverage muon veto. The new cryostat has a larger volume (50 l) and can host up to 120 detectors. The detectors are fixed on Cu plates, each plate can host up to 12 detectors. This compact arrangement (Fig. 2.5) will allow increasing the number of neutron coincidences.

The cryostat is nitrogen free, with three pulse tubes and one helium cold vapor reliquefier, having therefore a low helium consumption. The whole setup is situated inside a clean room ($\sim$130 m^3) supplied with deradonized air (0.1 Bq/m^3). The detector holders have also been optimized for low radioactivity, being only made out of Teflon and copper.

By diminishing the radioactive background and increasing the detection mass, EDELWEISS II should gain a factor 100 in sensitivity compared to EDELWEISS I.

This chapter presents the detection technique of EDELWEISS, the final results and limitations of the first stage of the experiment as well as the main improvements brought to EDELWEISS II. It is shown that one of the important issues in EDELWEISS is the neutron background that can mimic WIMP events. In the future chapters we will see one way of distinguishing between WIMP and neutron events by using light targets as complementary to Ge detectors.

Chapter 3

Theoretical Motivation for the Use of Light Targets in a Dark Matter Search

Abstract

Le bruit de fond radioactif a été une des limites importantes dans EDELWEISS I. Les neutrons pouvant donner des reculs de même type que les WIMPs, la compréhension du bruit de fond neutron est essentielle pour augmenter la sensibilité de l'expérience. Un des moyens de distinguer entre un signal WIMP et un signal neutron est de diversifier le cibles utilisées. Le taux d'événements WIMP et neutron est calculé pour différents cristaux qui peuvent servir comme cible pour une recherche de matière noire.

3.1 Interaction between WIMPs and ordinary matter

In the first two chapters we have seen the different strategies for detecting dark matter as well as the principle of EDELWEISS detectors. The topic of this thesis is the investigation of the possibility of using detectors based on the simultaneous measurement of heat and scintillation within EDELWEISS. In this chapter, the importance of using different targets in the search for dark matter is shown by calculating the event rate of WIMPs in different detectors. The following calculations follow those of (Lewin and Smith 1996) and (Kamionkowski 1996).

3.1.1 Theoretical framework

Let us consider a density n of particles per m^3 with a velocity v. The elastic scattering event rate in a crystal per kg of detector mass and per time is:

$$R = \frac{N_0}{A} \cdot \sigma v n \tag{3.1}$$

with N_0 the Avogadro's number, A the atomic mass of the target and σ the scattering cross section of WIMPs on the nucleus. The differential event rate is:

$$\frac{dR}{dE_R} = \frac{N_0}{A} \cdot vn \frac{d\sigma_{\omega-N}}{dE_R} \tag{3.2}$$

We have seen in the first chapter that in order to explain the rotational curves of the galaxies, one can consider a WIMP halo with a maxwellien velocity distribution:

$$f(v)d^3v = \frac{e^{-v^2/v_0^2}}{\pi^{3/2}v_0^3}d^3v \tag{3.3}$$

with v_0 = 230 km/s. Taking into account this distribution, we can integrate the event rate for all WIMP velocities and obtain:

$$\frac{dR}{dE_R} = \frac{\rho N_A}{\sqrt{\pi}m_\omega m_r^2 v_0}\sigma_{\omega-N} \tag{3.4}$$

with m_ω the WIMP mass and $m_r = \frac{m_\omega A}{m_\omega + A}$.

Until now, we have neglected the velocity of the Earth and Sun, as well as the form factor correction that takes into account the nuclear radius. Therefore, we can write the differential event rate as:

$$\frac{dR}{dE_R} = \frac{\rho N_A}{\sqrt{\pi}m_\omega m_r^2 v_0}\sigma_{\omega-N} \cdot F^2(E_R)T(E_R) \tag{3.5}$$

where $F^2(E_R)$ is the form factor and $T(E_R)$ the correction due to the fact that the detector is situated on the Earth which is in orbit around the Sun, moving through the galaxy.

The correction factor that takes into account the speed of the detector can be written:

$$T(E_R) = \frac{\sqrt{\pi}}{4v_{earth}} \cdot v_0\Big[erf\Big(\frac{v_{min}+v_{earth}}{v_0}\Big) - erf\Big(\frac{v_{min}+v_{earth}}{v_0}\Big)\Big] \tag{3.6}$$

where $v_{min} = \sqrt{\frac{E_R \cdot M_{target}}{2m_r^2}}$. There is one further parameter to take into account, which is the fact that a particle with a velocity greater than a certain value (v_{esc}) cannot remain gravitationally bound, escaping the galaxy. In order to deduce the previous equation, we have considered $v_{esc} \to \infty$. More generally:

$$\frac{dR}{dE_R}(v_{earth}, v_{escape}) = \frac{k_0}{k_1}\frac{dR}{dE_R}(vearth, \infty)\Big[T(E_R) - exp(-\frac{v_{esc}^2}{v_0^2})\Big] \tag{3.7}$$

with:

$$k_0 = (\pi v_0^2)^{3/2} \tag{3.8}$$

$$k_1 = k_0\left[erf(\frac{v_{esc}}{v_0}) - \frac{2}{\sqrt{\pi}}\frac{v_{esc}}{v_0}e^{-\frac{v_{esc}^2}{v_0^2}}\right] \tag{3.9}$$

When the momentum transfer $q = (2M_{target}E_R)^{1/2}$ becomes important (more than 1 MeV), that is the wavelength h/q is of the same order of magnitude as the nuclear

radius, we need to take into account a nuclear form factor correction. The correction depends on whether we consider a spin-independent or spin-dependent interaction between WIMPs and our chosen target. There are several possible approximations for the expression of the form factor. The ones used for these calculations are, for spin-independent interactions (Lewin and Smith 1996):

$$F(q) \;=\; 3\frac{sin(qr_n) - qr_n cos(qr_n)}{(qr_n)^3} exp\Big[-\frac{(qs)^2}{2}\Big] \tag{3.10}$$

where r_n is the nuclear radius, that can be approximated by:

$$r_n^2 \;=\; c^2 + \frac{7}{3}\pi^2 a^2 - 5s^2 \tag{3.11}$$

with $c \;=\; 1.23A^{1/3} - 0.6\;(fm)$, $a \;=\; 0.52\;(fm)$ and $s \;=\; 0.9\;(fm)$.

In the case of spin-dependent interactions, we can write the form factor as (Lewin and Smith 1996):

$$F(q) = \begin{cases} sin^2(qr_n)/(qr_n)^2 & \text{if } qr_n < 2.55 \text{ or } qr_n > 4.5 \\ constant = 0.047 & \text{if } 2.55 < qr_n < 4.5 \end{cases} \tag{3.12}$$

These correction factors have an important effect on heavy targets. Fig. 3.1 shows this effect on the differential event rate spectrum in Ge.

In order to compare the event rate of WIMPs in different targets, we need to express it as a function of the scattering cross section on protons. The elastic scattering cross section depends on the type of interaction considered: either spin-independent or spin-dependent coupling between WIMPs and nucleons. For spin-independent interactions, we can express the cross section on the target as a fuction of the cross section on protons as:

$$\sigma^{SI}_{\omega-N} \;=\; \Big(\frac{m_\omega + M_p}{m_\omega + M_{target}}\Big)^{-2} \cdot \sigma_{\omega-p} \cdot A^2 \tag{3.13}$$

For spin-dependent interactions, the cross section can be written:

$$\sigma^{SD}_{\omega-N} \;=\; \frac{32}{\pi} G_F^2 m_r^2 \frac{J+1}{J} (a_p < S_p > + a_n < S_n >)^2 \cdot \sigma_{\omega-p} \tag{3.14}$$

where J is the total angular momentum of the nucleus, $< S_p >$ ($< S_n >$) is the expectation value of the spin contribution of the proton (neutron) group in the nucleus and a_p, a_n the coupling constants between WIMPs and protons or neutrons.

I have briefly shown how we can calculate the event rate of WIMPs in a chosen crystal. Now we will see how these results apply to targets typically used in dark matter experiments.

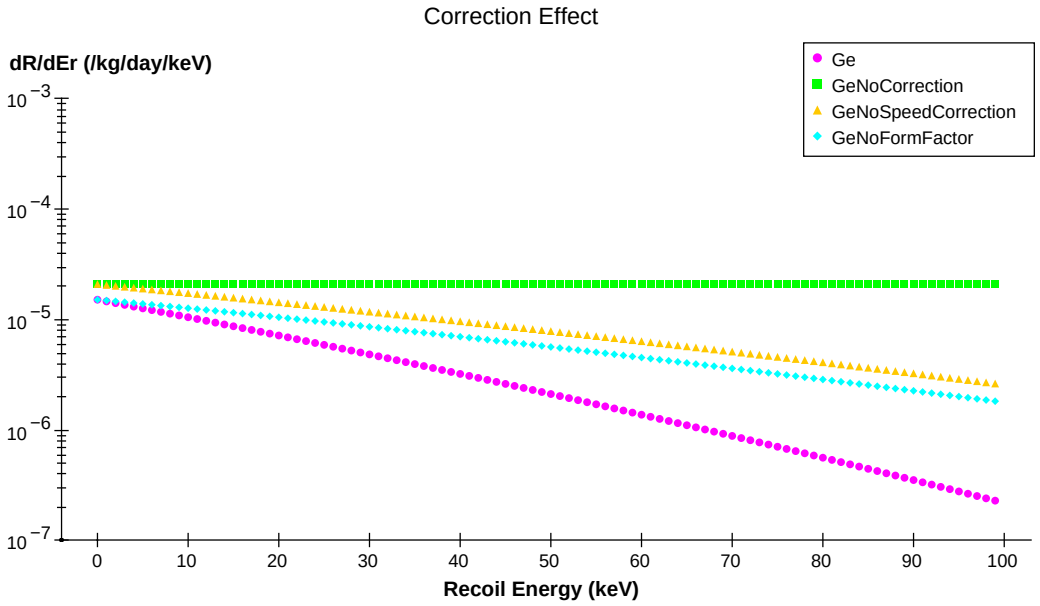

Figure 3.1: *Effects of different correction factors on the differential event rate, considering a WIMP mass of 100 GeV and an elastic scattering cross section on nucleons of 10−6 pb. Circles show the spectrum when we take into account all correction factors, squares: the spectrum without any speed or form factor correction, triangles: there is a form factor correction but no velocity correction and diamonds: there is no form factor correction and a velocity factor correction.*

3.1.2 Spin-independent interactions

As shown in equation (3.13), the cross section for spin-independent interactions depends on the square of the atomic mass of the target. Therefore, the event rate will be higher in heavier targets. Fig. 3.2 shows the differential event rate in $CaWO_4$, Ge, Si, LiF and Al_2O_3 for a WIMP mass of 100 GeV and an elastic scattering cross section of 10^{-6} pb. The standard astrophysical assumptions have been made, considering ρ_0 = 0.3 GeV/cm^3, v_0 = 220 km/s, v_{escape} = 650 km/s, v_{earth} = 235 km/s.

We can see that if an experiment using Ge and sapphire crystals saw a WIMP signal, there would be more events in Ge than in sapphire and this could be an important hint that the signal really comes from WIMPs.

In the case of lighter WIMPs, this tendency is inverted. Fig. 3.3 shows the same spectra for a 20 GeV WIMP. We can see that above 30 keV, sapphire is more efficient for detecting light WIMPs than Ge. This is explained by the fact that the recoil energy will be higher for targets having the same mass as the interacting particle.

In order to distinguish between WIMPs of different masses, we also have access to

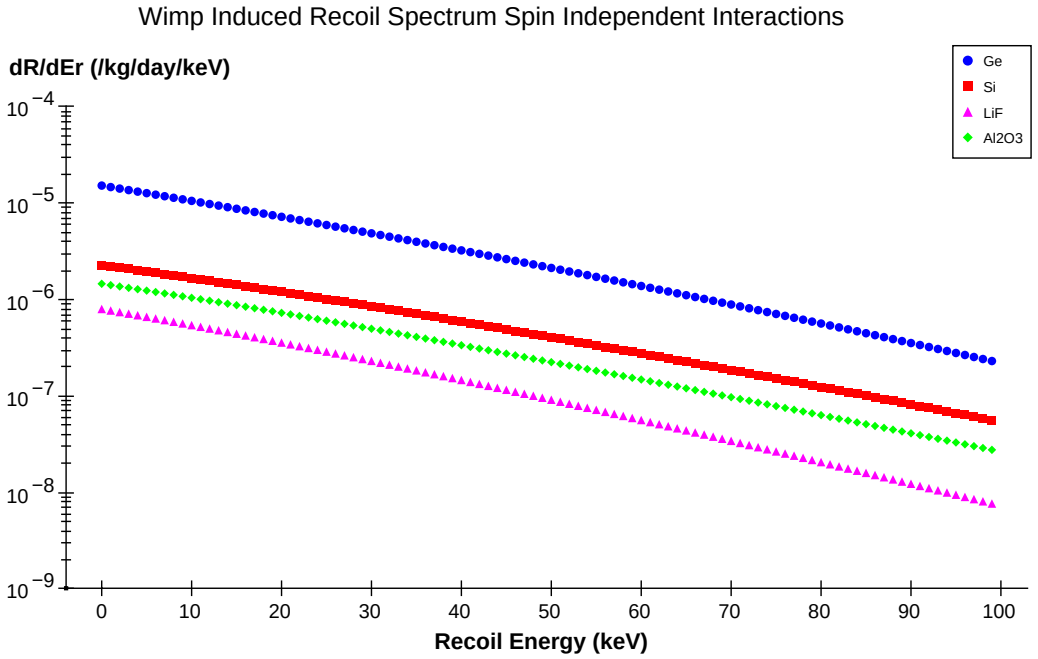

Figure 3.2: *Interaction event rate of WIMPs in $CaWO_4$, Ge, Si, LiF and Al_2O_3 for a WIMP mass of 100 GeV and an elastic scattering cross section of 10^{-6} pb. The event rate is higher in heavy crystals like Ge than in lighter ones like Al_2O_3.*

the shape of the recoil spectrum in the target, which will be different for heavy and light WIMPs (Sanglard 2005).

3.1.3 Spin-dependent interactions

For spin-dependent interactions, a crucial role is played by the isotopic abundance of elements having a non-zero angular momentum. For instance, sapphire is an interesting crystal for spin dependent interactions, because of the ^{27}Al that has an angular momentum of 3/2 and an isotopic abundance of 100%, while natural Ge contains only 7.7% ^{73}Ge, with an angular momentum of 9/2.

element	^{6}Li	^{7}Li	^{19}F	^{27}Al	^{29}Si	^{73}Ge
J	1	3/2	1/2	3/2	1/2	9/2
abundance(%)	7.5	92.5	100	100	4.7	7.7
S_p	0.5	0.497	0.441	0.343	-0.002	0.03
S_n	0.5	0.004	-0.109	0.03	0.13	0.378

Fig. 3.4 is showing the differential event rate in Ge, Si, LiF and Al_2O_3 if only the

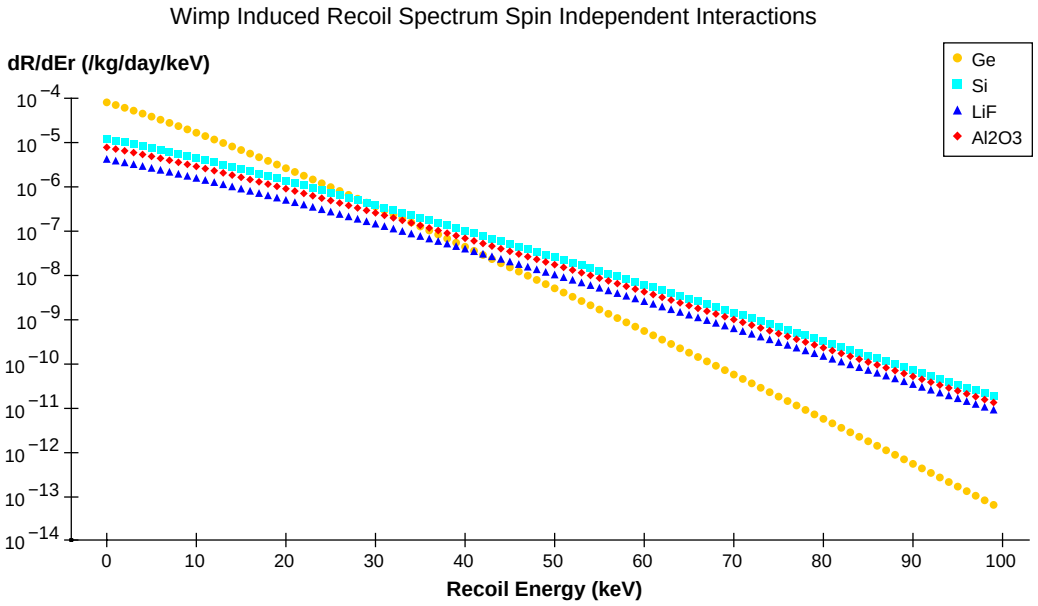

Figure 3.3: *Interaction event rate of WIMPs in $CaWO_4$, Ge, Si, LiF and Al_2O_3 for a WIMP mass of 20 GeV and an elastic scattering cross section of 10^{-6} pb. The event rate is higher in light crystals like Al_2O_3 than in heavy ones like Ge.*

spin-dependent coupling is taken into account. We can see that if EDELWEISS used sapphire detectors together with the Ge ones, this would increase the sensitivity of the experiment to spin-dependent interactions.

Up to now, we have shown that for all types of interactions Ge and sapphire have a different behaviour. This can be a useful WIMP signature for dark matter searches.

3.2 Interaction between neutrons and dark matter detectors

In the previous chapter, it has been shown that neutrons are the most dangerous source of background because they can mimic a WIMP signal. Indeed, a neutron having an energy of 0.5 MeV or a WIMP of 100 GeV with an energy of 30 keV give recoil energies of the same order of magnitude (about 30 keV) (Chabert 2004). This means that WIMPs with a mass between 1 and 10 MeV produce the same recoil energies in germanium as neutrons with an energy between 1 and 10 MeV. We will now see which are the main sources of neutrons in the Modane Underground Laboratory and how we can have an idea if the events detected come from WIMPs or neutrons by diversifying our targets.

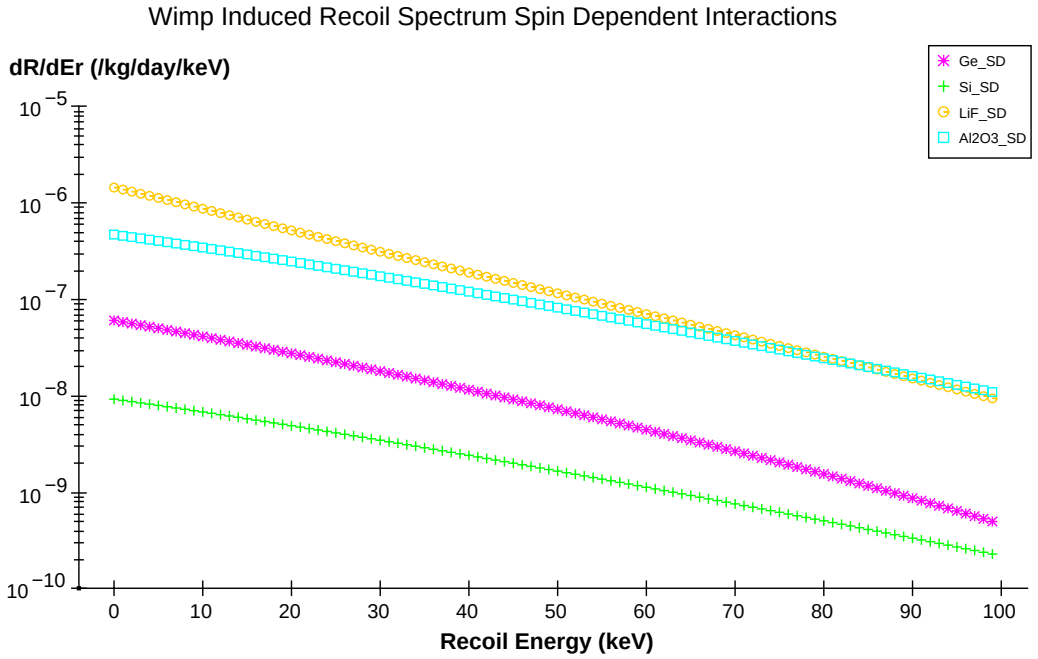

Figure 3.4: *Interaction event rate of WIMPs in Ge, Si, LiF and Al_2O_3 for spin-dependent coupling. LiF and Al_2O_3 are more interesting for SD interactions than Ge.*

3.2.1 The origin of neutrons in Modane Underground Laboratory

The EDELWEISS experiment is protected by a polyethylene shielding in order to stop low energy neutrons. Monte-Carlo simulations have shown that the neutron flux is reduced by a factor of about 100 by 30 cm of shielding and of about 1000 by 50 cm for neutrons having energies between 1 and 10 MeV. Therefore, the most dangerous neutrons that can cross the shielding and interact with the detectors are the ones having high energies (several GeV).

In a deep underground laboratory, the neutron background mainly comes from three sources, as shown in Fig. 3.5 (Chazal 1997):

- The natural radioactivity of the rock, due to the spontaneous fission of uranium and thorium (less than 10 MeV).
- Reactions of the type (α, n) given by the alpha particles emitted by uranium, thorium and their daughters interacting with the rock (less than 10 MeV).
- The muons interacting with materials around the experiment (up to several GeV).

Certain elements like thorium and uranium have radioactive isotopes with a lifetime of the same order of magnitude as the age of the Earth. Their daughters can be found in

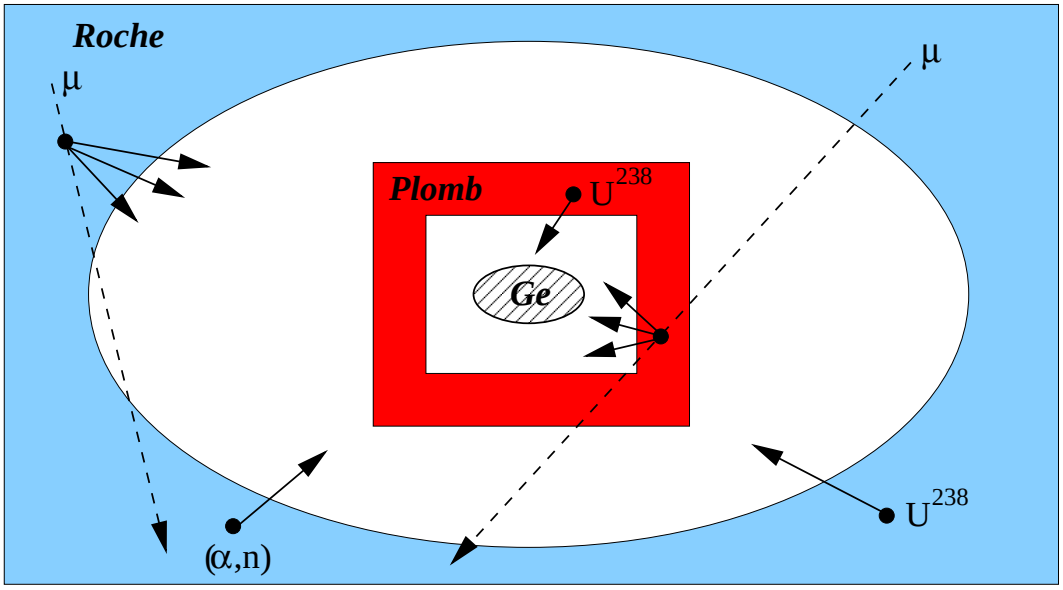

Figure 3.5: *Sources of neutrons in an underground laboratory: (α, n) reactions, natural radiaoctivity from the rock and products of muon interactions.*

many materials like the rock in which the underground tunnel has been built. Uranuim has no stable isotope. In natural state, uranium is made out of 99.275% ^{238}U and of 0.72 ^{235}U plus traces of other isotopes. The half-lives are:

$T_{1/2}(^{238}U)$ = 4.468 x 10^9 years
$T_{1/2}(^{235}U)$ = 7.04 x 10^8 years

Thorium is only made out of radioactive ^{232}Th with the half-life:

$T_{1/2}(^{232}Th)$ = 1.28 x 10^{10} years

The main fission taking place in the rock is that of ^{238}U, producing neutrons having an average energy of about 2 MeV.

Another source of neutrons are the (α, n) reactions with light elements from the rock. This kind of neutrons have an average energy of about 3.5 MeV.

A muon can couple to a proton in a nucleus by weak interaction: $\mu^- + p \rightarrow n + \nu_\mu$, creating a neutron with an energy between 6 MeV and a few dozens of MeV. Muons can also produce neutrons by photonuclear effect when they scatter inelastically on a nucleus: $\mu + (Z, A) \rightarrow \mu' + (Z, A') + xn + ...$ This process creates fast neutrons that can have energies much higher than 10 MeV. Therefore, this kind of neutrons can easily cross the shielding and interact with the detectors.

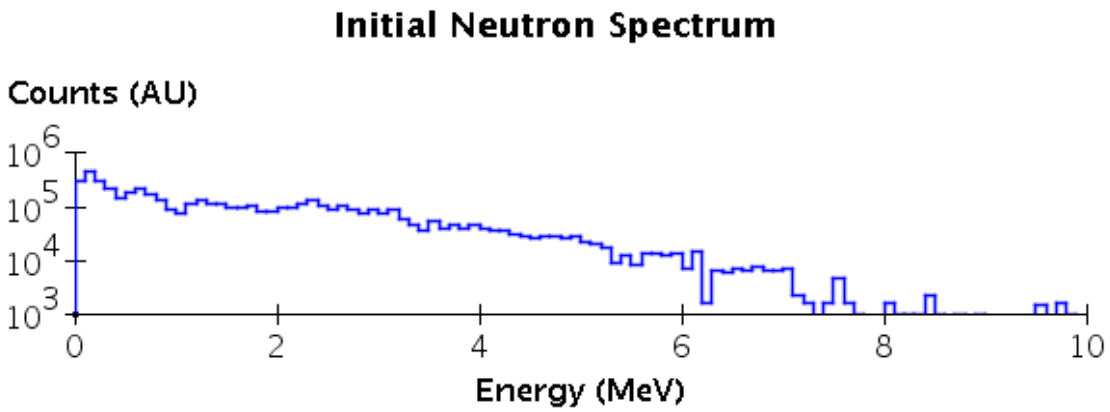

Figure 3.6: *Neutron energy spectrum in Modane Underground Laboratory.*

The EDELWEISS collaboration has made a first measurement of the neutron flux in the laboratory, obtaining 4x10^{-6} n/cm^2/s (Chazal 1998). After improvement of the neutron simulation algorithms, it has been found that the neutron flux is 1.6x10^{-6} n/cm^2/s for neutrons with energies between 1 and 10 MeV (Chabert 2004). The energy spectrum of these neutrons is shown in Fig. 3.6.

Thanks to Monte-Carlo simulations, we can find the event rate of neutrons in targets that are interesting for dark matter detection. Fig 3.7 shows the differential event rate in Ge, Si, LiF and Al_2O_3.

The energy transfer is more efficient when the order of magnitude of the target mass is close to that of the interacting particle. Therefore, the recoil energy in light targets will be higher than in heavy ones. If we integrate the differential event rate above a threshold, a sapphire target will see more neutron events than a Ge one. This means that an experiment using multiple targets will see a difference in the neutron event rate in the different detectors.

We have seen in this chapter that the use of sapphire as complementary target to Ge is interesting in order to distinguish between a neutron and a WIMP signal, as well as for the detection of light WIMPs or WIMPs that have a spin-dependent coupling with the ordinary matter. In order to distinguish between nuclear and electronic recoils, a sapphire bolometer has to measure two signals simultaneously: heat and scintillation. The heat signal has already been studied and it is known that sapphire has low heat capacity that makes it perfect for 20 mK tests. Before this thesis, it was difficult to say whether sapphire could be a good cryogenic scintillator. Therefore, in the following chapters, I will describe the scintillation tests performed in order to define what kind of sapphire crystals should be used within a cryogenic dark matter search.

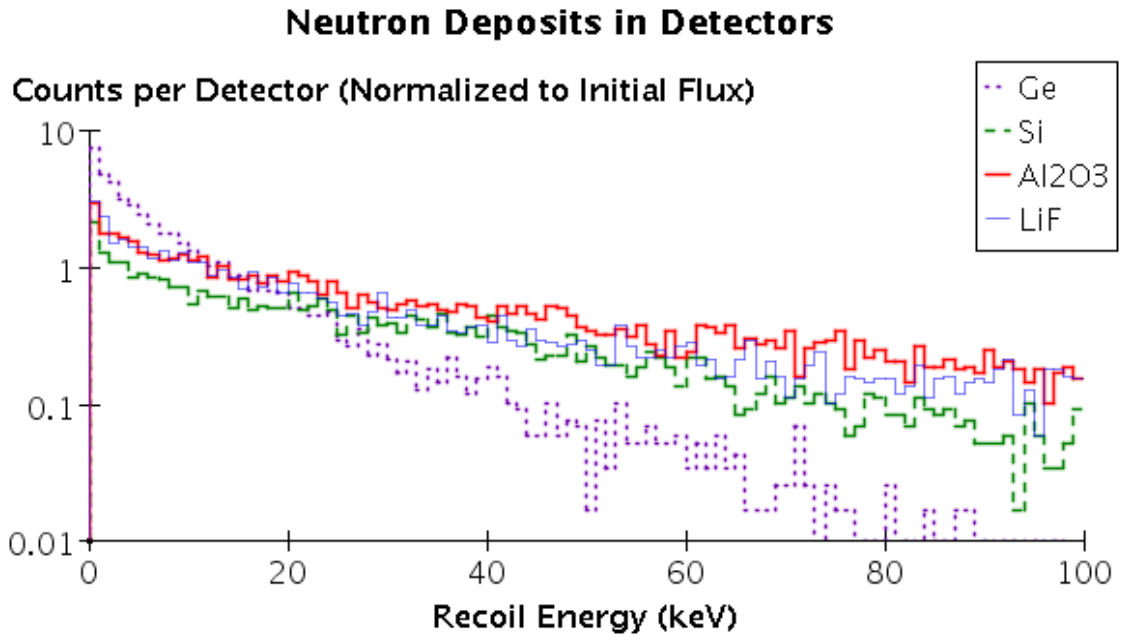

Figure 3.7: *Neutron simulated event rate in targets that can be used in dark matter searches: Ge, Si, LiF and Al_2O_3. The integrated event rate above a threshold is higher in Al_2O_3 than in Ge.*

Chapter 4

Study of Scintillation by Spectroscopic Characterization

Abstract

Le saphir est un cristal léger qui pourrait être utilisé dans une expérience de recherche de matière noire en tant que détecteur scintillation-chaleur, de manière complémentaire avec les cibles de masse atomique élevée déjà existantes comme le germanium. Le saphir est déjà connu comme un bon bolomètre chaleur. Nous verrons par la suite comment les cristaux peuvent tre caractérisés du point du vue de l'émission de lumière, afin de trouver les scintillateurs les plus efficaces.

4.1 Introduction to the problem of crystal scintillation

One of the main goals of my thesis was to define in what conditions sapphire could make an interesting low temperature scintillator. In order to present the different spectroscopic characterization tests performed on sapphire samples, some general understanding of the scintillation process is essential.

The electronic energy states in an inorganic crystal lattice consist of a series of energy bands (Birks 1964). A diagram of the energy bands in the crystals is shown in Fig. 4.1.

In the normal state, the valence band is completely filled, while the conduction band is empty. The valence band is separated from the conduction band by an energy gap of a few electron-volts. When a high energy photon interacts with the crystal, several electrons and holes are excited to either the upper level of the valence band or the lower level of the conduction band. Electrons in the valence band may be raised in the conduction band by the absorption of an energy at least equal to the energy gap, leaving holes in the valence band. Alternatively, the excited electron may remain bound to the positive hole, creating an exciton. The exciton carries no net charge but is free to migrate through the crystal lattice. The exciton band corresponds to a band of energies below the conduction band. This structure applies to insulators having a perfect crystal lattice. In practice, variations due to lattice defects and impurities occur in the energy bands, producing local electronic energy levels in the forbidden region. If these levels

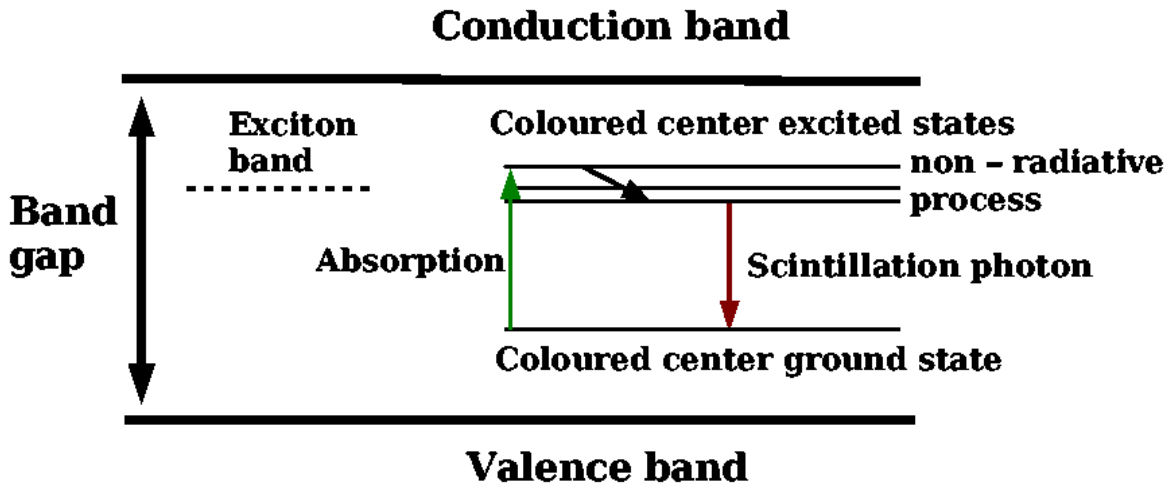

Figure 4.1: *Energy bands in a crystal. In the normal state, the lower energy bands are completely filled, while the higher bands are empty.*

are unoccupied, electrons or excitons moving in the conduction band may enter these local energy levels. There are three main types of centers:

- Luminescence centers, in which the transition to the ground state of the center is accompanied by photon emission.
- Quenching centers, in which thermal dissipation of excitation energy occurs without light emission.
- Traps that may have metastable levels from which the electrons(holes) or excitons may only return to the conduction band(valence band) by acquiring thermal energy. Once in the conduction band, they return to the valence band by photon emission. This process carries the name of thermoluminescence.

The luminescence centers can have several origins: specific impurities that are added to the crystal, stoichiometric excess of one of the constituents of the solid, defects in the lattice. To sum up, a crystal can scintillate if there are energy bands within the forbidden band created by specific activators.

4.2 Sapphire properties

Synthetic sapphire is a single crystal form of corundum, Al_2O_3 , also known as alpha-alumina or alumina. The combination of favourable chemical, electrical, mechanical,

optical, surface, thermal and durability properties make sapphire a material with numerous applications (Dobrovinskaya et al. 2002). In aerospace, sapphire is used for its durability and resistance to corrosion, often in combination with the ability to withstand high heat while having a very broad transmission range. The applications include Forward Looking Infra Red Windows (thanks to its optical clarity over a broad spectral range), windows that can resist erosion in salt and blowing sand environments, lamps, where the capacity to resist at high temperatures is used. In medicine, sapphire is used in surgical systems for laser transmission and in contact with body fluids (endoscope lenses, knives). Sapphire is also useful in the watch industry, for scratchproof watch glasses. In optics, sapphire applications range from laser crystals to lightguides, lenses or windows. Cr:Al_2O_3 crystals have been used for building the first solid-state laser in 1960 (Maiman 1960), being recently replaced by Ti:Al_2O_3 (Moulton 1986). In jewelry, the gem known as sapphire is blue, but Al_2O_3 doped with elements like Cr, Ti, Fe, V, Be can have different colours: red (ruby), pink, purple, orange, yellow, green.

Sapphire hardness is 9 Mohs, being the third hardest material after diamond (10) and SiC (9.5). The melting point is very high, 2030 °C. The crystal is insoluble in water, HNO_3, H_2SO_4, HCl, HF. The density is 3.98 g/cm^3. The optical transparency range is 170-5500 nm and it remains transparent even after exposure to high doses of radiation and high-energy electron beams. It is a good insulator with a band gap of 9 eV. Sapphire crystalises in a rhomboidal system and has a hexagonal symmetry.

Sapphire single crystals can be grown by several methods. The historically first (developed at the end of the 19th century) and easiest method used for sapphire growth is *Verneuil* (flame fusion). The principle of the process involves melting Al_2O_3 powder on an oxyhydrogen flame. As the powder passes through the flame, small droplets form and fall on a support rod placed below. As more droplets fall, a single crystal called a "boule" starts to form and the support is slowly moved downwards, allowing the base of the boule to crystallise while the tip remains liquid. Very long cylinders can be formed using this method. Although the cost is low, this method has some drawbacks. Defects easily appear in the crystal lattice and for doped crystals there is also a gradient in the doping concentration between the top and the bottom of the cylinder. Higher quality crystals can be obtained using the *Czochralski* method. This method consists in pulling a crystal from a crucibile at a melt temperature either constant or varying in a controlled manner. Unlike the Verneuil method, Czochralski allows to substantially stabilize the thermodynamic parameters of the growth process (like the redox potential of the growth atmosphere), the melt temperature and temperature distribution in the crystal. The main drawback of the method is the presence of the crucibile that can be a source of unwanted impurities in the crystal. Besides these two main methods, numerous other growth techniques exist: Bridgman-Stockbarger, Kyropoulos, Heat Exchange Method, Stepanov, Flux Method, Internal Crystallization, etc. The right method has to

be chosen according to the requirements of each particular application. For instance, impurities in the lattice can be a problem for window manufacturing but can have interesting scintillation properties.

I have shown here some of the main properties of sapphire that make it a material with numerous applications. Recently, Al_2O_3 has also started to be investigated by astroparticle physicists as a possible target for dark matter detection.

4.3 Sapphire scintillation: state of the art

Before the beginning of this thesis, some indication existed that certain sapphire samples could be interesting low temperature scintillators. The ROSEBUD collaboration had demonstrated that certain nominally pure sapphire crystals could be good scintillators at 20 mK (Coron 2004). The origin of this scintillation was not completely understood, being attributed to the presence of Cr^{3+}impurities in nominally pure crystals. We will see in this chapter that the only presence of Cr^{3+}can not explain the important low temperature scintillation measured by ROSEBUD. Another encouraging set of tests had been performed on Ti:Al_2O_3 with a Ti concentration of the order of 1000 ppm, showing that less concentrated samples could scintillate more than the more concentrated ones (Mikhailik 2005).

Several low temperature tests have been performed on both nominally pure and doped sapphire crystals of different sizes, shapes, origins, with both Ge and Si light detectors. Some of the results are shown in the Table 4.1 (Petricca and De Marcillac n.d.):

Crystal	Shape	Light yield (%)	Light Detector
IAS26 - B213	50 g cylinder	1.3	Ge
IAS03 - A080	5 g cube	1.27	Ge
IAS15 - A107	50 g cylinder	0.25	Si
MPP3	20x10x5 mm^3	1.4	Si
MPP4	20x10x5 mm^3	1.4	Si
IPNL1.3	5 g cube	0.8	Ge

Table 4.1: *Cryogenic gamma scintillation light yield (fraction of energy deposited in the crystal and seen in the light detector) of different crystals. Light yields vary by a factor of about 6 between the good and the bad scintillators.*

These tests show differences of a factor of 6 between the light yields (the fraction of energy of the incoming particle seen in the light detector) of different crystals. While a crystal having a light yield of 1.4 % is very interesting for building dark matter search detectors, crystals having a light yield of only 0.25 % should be avoided. In order to tell good scintillators from inefficient ones, several different approaches are possible. Each

crystal that will be used as scintillating detector can be tested directly at 20 mK. This method has the advantage of giving a reliable answer on the actual low temperature behaviour, but is time and money consuming. Another way of dealing with this problem is to find a connection between the room temperature scintillation and the low temperature one. The advantage is that room temperature scintillation tests can be performed fast and easily, but they may not give a definite answer if crystals with similar room temperature scintillation spectra behave differently at low temperature (e.g. if there are defects in the lattice that only trap electrons or holes at low temperature). A different approach consists in finding crystal growth conditions that always lead to good low temperature scintillators. This method cannot tell if a randomly chosen crystal is a good scintillator or not, the purpose is just to find the criteria that ensure that good scintillating crystals can be obtained in a reproducible manner. During my PhD, I followed this approach, defining conditions that lead to good scintillating properties. The first step was to understand why crystals that were nominally pure emitted light at low temperature. Once the origin of the scintillation understood, I did systematic tests on crystals having controlled growth conditions in order to find the most efficient scintillators. The methods of spectroscopic characterization that I used are: scintillation tests using X ray excitation, that give the quantity of light emitted by every crystal and the shape of the spectrum between the room temperature and 30 K; fluorescence and optical absorption that are used for determining the quantity of impurity in crystals and thermoluminescence that gives additional information on the evolution of the quantity of light as a function of temperature.

4.4 X ray scintillation

4.4.1 Experimental setup

All scintillation tests have been done thanks to a collaboration between IAS[1], IPNL[2], LPCML[3] and MPP[4], within the SciCryo project funded by the ANR[5] in 2005. For the scintillation tests, I have used an Inel XRG 3000 X ray generator. The experimental setup is shown in Fig. 4.4.1.

The Bremsstrahlung X rays are produced by electrons accelerated at 40 kV and 35 mA bombarding a tungsten anode (Dujardin and Ledoux n.d.). The X ray flux is stable at less than 5%. The X rays induce crystal scintillation which is guided by an optical

[1]Institut d'Astrophysique Spatiale, INSU - Université Paris XI
[2]Institut de Physique Nucléaire de Lyon, IN2P3 - Université Claude Bernard Lyon 1
[3]Laboratoire de Physico-Chimie des Materiaux Luminescents, Université Claude Bernard Lyon 1
[4]Max Planck Physik Munich
[5]Agence Nationale de la Recherche

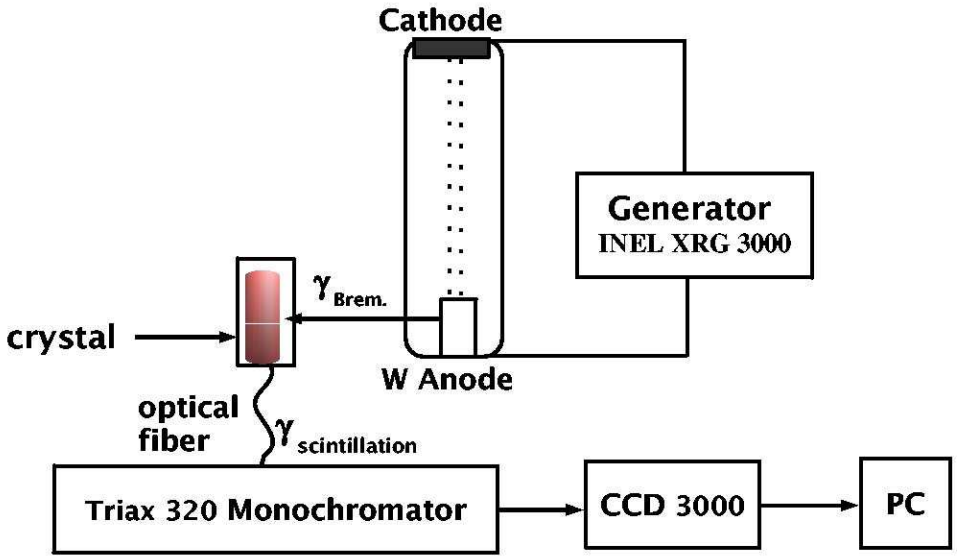

Figure 4.2: *A scheme of the experimental apparatus for X ray scintillation tests.*

fiber towards a monochromator diffraction grating Triax 320 Jobin-Yvon separating the wavelengths and sending them to a CCD 3000 camera. The detector is sensitive to the number of photons, therefore all spectra show the number of photons detected at each wavelength. The CCD sends the information to a computer. The crystals can be cooled down to 30 K with a cryostat with optical windows. The cryostat is mechanically cooled.

The spectra have been taken between 250 and 1000 nm, corresponding to the sensitivity range of the experimental setup. A diffraction grating not only gives first order intensity maxima but also multiple order maxima (i.e. a peak that appears at 400 nm will also appear at 800 nm, 1200 nm...):

$$d \sin\theta = n\lambda \tag{4.1}$$

where n is the order number, λ the wavelength, d the distance between grating lines and θ the angle of diffraction. Therefore, I have used Kodak high-pass filters with cuts at 320, 400 and 600 nm (Fig. 4.3).

Thus, the total range 250 - 1000 nm is divided into 5 spectral regions with a filter corresponding to each region (Table 4.2).

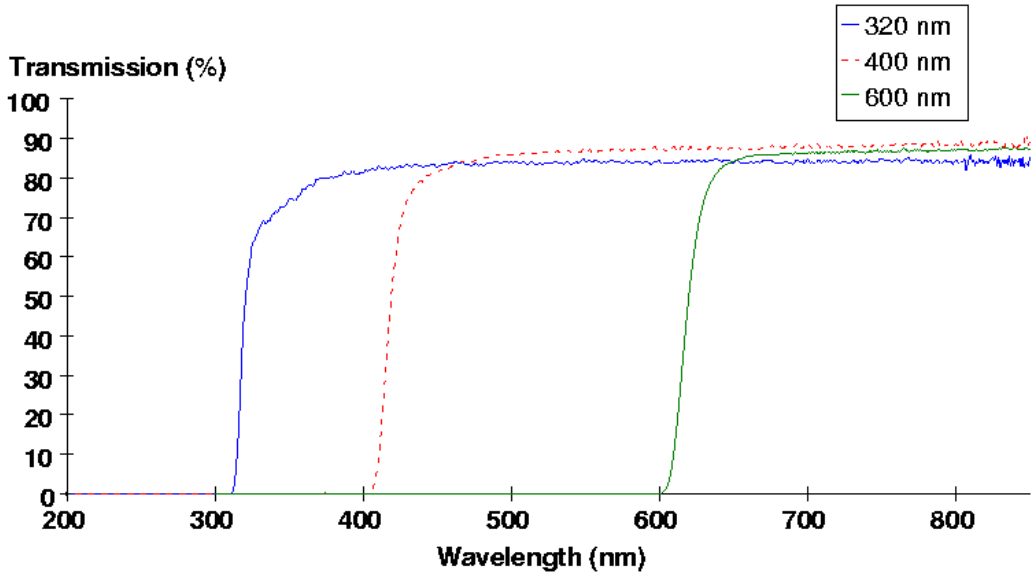

Figure 4.3: *Transmission spectra of the filters used for scintillation tests measured by optical absorption.*

center (nm)	range (nm)	computer cuts (nm)	filter (nm)
280	143 - 419	250 - 340	-
400	263 - 538	340 - 520	320
520	384 - 658	520 - 655	400
750	615 - 886	655 - 850	600
980	847 - 1114	850 - 1000	610

Table 4.2: *Use of filters for measuring the scintillation spectrum.*

4.4.2 Data analysis

The first step in the data analysis is the spectra concatenation. The five parts are put together in one single spectrum. The computer cuts (Table 4.2) are chosen in order to have a maximum transmission for each filter. Each spectrum is multiplied by the transmission efficiency corresponding to the filter (about 85%). Then the spectra are corrected for the detector response. The calibration of the detection system has been done using an Oriel 63358 tungsten lamp. For that, we place the lamp at 50 cm of the optical fiber and we measure the spectrum. The real spectrum, indicated by Oriel is given by the function:

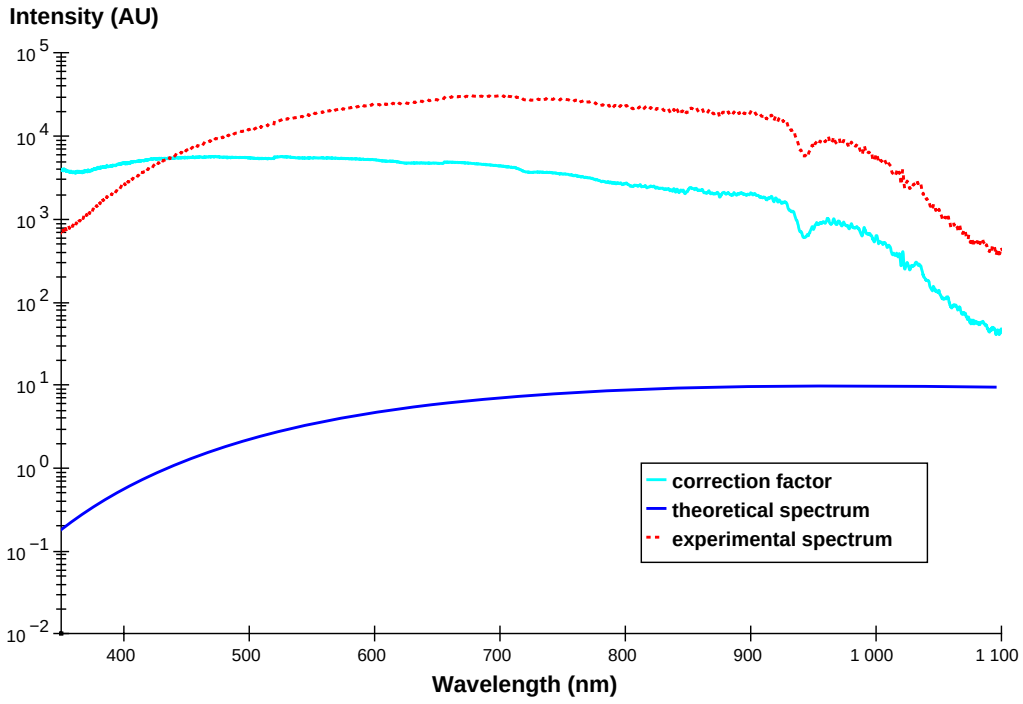

Figure 4.4: *The detector response has been determined using a tungsten lamp. The correction factor is given by the ratio between the lamp spectrum given by the manufacturer and the one measured with our experimental setup.*

$$Intensity = \frac{1}{\lambda^5} e^{A+\frac{B}{\lambda}} \cdot (C + \frac{D}{\lambda} + \frac{E}{\lambda^2} + \frac{F}{\lambda^3} + \frac{G}{\lambda^4} + \frac{H}{\lambda^5}) \tag{4.2}$$

with:
A = 41.7265
B = -4959.48
C = 0.65866
D = 910.029
E = -844063
F = $3.94926 \cdot 10^8$
G = $-9.27579 \cdot 10^{10}$
H = $8.46036 \cdot 10^{12}$
The ratio between the measured spectrum and the theoretical one gives the efficiency of the detection system, that is the correction factor (Fig. 4.4). Each experimental spectrum is multiplied by this correction factor in order to obtain the real scintillation spectrum.

The spectrum obtained this way usually contains not only the signal due to crystal

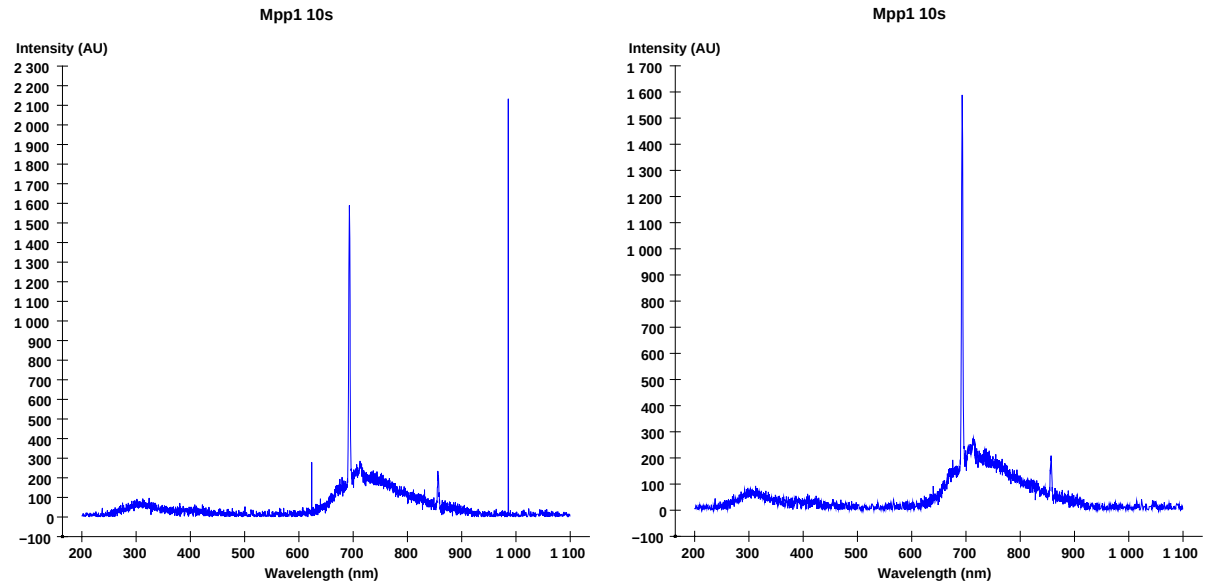

Figure 4.5: *An example of "cosmic hits" at 620 nm and 980 nm (left). These hits are eliminated during data analysis (right), without altering the intensity of the Cr peak (1588 A.U.)*

scintillation, but also a few hits probably coming from cosmic rays interacting with the CCD during data taking (Fig. 4.5).

When eliminating the "cosmic hits" the algorithm has to take into account the difference between these hits (620 nm and 980 nm in Fig. 4.5) and the Cr peak (about 690 nm). The main difference is that noise peaks usually lie on no more than 2 channels while the Cr peak is much larger (about 17 channels). In order to look for outliers, the algorithm first calculates the derivative at each point of the spectrum; it is among the derivatives that we look for outliers. In order to decide whether a point is an outlier or not, we calculate the average value for a certain number of points (the reference array) before and after the given point (without taking it into account). If the difference between the value of the point and the average value is superior to the standard deviation multiplied by a certain number, then the point is an outlier and it is eliminated from the spectrum. In the case of our spectra the algorithm is applied twice, the reference array having 20 points (10 of each side of the studied point). When applying it for 4 times the standard deviation, no other point than the actual oulier is eliminated, but some of the outliers may remain (algorithm useful when there are about 2 or 3 outliers in the spectrum). In the case of several outliers, we apply the algorithm for twice the standard deviation. A few points that are not outliers are also eliminated, but none belonging to the 693 nm Cr peak.

Once the different parts of the spectrum put together and the outliers eliminated,

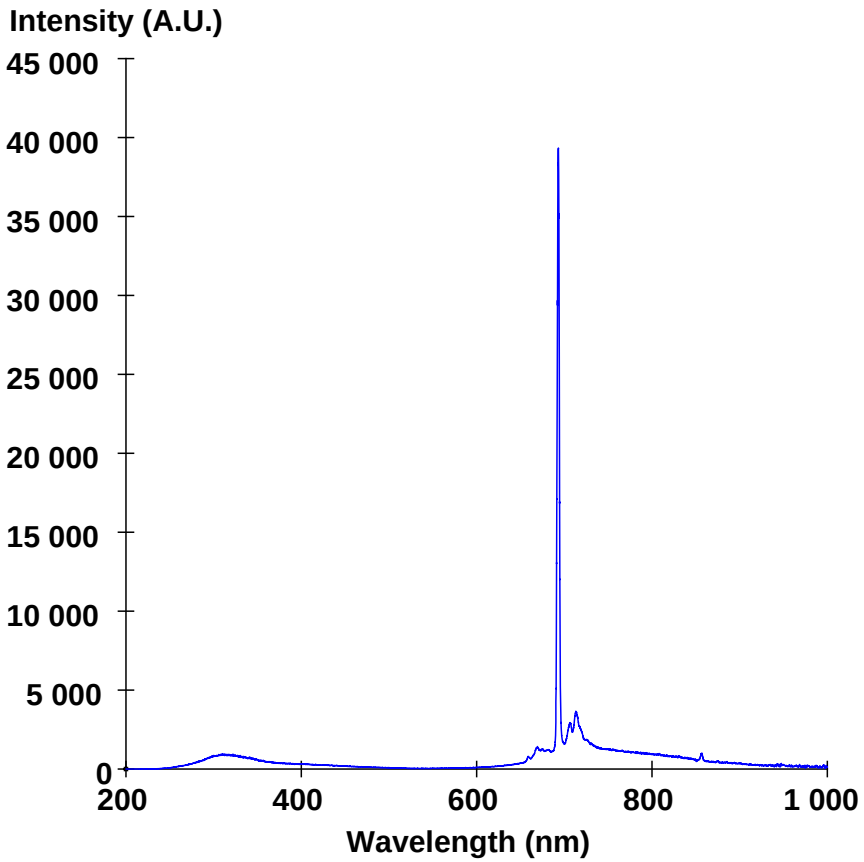

Figure 4.6: *An example of scintillation spectrum of nominally pure sapphire having a ppm level of Cr^{3+} impurities. The R_1 and R_2 zero - phonon lines are at 693 nm (not resolved) accompanied on both sides within 50 nm by several vibrational satellites.*

the spectrum, representing the number of photons as a function of wavelength, can be plotted.

4.4.3 Nominally pure crystals

Several nominally pure sapphire crystals have been analysed using the X rays. All of them show room temperature scintillation. This scintillation can be produced by impurities in the crystal (like Cr^{3+}, Ti^{3+}, Ti^{4+}) even at ppm levels or by other coloured centers. An example of scintillation peak due to Cr^{3+} impurities is shown in Fig. 4.6.

By fitting the peak, we get a mean value of 693 nm and a FWHM of 4 nm, which corresponds to the scintillation spectra shown in literature for chromium doped sapphire (Nelson and Sturge 1964). It represents the R_1 and R_2 zero-phonon lines of ruby,

which are not resolved with the sensibility of our detection system and at room temperature. The R lines are accompanied by vibrational side bands which are created by transitions including the interaction with phonons. When creating or destroying phonons in a transition, the photon energy is reduced or enhanced by the energy of the phonons, which explains the vibrational satellites of the R lines.

The other scintillation peak of the spectrum has weaker intensity and lies at 300 nm, having a FWHM of about 100 nm. The origin of this peak is not yet clear. It is known that the F^+ coloured centers (i.e. oxygen vacancies with one trapped electron) give an emission band at 330 nm (Vallayer 2001). Another hypothesis is that this scintillation peak is the emission of excitons localised at Ti^{3+} ions (Mikhailik 2005). Further study is needed in order to come to a final conclusion.

Another kind of scintillation encountered in nominally pure crystals during the X ray tests is the one due to Ti^{3+}. An example of such a spectrum is given in Fig. 4.7. It is a broad peak, centered at 750 nm with a FWHM of about 140 nm which is the well known Ti^{3+} scintillation peak in $Al_2O_3 : Ti$ (Grinberg 1993).

During the tests, I have also found that some nominally pure crystals had a scintillation peak in the blue region, with a mean value of 415 nm and a FWHM of about 80 nm, as shown in Fig. 4.8.

Several hypothesis are also proposed in the literature in order to explain this scintillation. One of them concerns the F coloured centers (oxygen vacancies) scintillation (Vallayer 2001). Another one suggests a 420 nm scintillation peak induced in sapphire crystals by Ti^{4+} (Blasse 1990). It is difficult at this point in the analysis to say whether one hypothesis or the other or even both of them explain the scintillation noticed at 415 nm. One interesting aspect is that we have noticed an enhanced 415 nm scintillation in two of our crystals, one of 215 mg and the other one of 60 mg, belonging to the same batch. We also know that Ti has a broad absorption band between 400 and 600 nm, so the emission peak at 415 nm is inside this absorption band. The fact that both crystals having this scintillation are small may signify that in larger crystals all or part of the 415 nm emission is absorbed by Ti.

To sum up, the main scintillation peaks encountered in nominally pure sapphire during our tests are:

- 693 nm : Cr^{3+} line (FWHM = 4 nm)
- 750 nm : broad peak due to Ti^{3+} (FWHM = 140 nm)
- 300 nm : F^+ coloured centers and/or excitons localised at Ti^{3+} ions and/or other
- 415 nm : F coloured centers and/or Ti^{4+}

By now, we have seen crystals that show two or three of these peaks, nevertheless there are crystals where all types of scintillation are encountered as shown in Fig. 4.9

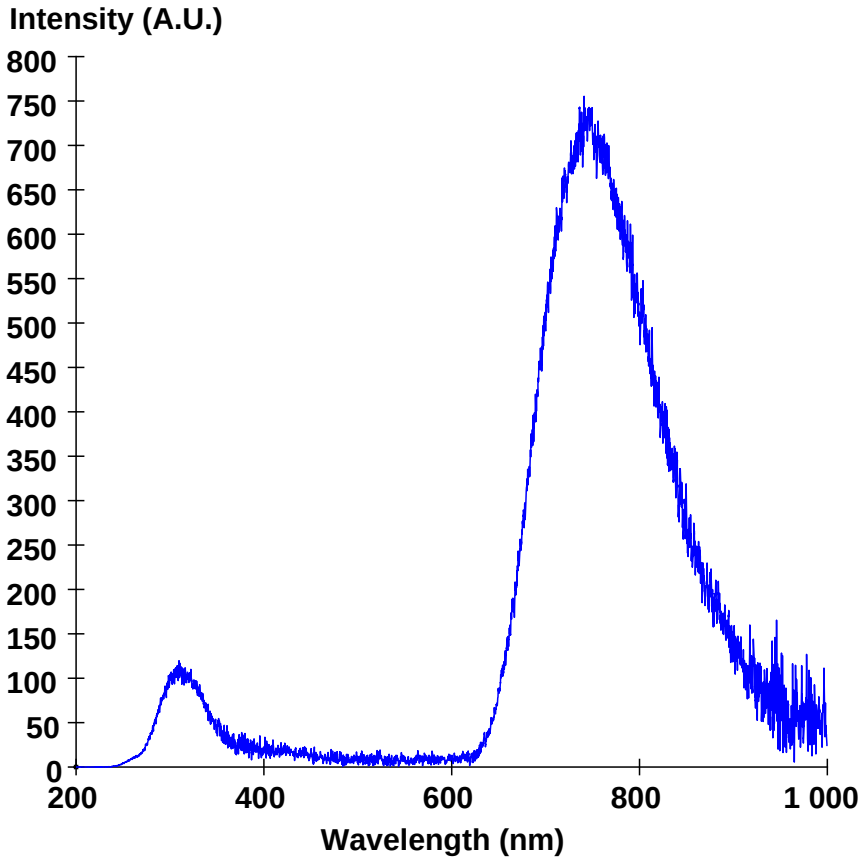

Figure 4.7: *Scintillation spectra of nominally pure sapphire having a ppm level of Ti^{3+} impurities; Ti^{3+} gives a broad scintillation peak centered at 750 nm.*

Since nominally pure crystals can have different types of scintillation spectra, it is interesting to know what kind of impurities are more favourable for the light yield. In order to compare the light yield of different crystals, they need to have the same size, shape, polishing and they have to be kept at the same position towards the detector and the excitation source. Fig. 4.10 shows the comparison between two crystals, one containing Cr impurities and the other one containing Ti.

We can see that from the standpoint of the integrated light yield, Ti that has a broad scintillation band is more interesting than Cr, having just a thin line with few photons. In order to confirm which is the ”useful” doping element for good scintillating properties, we need to check the evolution of the two main spectra (the ones dominated by Ti and the ones dominated by Cr) at low temperature.

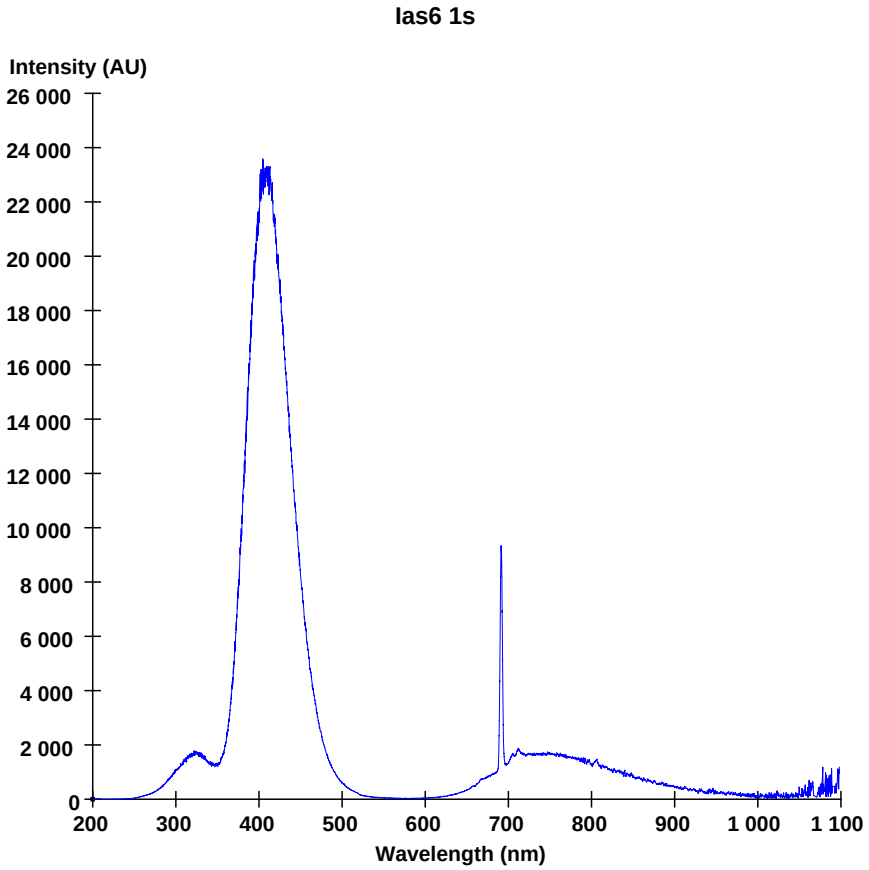

Figure 4.8: *Scintillation induced by coloured centers and/or Ti^{4+} in nominally pure sapphire (400 nm peak).*

4.4.4 Low temperature light yield evolution

So far, we have seen that nominally pure Al_2O_3 with small quantities of $Ti^{3+}$is a promising room temperature scintillator. I have also shown that another source of scintillation at room temperature is the presence of Cr^{3+}, which is less interesting from the point of view of the number of photons contained in the peak. The next step is to check how these spectra change at low temperature by cooling down the crystals with an optical cryostat.

Fig. 4.11 shows the evolution of a nominally pure sapphire crystal with traces of Cr^{3+}between the room temperature and 30 K.

We can see that even though the intensity of the Cr line is considerably enhanced, we measure a 20% decrease in the overall integrated light yield when decreasing the temperature. This result, associated to the room temperature one gives indication that $Cr^{3+}$is not the best choice of doping for efficient low temperature scintillators.

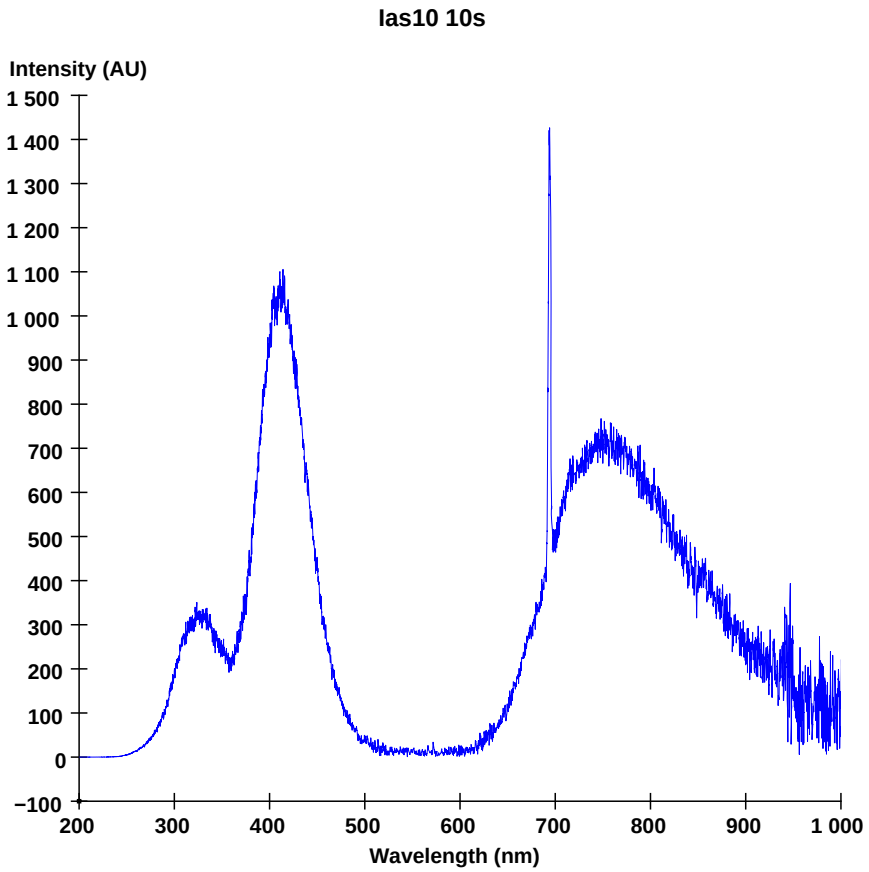

Figure 4.9: *One crystal can show several scintillation peaks: 300 nm, 415 nm, 693 nm, 750 nm*

Fig. 4.12 shows the evolution of a crystal containing Ti^{3+}doping between room temperature and 30 K. We can see that there is an overall increase of a factor of about 2 in the integrated light yield.

This increase in the light yield between room temperature and 30 K gives a positive indication that Ti:Al_2O_3 can be an useful crystal for building scintillating low temperature detectors.

4.4.5 Room temperature scintillation tests of Ti:Al_2O_3

Tests done on several randomly chosen crystals show that they all contain impurities and scintillate and that the most promising impurity for low temperature scintillation is Ti^{3+}. In order to find the optimum concentration for a maximum light yield, I have tested five crystals with controlled Ti doping: 10, 50, 100, 500 and 1000 ppm. All crystals have the same shape and size, 20 x 10 x 5 mm^3 and are polished in the same way. All

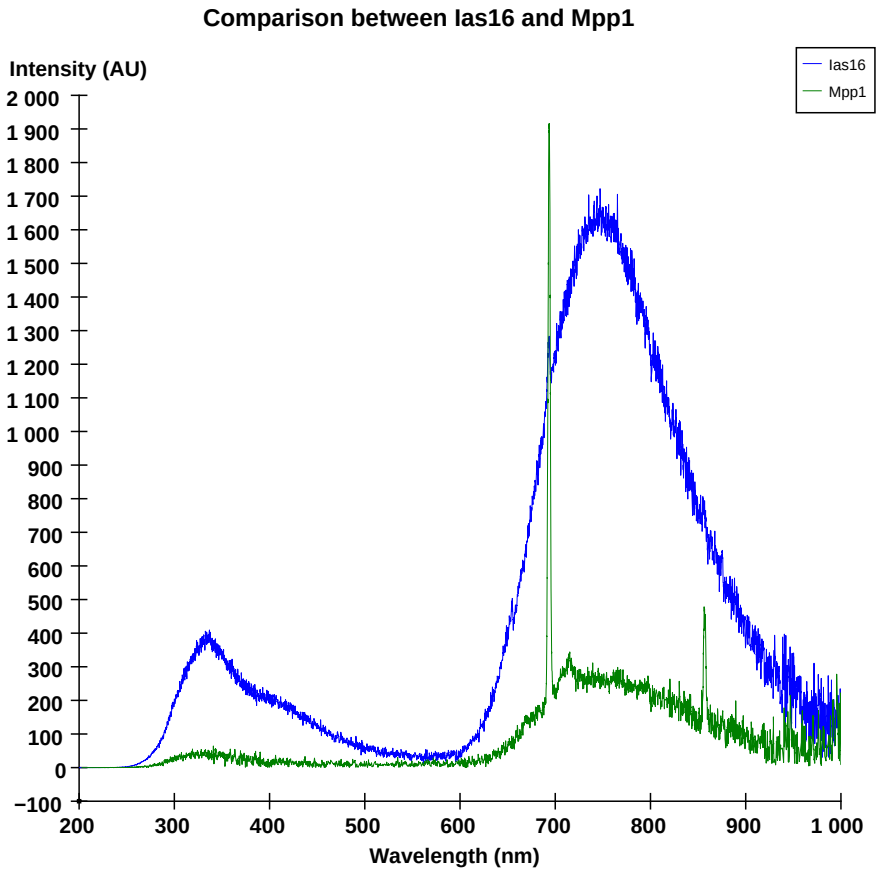

Figure 4.10: *Comparison between two crystals of the same size, geometry (cylinders with h = 40 mm and ϕ = 40 mm), position versus the X rays and the optical fiber and for the same time of exposure. When superposing the two spectra we can see that the crystal containing Ti impurities (IAS 16) scintillates more than the crystal containing Cr (MPP 1).*

are Czochralski grown in a redox potential of -230 kJ/mol, and C oriented. They have been fabricated by The Institute for Single Crystals (ISC), Ukraine.

In order to compare the spectra of the five crystals, they have been kept in a fixed geometry towards the X rays and the optical fiber using a teflon holder (Fig. 4.13).

Fig. 4.14 shows the comparison between the five spectra at room temperature. The main scintillation occuring in the five spectra is the one due to Ti^{3+}at 750 nm; we also see the 300 nm peak and a peak in the blue region at 400 nm for the less concentrated samples (10 and 50 ppm).

In order to find the best concentration for an optimum light yield, we need to calculate the integrated light yield for each spectrum. Fig. 4.15 is showing the light yield of the five crystals integrated on the range 200 - 900 nm.

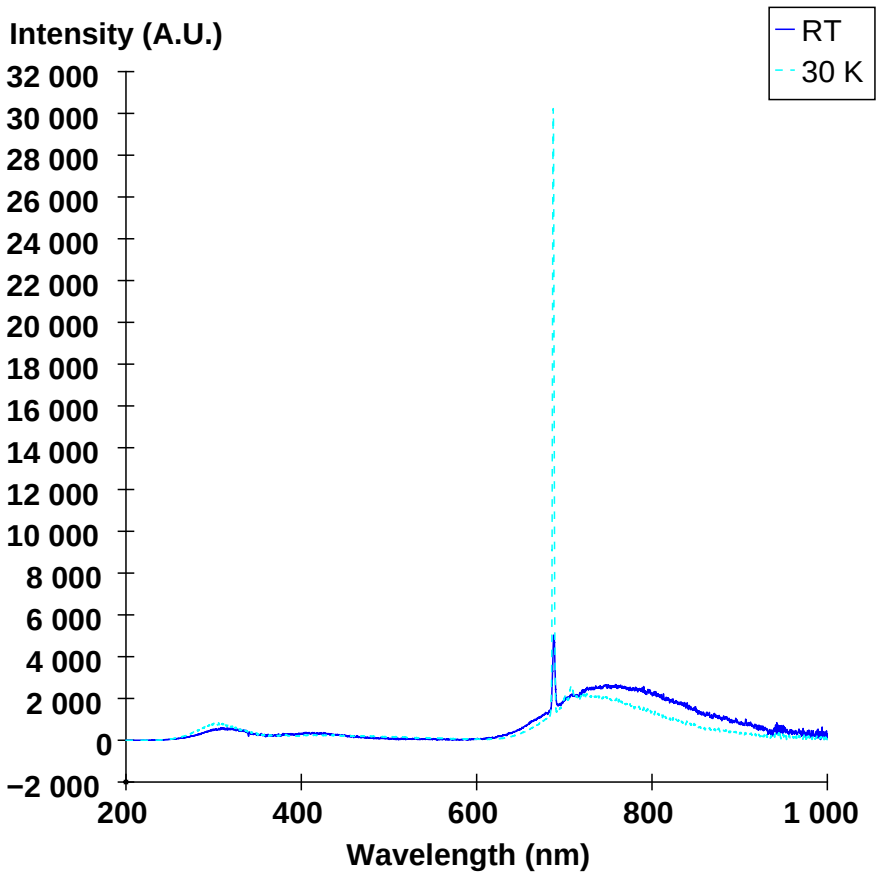

Figure 4.11: *Evolution of a nominally pure sapphire crystal with traces of Cr between the room temperature and 30 K.*

We can see that in the five crystals considered, the best Ti concentration for a maximum light yield is 100 ppm. Another interesting feature is that there is only a 35% difference between the best and the less efficient scintillator on the range 10 - 500 ppm. Since the main purpose of this test is to study the quantity of light as a function of Ti concentration, Fig. 4.16 is showing the integrated light yield on the range 600 - 900 nm, corresponding to the Ti^{3+}peak.

On this range, the crystal with 100 ppm of Ti remains the most efficient scintillator. The difference between the best and the worst scintillator is reduced to 25% for concentrations between 10 and 500 ppm. All this leads to the conclusion that in order to obtain efficient room temperature scintillators, the precision of Ti concentration between 10 and 500 ppm is not mandatory.

Low temperature tests were performed for the four best scintillators. Another reason why high concentrations of Ti^{3+}should be avoided for low temperature scintillators

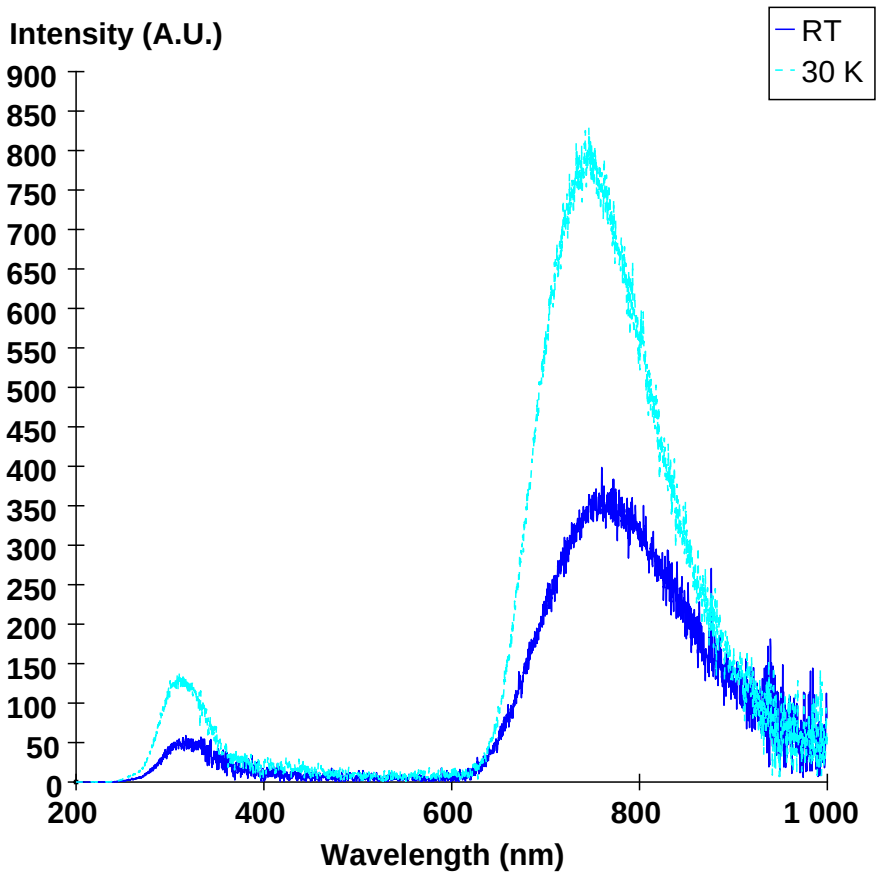

Figure 4.12: *Evolution of a sapphire containing Ti between the room temperature and 30 K. There is a factor of 2 between the two light yields.*

is that that heat capacity can dramatically increase at low temperature in the presence of paramagnetic impurities such as Ti^{3+}, making the crystal inefficient as heat bolometer (Pobell 1996).

4.4.6 Low temperature scintillation tests of Ti:Al_2O_3

The four Ti:Al_2O_3 crystals have been tested in the temperature range 30 - 300 K in order to determine the evolution of the quantity of light as a function of temperature. The typical change in a spectrum between the room temperature and 30 K is shown in Fig. 4.17.

There is a factor of about two between the room temperature and the low temperature light yield. We notice an increase in the near IR and UV scintillation, while the blue emission is diminished at low temperature.

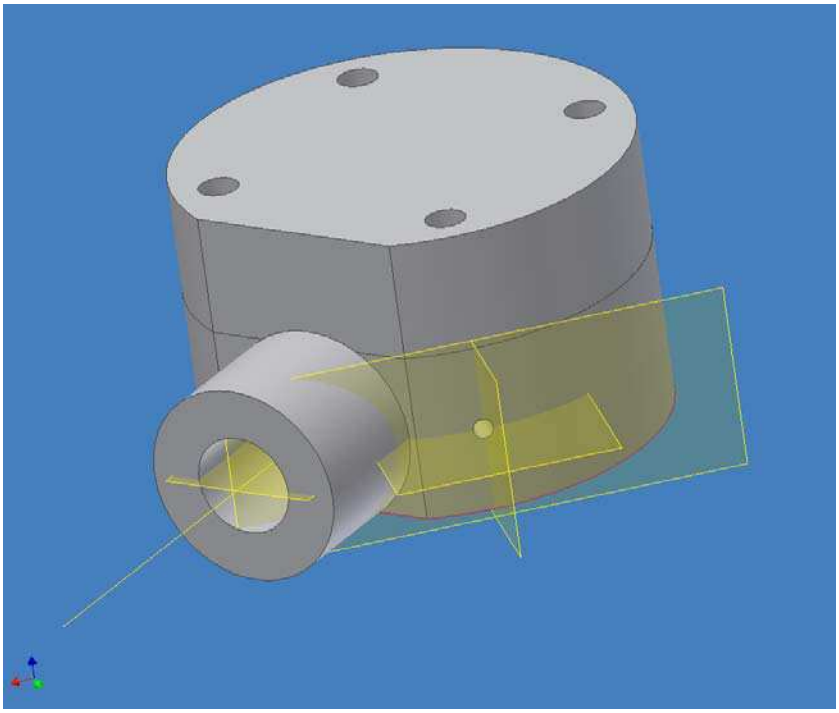

Figure 4.13: *Teflon holder that allows keeping 20 x 10 x 5 mm^3 crystals in a fixed geometry. The crystal is inside the cylinder, the optical fiber is fixed on the holder and the X ray flux reaches the crystal through a 2 mm whole in the teflon (where the white areas cross).*

In order to find which scintillator is most efficient, we have to compare the integrated light yield of crystals placed in a setup that keeps them in a fixed geometry. As shown earlier in this chapter, this is easy to do at room temperature using a teflon holder. When the crystals need to be tested in the cryostat, the setup is more complex and the cryostat or the crystal holder can easily move when changing the samples, which means that not all the samples are at the same position. Therefore, in order to compare the low temperature scintillation, I have normalized each room temperature spectrum in the cryostat to the spectrum obtained in the teflon holder. I have obtained the normalization factor by finding a function that fits the Ti^{3+}peak and determining the value of the function at 760 nm, where the peak reaches its maximum intensity. The normalization factor is $I_{teflon}/I_{cryostat}$ at 760 nm.

Fig. 4.18 shows the comparison between the four crystals at 45 K. When calculating the integrated light yield in the range 200 - 900 nm (Fig. 4.19), the result is similar to the one obtained at room temperature.

The difference between the light yield coming from the most and the less efficient scintillator is only 20%. The best scintillator on the whole range is the crystal with 50 ppm of Ti, but the quantity the light is practically the same for 50 and 100 ppm.

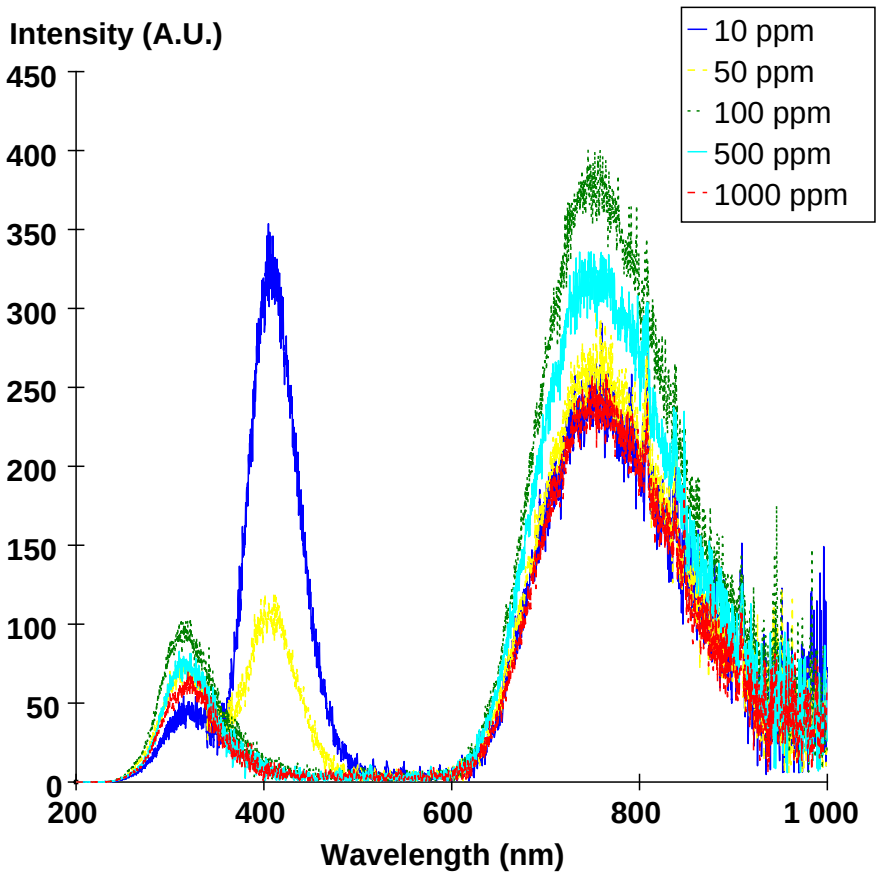

Figure 4.14: *Room temperature scintillation spectra of Ti:Al_2O_3 with Ti concentrations of 10, 50, 100, 500 and 1000 ppm.*

When we take into account only the near IR scintillation corresponding to the Ti^{3+}peak (Fig. 4.20), we can see that the best scintillator is the crystal with 100 ppm of Ti, which emits 30% more light than the one with 10 ppm.

So far, we have seen the comparison between the four crystals at both room temperature and 45 K. The conclusion is that the best scintillator is the sapphire containing 100 ppm of Ti, and that the difference between the light yield of crystals with concentrations from 10 to 500 ppm is small. The detectors in the EDELWEISS experiment work at 20 mK, so in an ideal test we should study the scintillation spectrum at this temperature. Nevertheless, in order to obtain the scintillation spectra, we need a strong source of excitation, like the X ray flux. In a dilution cryostat, the first effect of such an excitation would be the heating of the cryostat. It is therefore very difficult to imagine such a test. Therefore, we have to try to understand the behaviour of the quantity of light as a function of temperature on the temperature range where we can use the experimental

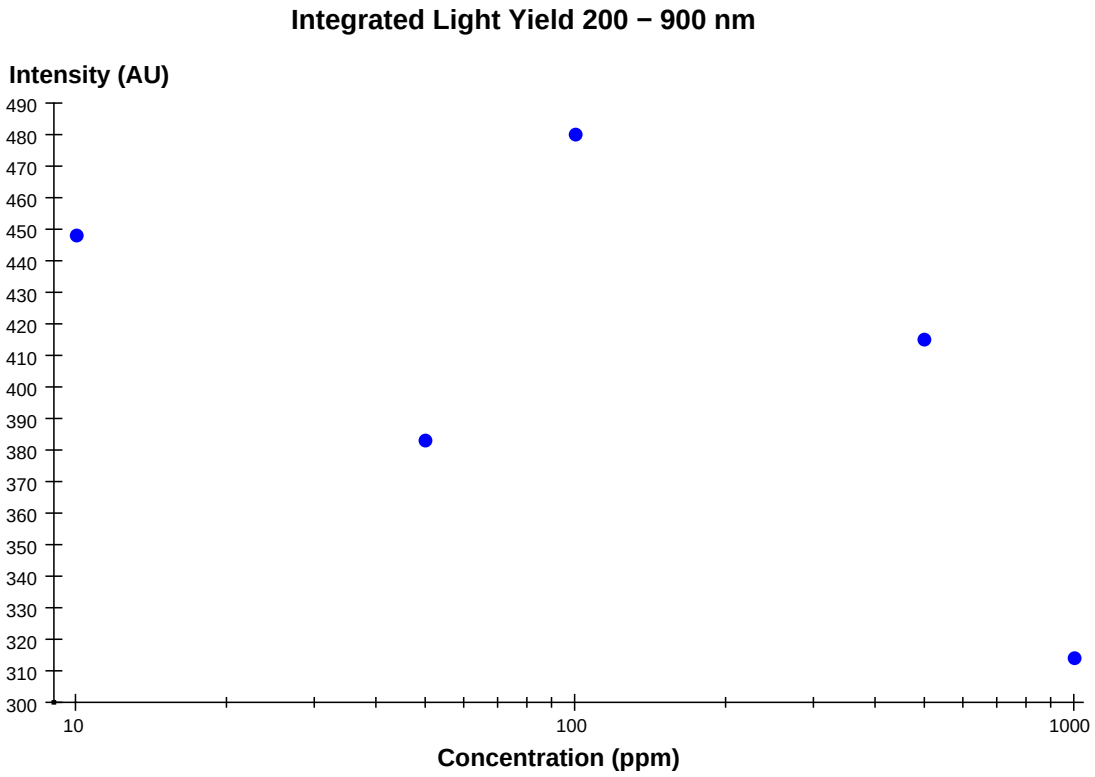

Figure 4.15: *Comparison between the room temperature light yield of crystals having different Ti concentrations on the range 200 - 900 nm. The crystal with 100 ppm of Ti has the highest light yield, while the most concentrated sample is the less efficient scintillator.*

setup and try to extrapolate this behaviour for lower temperatures.

4.4.7 Evolution of Ti:Al_2O_3 scintillation properties

Fig. 4.21 is showing the evolution of the light yield of the four Ti:Al_2O_3 crystals on the range 200 - 900 nm, at several temperatures between 45 and 300 K. The light yield of each crystal has been normalized to the room temperature scintillation. The first measure is done at room temperature, then the crystal is cooled down to the base temperature of the cryostat (about 30 K) and the intermediate points are measured when warming up the cryostat.

We can see that the overall increase in the total light yield is compatible with a factor of two, the exact value depending on the crystal. The behaviour reported for more concentrated samples (Mikhailik 2005) is that the total light yield increases down to a temperature of about 150 K and remains practically constant between 150 and 45 K. This is consistent with what is seen for the 500 ppm crystal. The less concentrated samples

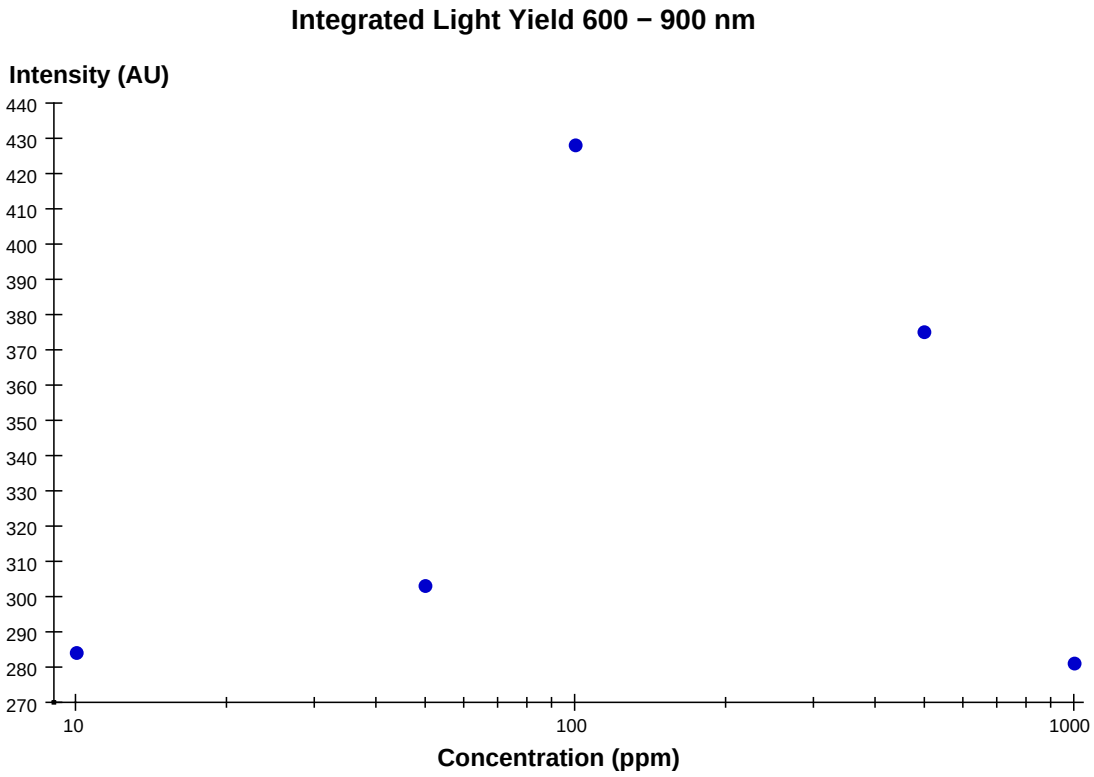

Figure 4.16: *Comparison between the room temperature light yield of crystals having different Ti concentrations on the range 600 - 900 nm. The crystal with 100 ppm of Ti remains the most efficient scintillator.*

(10 and 50 ppm) appear to have a light yield that keeps increasing with a slight slope even at lower temperatures for both the 200 - 900 and 600 - 900 nm range (Fig. 4.22).

The less concentrated samples are also the ones improving their scintillation efficiency the most between room temperature and 45 K. Some of the crystals have a particular behaviour around 100 K, with a sudden increase in the light yield when warming up the crystal. This effect is enhanced for the 50 ppm crystal. This kind of effect can be explained by the presence of metastable levels in the forbidden band that play the role of traps for charge carriers. These traps are filled when the crystal is exposed to X ray radiation at low temperature. For the electron at the metastable level to be able to recombine with a hole it should first be transfered to the conduction band. The energy needed for the transfer can come from different sources: an electric field, infrared light or from warming up the crystal. The *thermoluminescence* is the property of certain crystals of emitting light when they are heated if they have beeen previously exposed to a natural or artificial source of radiation.

In order to test this effect, the crystal is cooled down to 10 K and then heated up

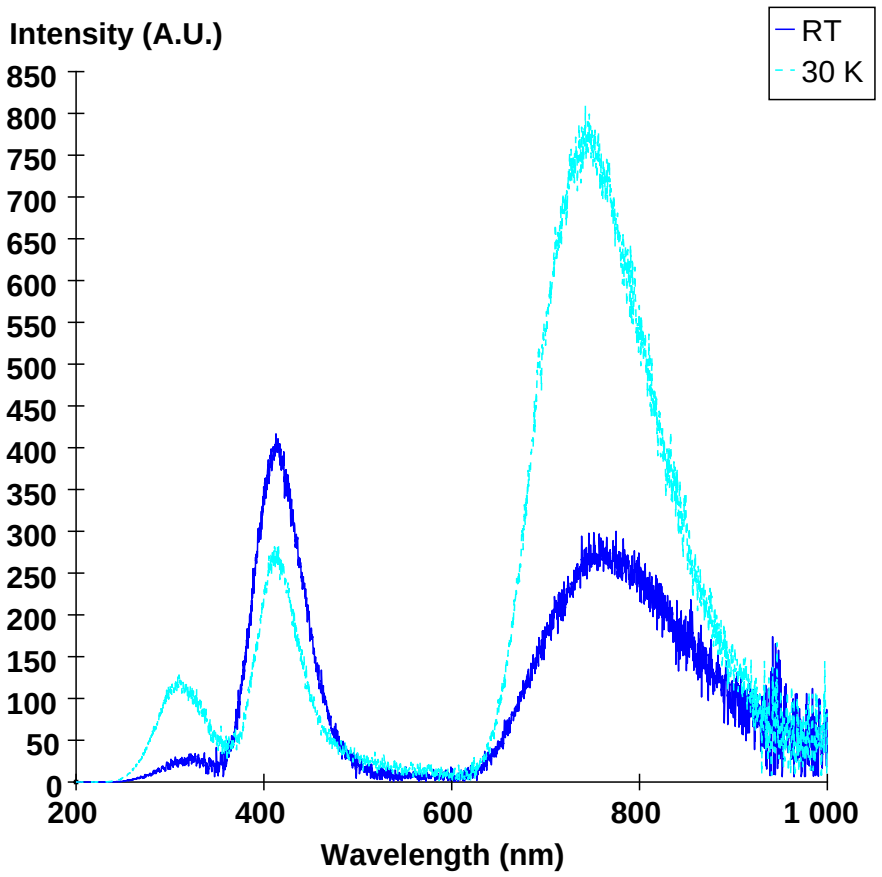

Figure 4.17: *Scintillation spectrum of a Ti:Al_2O_3 crystal with a Ti concentration of 10 ppm between the room temperature (RT) and 30 K. We can see that there is an increase in the total light yield.*

while measuring the light yield at each temperature with a photomultiplier. Fig. 4.23 shows the thermoluminescence spectrum of the 50 ppm sample. We can see that there are several emission peaks between 50 and 100 K, with the dominant one at 100 K. This helps explaining the evolution of the quantity of emitted light as a function of temperature shown in Fig. 4.22. There are electrons trapped in the forbidden band beneath the Ti^{3+}level. At 100 K, these electrons obtain enough energy to get to the Ti^{3+}level and then fall back into the valence band through light emission. This effect explains the increase in the intensity of light between 80 and 100 K.

A systematic study of four Ti:Al_2O_3 crystals with Ti concentrations of 10, 50, 100 and 500 ppm showed that this range of concentrations is interesting from the point of view of the light yield for temperatures between 30 and 300 K. All crystals gain a factor of about two between the quantity of light emitted at room temperature and 30 K. While for

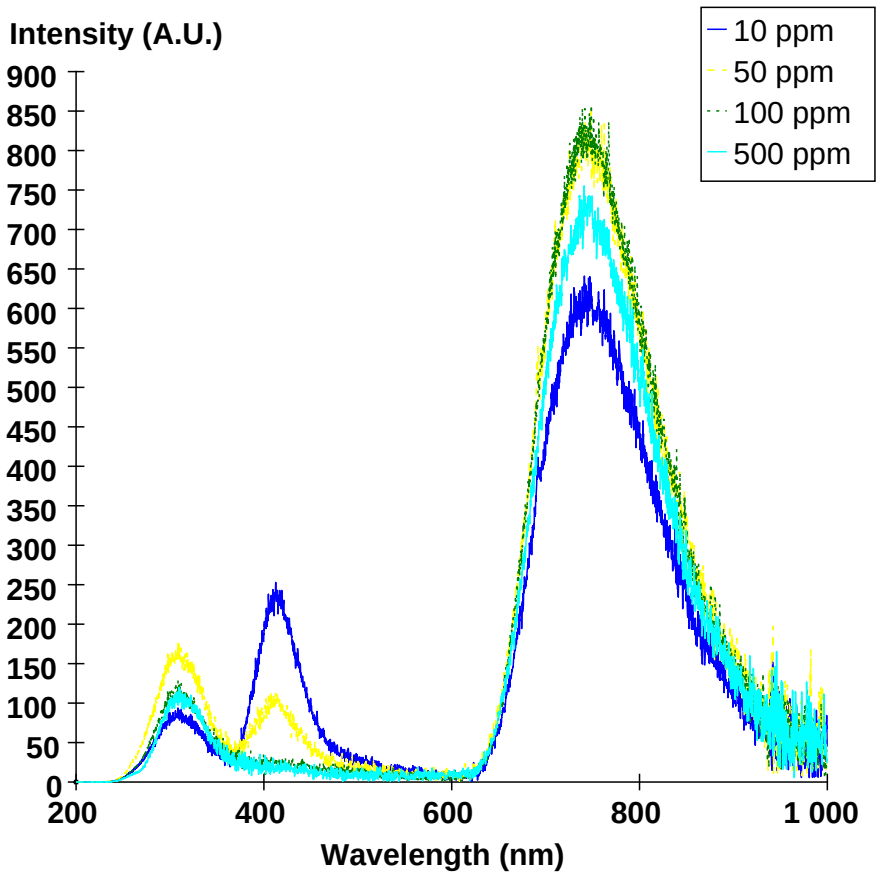

Figure 4.18: *Scintillation spectra of Ti:Al_2O_3 crystals with a Ti concentration of 10, 50, 100 and 500 ppm at 45 K.*

the most concentrated samples the quantity of light seems stable between 80 and 30 K, for the less concentrated, the light yield keeps increasing slightly, making it difficult to predict the exact behaviour at lower temperature. Nevertheless, taking into account the behaviour on the range 300 - 30 K, it is a reasonable assumption to consider that the quantity of light will have at least the value measured at 30 K, which is encouraging for future lower temperature tests.

Up to now, we have considered that the quantity of Ti indicated by the manufacturer corresponded to the actual Ti^{3+}concentration. This is not necessarily the case for all crystals, especially when the manufacturer does not guarantee the oxidation state of Ti in the crystal. We have also seen that even crystals that are sold as nominally pure can scintillate as a consequence of the presence of Ti in the lattice. This leads to the conclusion that in order to completely characterize a crystal and explain its scintillation properties, one needs a method to quantify the presence of impurities. In the following

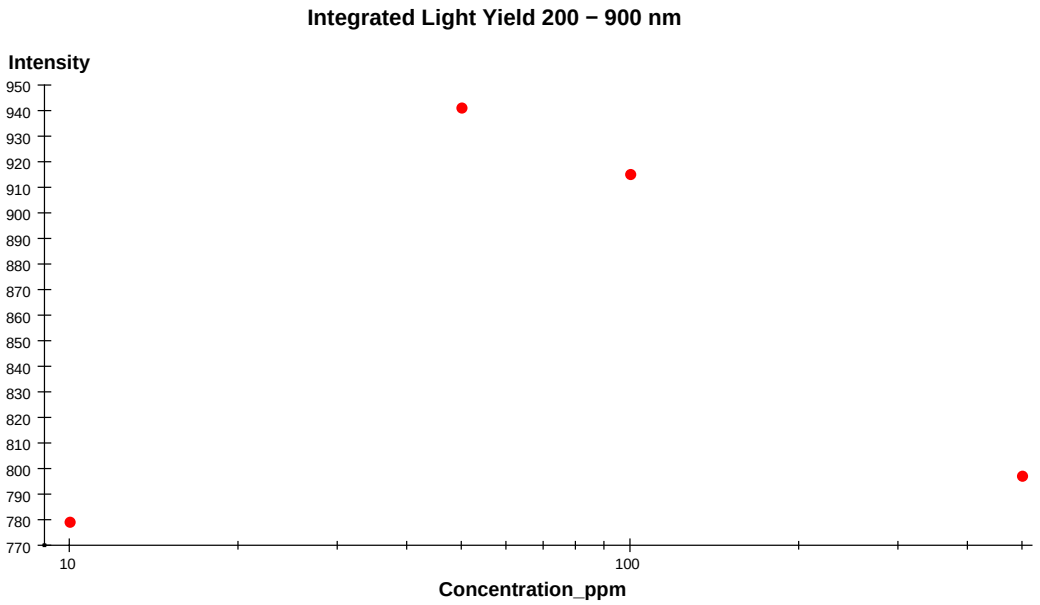

Figure 4.19: *Comparison between the light yield of crystals with 10, 50, 100 and 500 ppm of Ti at 45 K on the range 200 - 900 nm.*

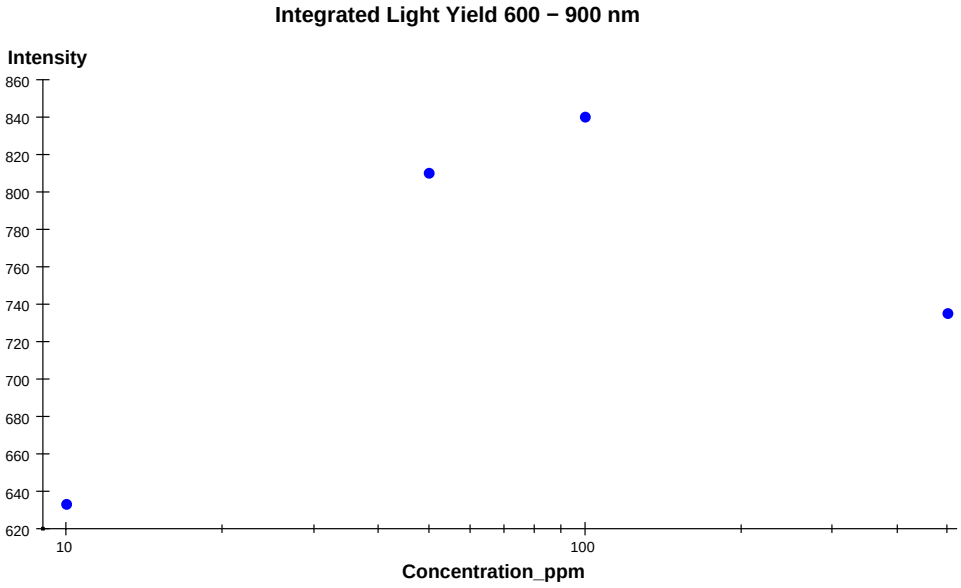

Figure 4.20: *Comparison between the light yield of crystals with 10, 50, 100 and 500 ppm of Ti at 45 K on the range 600 - 900 nm. The light yield remains practically constant for Ti concentrations between 50 and 100 ppm.*

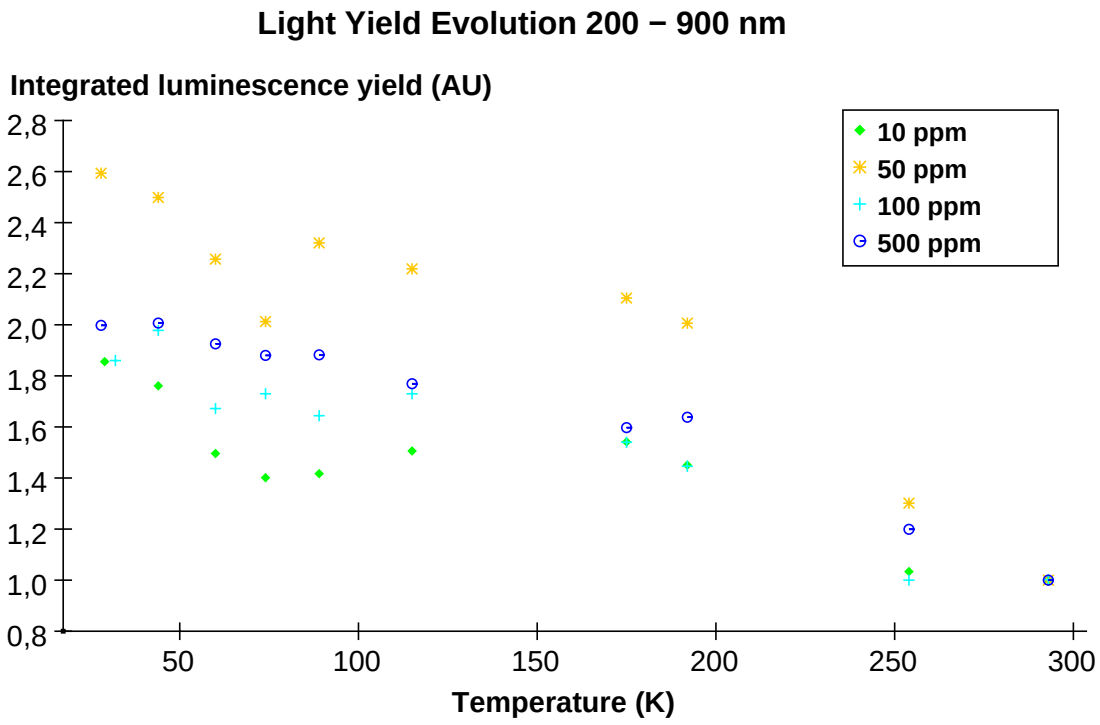

Figure 4.21: *Evolution of the light yield of crystals with 10, 50, 100 and 500 ppm of Ti between room temperature and 45 K on the range 200 - 900 nm. The quantity of light of each crystal is normalized to the room temperature intensity. There is an increase compatible with an average factor of two when decreasing the temperature.*

sections, I will present two optical methods that help getting additional information on the structure of a crystal: optical absorption and fluorescence.

4.5 Optical absorption

4.5.1 Experimental setup

The typical setup for optical absorption tests is shown in Fig. 4.24.

The initial light beam separates in two beams of the same intensity which pass through two identical slits. The sample to be measured is fixed behind one of the slits. By measuring the intensity of the two light beams, we can establish the doping concentration of the crystal using the Lambert-Beer equation:

$$I = I_0 exp[-cAl] \tag{4.3}$$

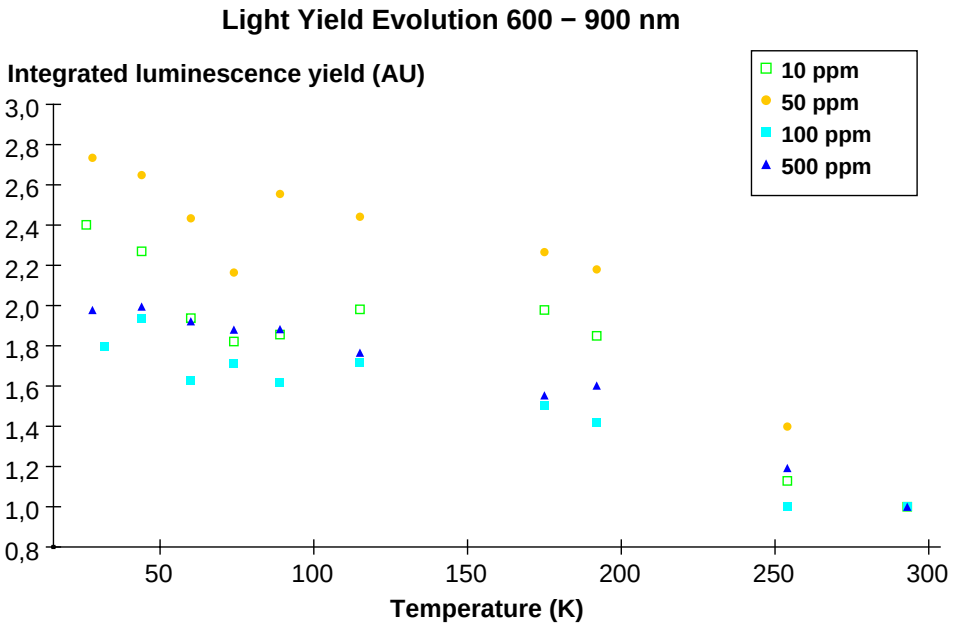

Figure 4.22: *Evolution of the light yield of crystals with 10, 50, 100 and 500 ppm of Ti between room temperature and 45 K on the range 600 - 900 nm.*

where I is the intensity of the beam, c the doping concentration, A the coefficient of absorption of the impurity and l the length of the optical path. What we usually measure is the absorbance, i.e. $-log_{10}(I/I_0)$. This leads to:

$$log_{10}\frac{I_0}{I} = cAl \cdot log_{10}e \tag{4.4}$$

The coefficient of absorption of each impurity can be found in the literature and the crystal length is known, so we can calculate the doping concentration. It is also useful to notice that there is a linear dependence between the absorbance and the crystal concentration. Therefore, we can easily check the doping concentration in several crystals by plotting the absorbance against concentration, using a few reference points which are in accordance with values given in literature. This kind of plot is useful for finding unknown concentrations in new samples, without having to calculate them systematically.

The method can be used for both room temperature and low temperature tests, with an optical cryostat. I have performed the room temperature tests using an experimental setup belonging to the LPCML and the low temperature tests in collaboration with the CRESST group at the Oxford University. The two setups being similar, I will only describe the Oxford experimental setup, the main difference being the presence of an optical cryostat for low temperature tests. In order to measure the absorption, I used a

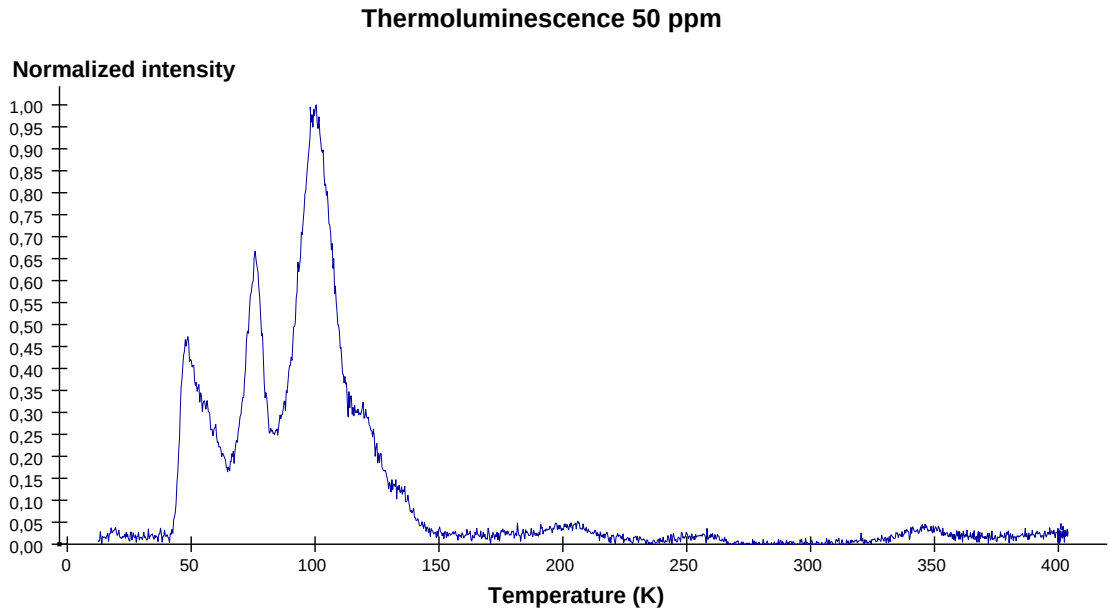

Figure 4.23: *Thermoluminescence spectrum of a Ti:Al_2O_3 crystal with 50 ppm of Ti. The presence of an important peak at a temperature of about 100 K explains an enhanced light yield measured at this temperature under X ray excitation.*

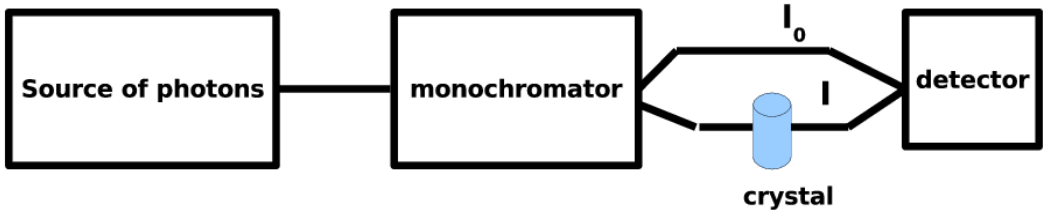

Figure 4.24: *Typical setup for absorption tests. The ratio between the intensity of the light crossing the crystal and the intensity of the light having the same optical path through air leads to the absorption coefficient of the crystal*

Perkin-Elmer Lambda 9 spectrophotometer and an exchange gas optical cryostat. The optical absorption can be determined in the range 200 - 3200 nm. This corresponds to three partial spectral ranges: UV from 185 to 319 nm, VIS from 319 to 860 nm and NIR from 860 nm. The light sources are a deuterium lamp for the UV range and a tungsten-halogen lamp for VIS and NIR ranges. The detectors are also different according to the wavelengths: a side window photomultiplier is used for the UV/VIS ranges and a PbS detector for the NIR range. Both the source and the detector change automatically during the measurement cycle. For each of the two light beams, the wavelengths

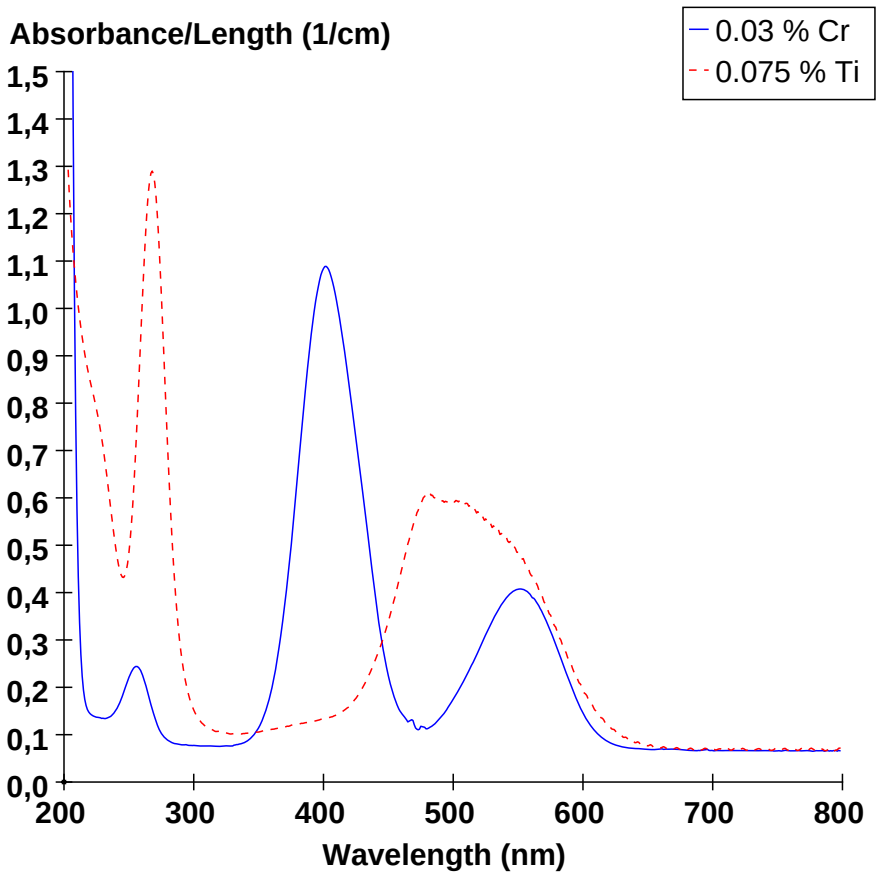

Figure 4.25: *Absorption spectra of two sapphire crystals, one doped with 0.03 wt % Cr and the other with 0.075 wt % Ti. Ti^{3+} absorption is characterized by a large band between 400 and 600 nm and Cr^{3+} absorption by three bands, at 250, 400 and 550 nm.*

are separated by a monochromator. Each monochromator has two gratings, one for UV/VIS and the other one for the NIR. Filters allow avoiding multiple order diffraction. There is a filter wheel, driven by a stepping motor to be in synchronization with the monochromators. Filter change is automatic at 2620, 1670, 1190, 810, 690, 562, 379 nm. The range of interest for sapphire crystals doped with Cr or Ti is 200 - 800 nm.

4.5.2 Room temperature absorption

We have seen in the previous section that the main two impurities with effects on the scintillation spectrum of a sapphire crystal are Cr and Ti. Fig. 4.25 is showing the absorption spectrum of two sapphire crystals, one doped with 0.03 wt % Cr and the other one with 0.075 wt % Ti.

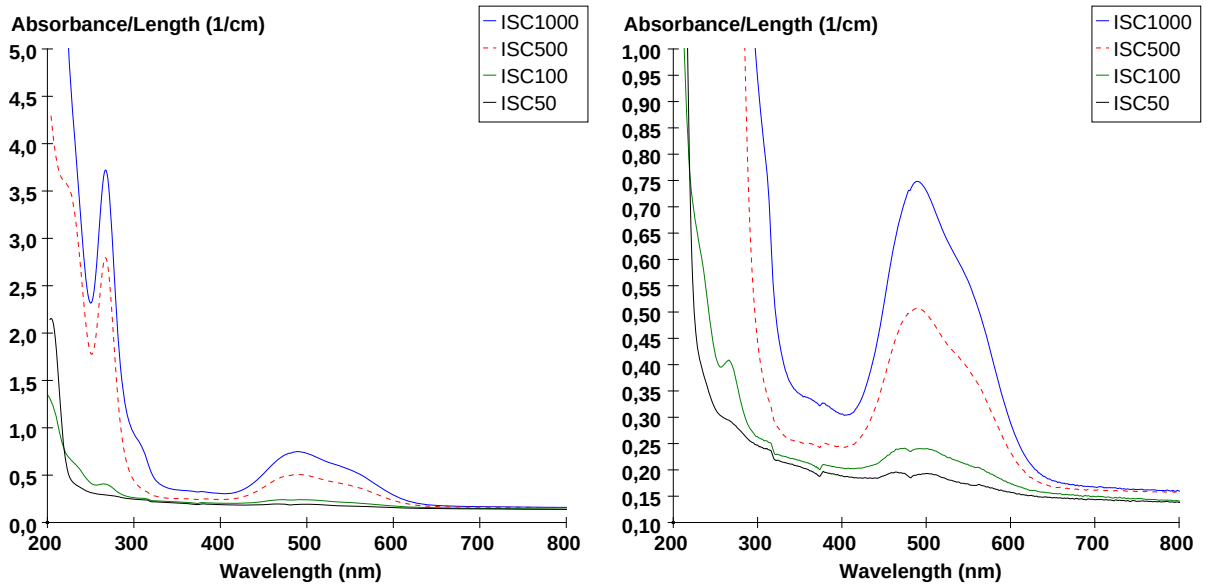

Figure 4.26: *Absorption spectra of Ti:Al_2O_3 with Ti concentrations of 1000, 500, 100 and 50 ppm. We can see that the minimum concentration we can measure with this method is 100 ppm.*

The absorption spectrum of $Ti^{3+}$is characterized by a large band between 400 and 600 nm (Lupei 1986). The crystal also shows a band at 266 nm and a shoulder at 220 nm. The 266 nm band is assigned to a bound excited state of Ti^{3+}, while the 220 nm shoulder is attributed to the presence of Ti^{4+}, being caused by the charge transfer in the O-Ti^{4+} pair (Wong 1995). Cr:Al_2O_3 has three absorption peaks at 250, 400 and 550 nm (Maiman 1961).

Using the optical absorption, I have tested five sapphire crystals with Ti concentrations of 1000, 500, 100, 50 and 10 ppm, corresponding to the five crystals tested with the X rays. All crystals are 20 x 10 x 5 mm^3 bricks. The room temperature spectra are shown in Fig. 4.26.

The method works well for finding the Ti concentration in the two crystals with 1000 and 500 ppm. The spectrum shows that it is difficult to distinguish the absorption peak of the 50 ppm crystal from the noise, 100 ppm being the lowest limit of detection. The next step is to check whether the three crystals have the Ti^{3+}concentration indicated by the manufacturer. Fig. 4.27 is showing the linear absorbance plotted against the Ti concentration for the crystals with 100, 500, 1000 ppm and another crystal with 750 ppm of Ti coming from a different manufacturer. The 750 ppm crystal is used as a reference, as its spectrum is in accordance with the absorption coefficient indicated in literature (Lupei 1986). The intensity of absorption is normalized for crystal length in order to compare crystals that may have a different size and is calculated by subtracting

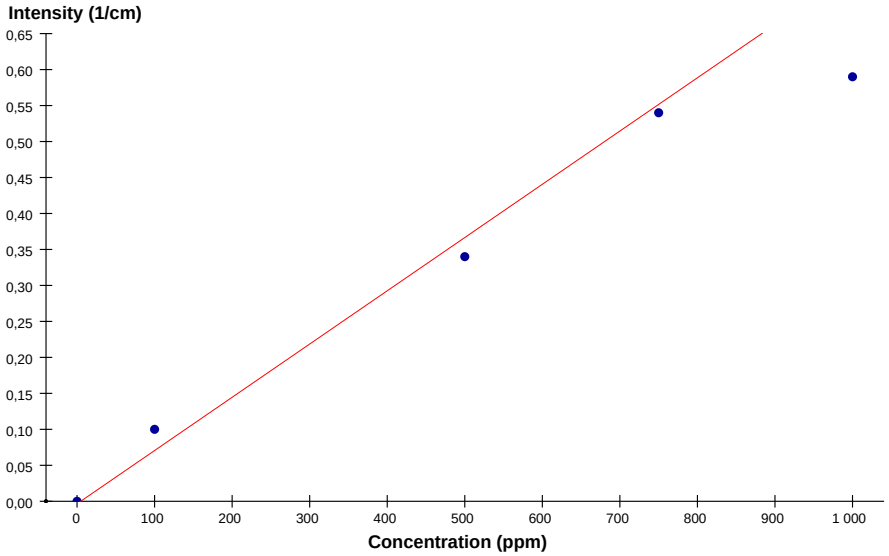

Figure 4.27: *Dependance of the intensity of the absorption peak on the Ti concentration.*

the value of the absorbance at 800 nm to the highest value of the Ti absorption band. According to the spectra in literature, there is no Ti^{3+}absorption at 800 nm, the reason why this value may be different from zero is due to crystal geometry and the fact that the two faces crossed by the light beam can not be perfectly parallel. Therefore this value corresponding to geometry losses needs to be subtracted in order to find the absolute value of Ti absorbance.

We can see that there is a linear dependance on the concentration range considered for the crystals with 100, 500 and 750 ppm, while the crystal with a nominal Ti concentration of 1000 ppm seems to contain less Ti than estimated by the manufacturer.

Another interesting feature is the study of the effect that the growth redox potential has on the Ti^{3+}concentration. In order to do this study, I have used three crystals of the size 5 x 5 x 1 mm^3 with a Ti concentration of 1000 ppm, grown in three different redox potentials: -230 kJ/mol, -30 kJ/mol, 120 kJ/mol. Fig. 4.28 is showing the three absorption spectra on the range 200 - 800 nm.

We can see that the shape of the absorption spectra depends strongly on the potential. The standard growth potential is -230 kJ/mol; crystals grown in this potential have between 98 and 100% of the Ti in the form Ti^{3+}. With a potential of -30 kJ/mol, 80% of the amount of Ti is kept as Ti^{3+}, which explains the decrease of the Ti^{3+}absorption band. It is also interesting to notice that the 266 nm band decreases with the decrease of the Ti^{3+}peak. This is an indication that this absorption is in close relation with the presence of Ti^{3+}in the crystals. In the same time, the absorption at lower wavelengths

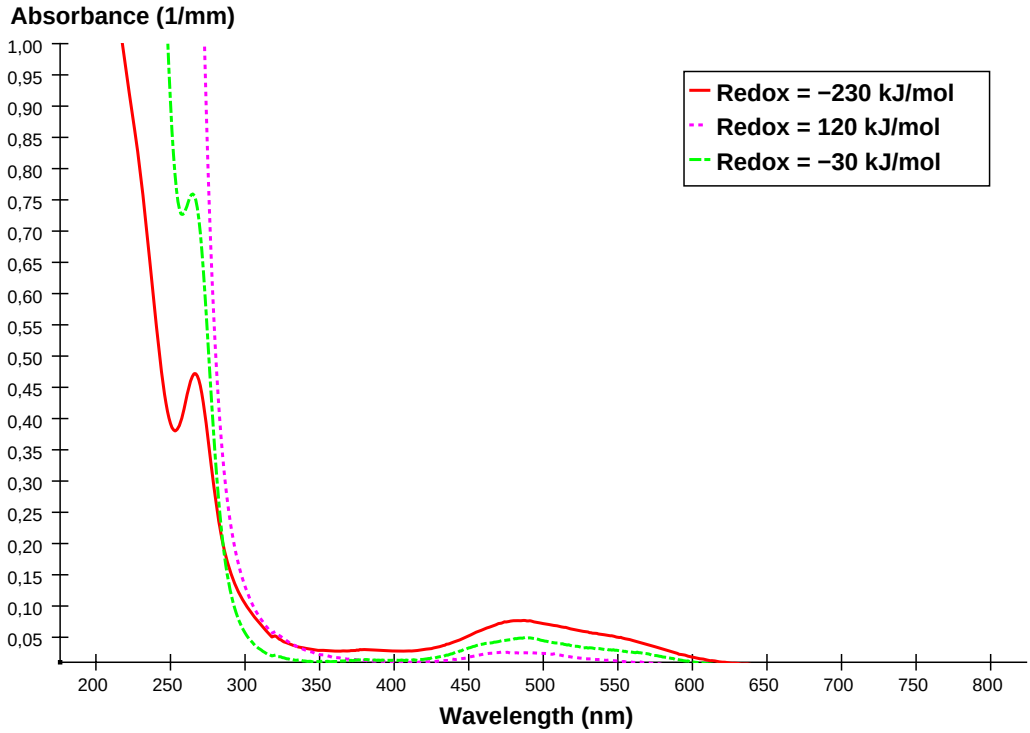

Figure 4.28: *Absorption spectra of Ti:Al_2O_3 crystals with 1000 ppm of Ti grown in different redox potentials: -230 kJ/mol, 120 kJ/mol, -30 kJ/mol. The quantity of Ti^{3+} in the crystals is found to depend strongly on the redox potential: while all Ti is found as Ti^{3+} in standard crystals, only 80% has this oxidation state when the crystal is obtained at -30 kJ/mol, and the concentration is reduced to 20% for the crystal grown at 120 kJ/mol.*

is enhanced. If 20% of the Ti concentration is not found as Ti^{3+}, it is likely that its oxidation state is 4+. This supports the attribution of the low wavelength absorption to the presence of Ti^{4+}. The effect is enhanced for a redox potential of 120 kJ/mol, where only 20% of the initial Ti is found as Ti^{3+}. This crystal is not transparent between 200 and 300 nm. This information is important for building windows with good transmission in the UV range.

4.5.3 Low temperature absorption

After having seen the room temperature absorption spectra and established the detection limits of our method, we can check whether there are changes in the absorption spectra at low temperature. Fig. 4.29 is showing the comparison between the room temperature and the low temperature absorption spectra of two crystals containing

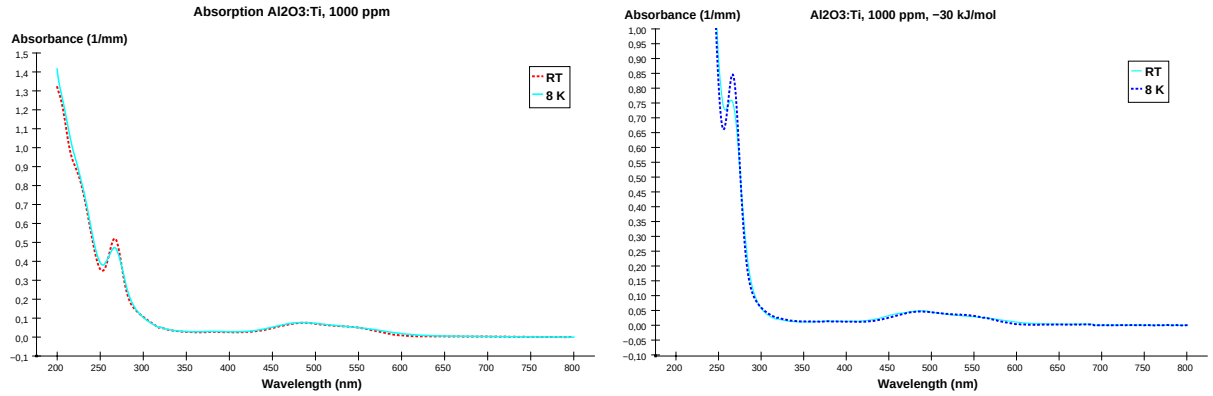

Figure 4.29: *Comparison between the room temperature and the 8 K absorption spectra of Ti:Al_2O_3 with Ti concentrations of 1000 ppm grown in a standard redox potential of -230 kJ/mol (left) and in a redox potential of -30 kJ/mol (right). The absorption band at 266 nm is hardly sensitive to temperature change for the standard crystal but increases significantly for the crystal grown at -30 kJ/mol.*

1000 ppm of Ti, one standard grown (-230 kJ/mol) and the other with a redox potential of -30 kJ/mol.

For the two crystals, the Ti^{3+}absorption band does not seem sensitive to temperature change. The 266 nm band has low dependence on the value of the temperature for the standard grown samples, but increases a lot between the room temperature and 8 K for the sample grown at -30 kJ/mol. Since there is little change with temperature for the standard crystals, this confirms that the 266 nm peak is in close correlation with the presence of Ti^{3+}. Nevertheless, its behaviour in differently grown crystals suggests that $Ti^{3+}$is not the only coloured center associated with this absorption and that it is correlated with other defects in the lattice.

We have seen in this chapter that the optical absorption allows determining the Ti concentration in crystals down to about 100 ppm. Among the crystals tested, we have found the same concentration as indicated by the manufacturer for the crystals with 100 and 500 ppm of Ti, while for the 1000 ppm sample, the concentration seems lower. The method is also sensitive to the oxidation state of the impurity and proves that the redox potential in which the sample has been grown determines whether all Ti is found as Ti^{3+}. The potential that insures a maximum Ti^{3+}concentration is -230 kJ/mol and should therefore be used in order to obtain crystals with a maximum near IR scintillation. As the optical absorption is not sensitive beneath 100 ppm and since one of the samples was found to have less Ti than indicated by the manufacturer, it is important to have at least one other optical method used for determining impurity concentration in crystals. This method is the fluorescence.

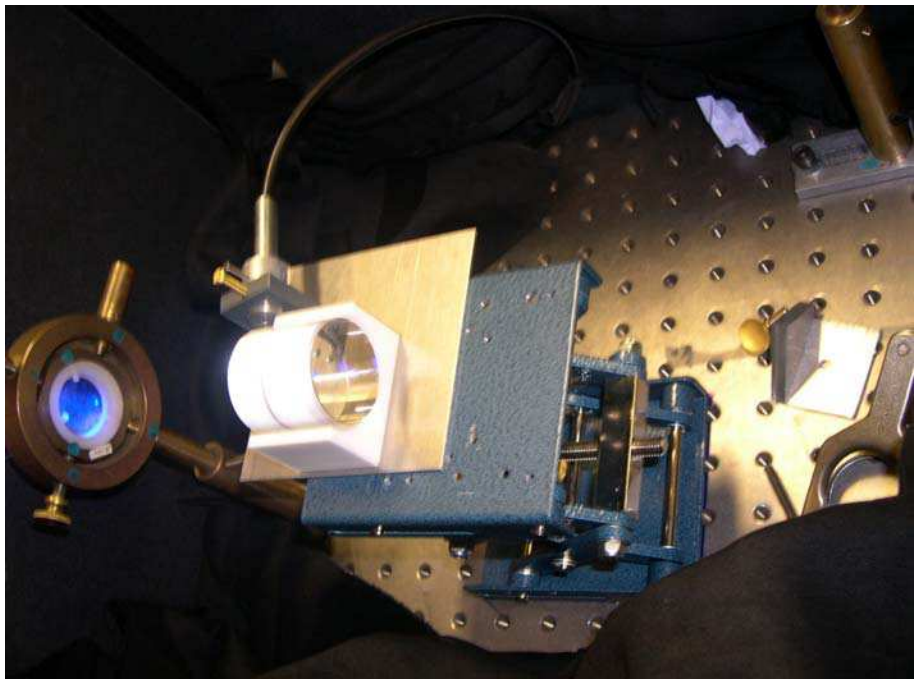

Figure 4.30: *Experimental setup for fluorescence tests. A 40 x 40 mm^3 sapphire crystal is excited with a beam of visible light.*

4.6 Fluorescence

The fluorescence is a method of spectroscopic characterization in which specific impurities are excited by visible light with a wavelength chosen in the absorption band of the impurity. All the fluorescence tests have been done at LPCML Lyon. The experimental setup is shown in Fig. 4.30.

The reading system is the same as for X ray scintillation. Crystal excitation is done with a Xenon lamp of 450 W coupled to a HD10 Jobin-Yvon Monochromator. The crystal is put in a teflon holder that keeps all samples in a fixed geometry. The teflon does not completely cover the samples in order to avoid reflection of the incident light that may saturate the reading system. Unlike X ray tests, this method of directly exciting each impurity with light of a wavelength in the absorption band of the dopant has the advantage of giving a response which is proportional to the doping concentration. In the case of the X ray excitation, an important amount of energy is transferred to the lattice which creates electrons, holes and defects in the lattice, the process is more complex so the quantity of light is not necessarily proportional to the doping concentration. In order to compare the light yield of different samples, they need to have the same size, shape and surface polishing.

We have seen in the previous sections that the main impurities having an important

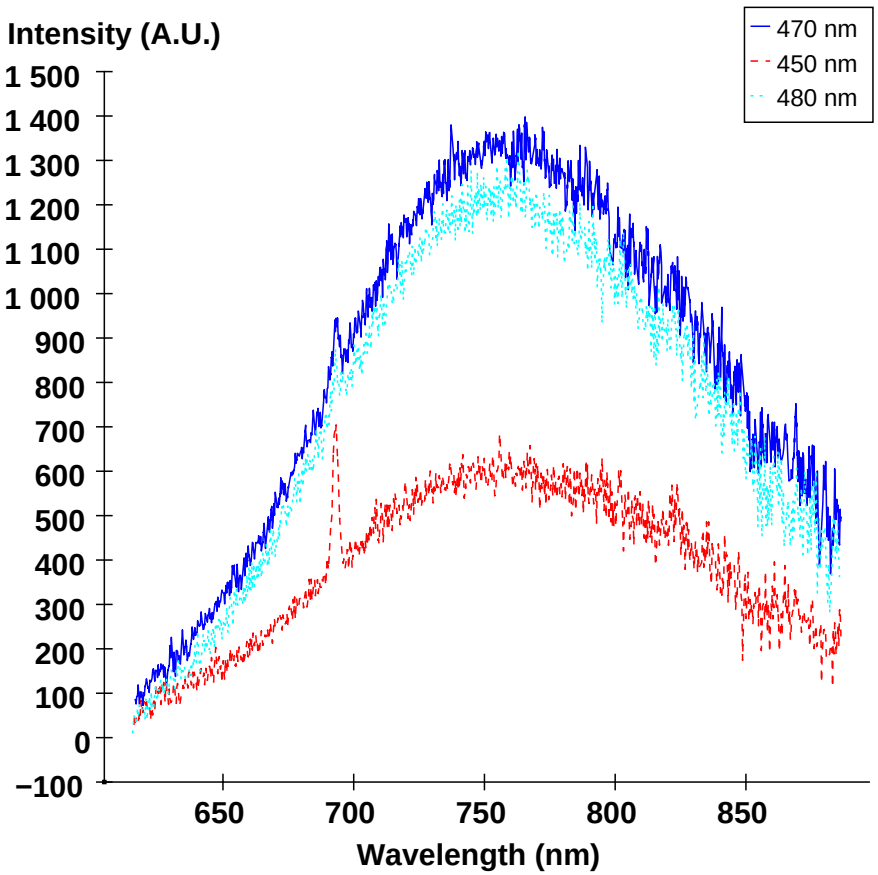

Figure 4.31: *Fluorescence tests performed on a nominally pure sapphire crystal with traces of Cr and Ti. By chosing several excitation wavelengths in the absorption band of Ti, we can see that the wavelength for a maximum Ti and a minimum Cr light emission is 470 nm.*

effect on sapphire scintillation are $Cr^{3+}$and Ti^{3+}. The absorption band of Ti lies between 400 and 600 nm, while Cr has two main absorption peaks at 410 and 565 nm (Fig. 4.25). In a crystal containing both Cr and Ti, the difficulty is to excite one type of impurity without exciting the other one, as the absorption bands overlap. Therefore, the first step when doing fluorescence tests is to find the optimum wavelength in the absorption band of Cr or Ti. Fig. 4.31 is showing fluorescence tests on a nominally pure sapphire crystal that shows both traces of Ti and Cr done in order to optimize the wavelength needed for Ti excitation.

We can see that the wavelength where there is a maximum Ti and a minimum Cr light emission is 470 nm. This result is coherent with the optical absorption spectrum which shows that 470 nm corresponds to an important intensity of the Ti band being situated between the two Cr absorption peaks.

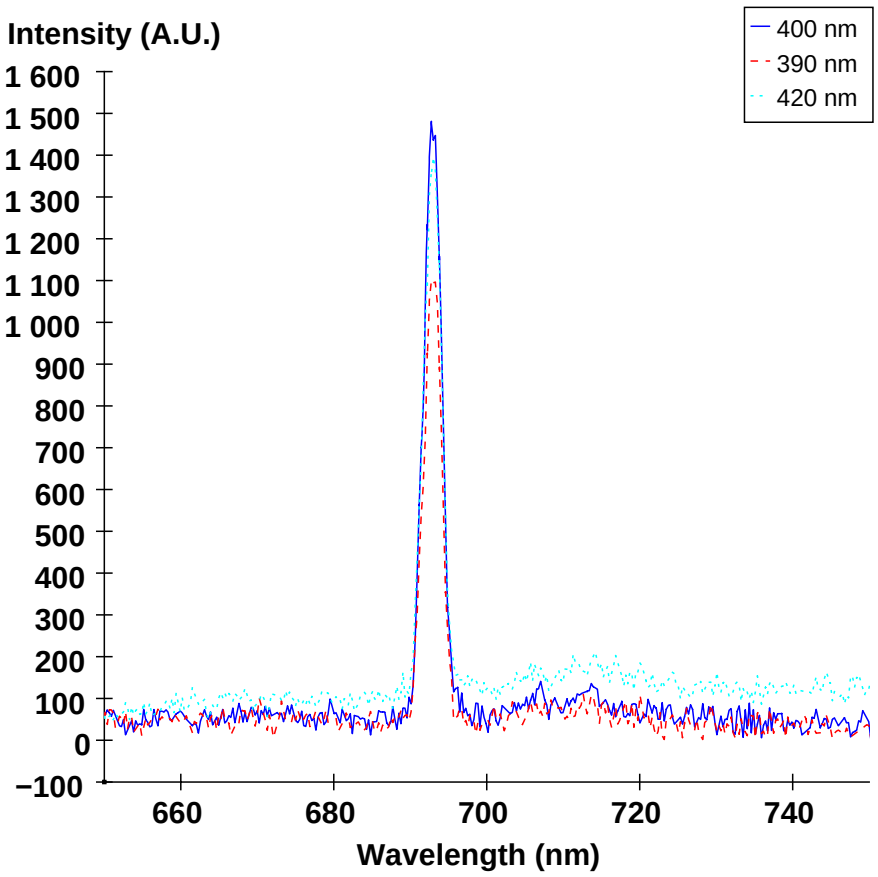

Figure 4.32: *Fluorescence tests performed on a nominally pure sapphire crystal with traces of Cr and Ti in order to optimize the Cr excitation wavelength. Results show 400 nm is a convenient wavelength for Cr excitation.*

Since the Ti absorption band is situated between 400 and 600 nm, a good choice for Cr excitation seems to be a wavelength beneath these values. Fig. 4.32 shows the tests performed on the same crystal in order to optimize the Cr excitation wavelegth.

A wavelength of 390 nm or 400 nm is useful for exciting Cr without Ti, while we can notice that at 420 nm both Cr and Ti scintillate. Since the sapphire crystal emits more light when the incoming light beam is at 400 nm, this wavelength has been chosen as optimum for Cr excitation.

The fluorescence can be very useful for the characterization of nominally pure sapphire crystals since it is sensitive even to ppm level impurity concentrations. Fig. 4.10 shows that two nominally pure sapphire crystals can have different scintillation spectra under the X rays. I have tested the same two crystals using the fluorescence method (Fig. 4.33).

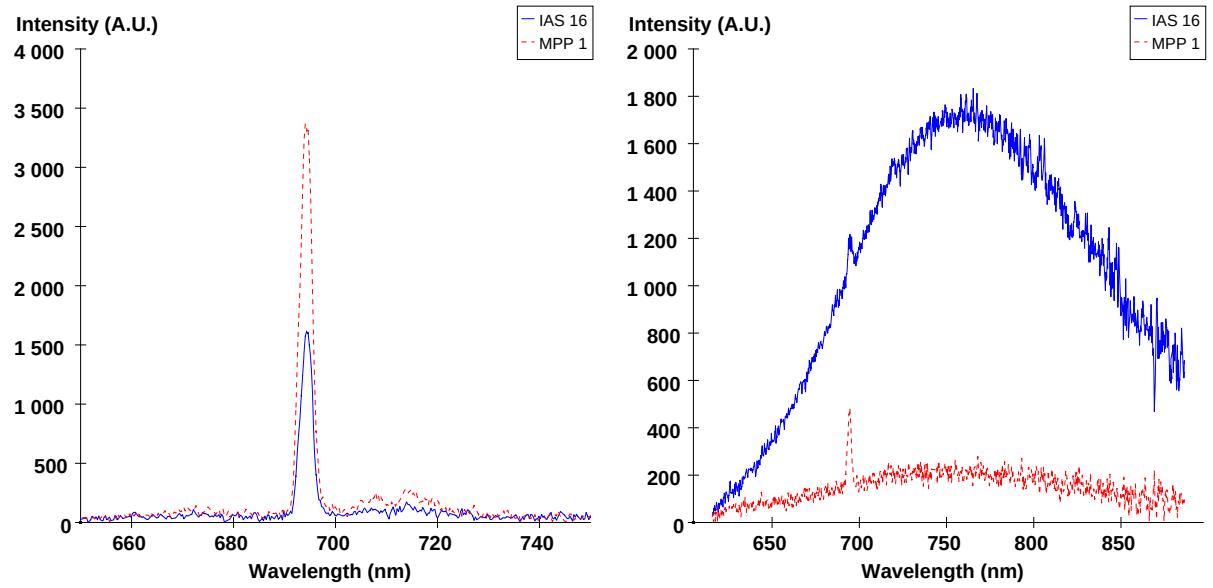

Figure 4.33: *Comparison between the fluorescence spectra of two nominally pure sapphire crystals. Cr^{3+} is excited with 400 nm light (left) and Ti^{3+} with 470 nm light (right). The spectra show that there is 2 times more Cr in MPP1, while IAS16 contains 8 times more Ti. This difference in concentration explains the different scintillation spectra measured under X ray excitation.*

Ti and Cr have been excited with the optimum wavelengths found previously: 400 nm for Cr and 470 nm for Ti. The spectra show that MPP1 has about twice more Cr than IAS16, while IAS16 contains about eight times more Ti. This difference in concentration explains the difference of scintillation spectra obtained under the X ray flux, where IAS16 mainly showed a Ti^{3+} light emission with a small Cr^{3+} peak and MPP1 had a dominant Cr^{3+} line. This test shows that fluorescence can succesfully explain scintillation properties of sapphire crystals with very small concentrations of Cr or Ti.

I have used fluorescence in order to check Ti concentration in the five Ti:Al_2O_3 crystals with nominally 10, 50, 100, 500 and 1000 ppm of Ti. Fig. 4.34 shows the emission spectra of the five crystals when the wavelength of excitation is 470 nm.

The spectra prove that the quantity of light emitted by each crystal depends on the Ti concentration indicated by the manufacturer. In order to check if the dependence is linear, it is necessary to plot the integrated quantity of light versus the Ti concentration (Fig. 4.35).

We can see that the dependence is linear for Ti concentrations between 10 and 500 ppm, while the 1000 ppm crystal appears to have less Ti than indicated by the manufacturer. These results confirm those obtained using the optical absorption, extending the range of sensitivity down to 10 ppm. The importance of this test is two fold: it is a way of

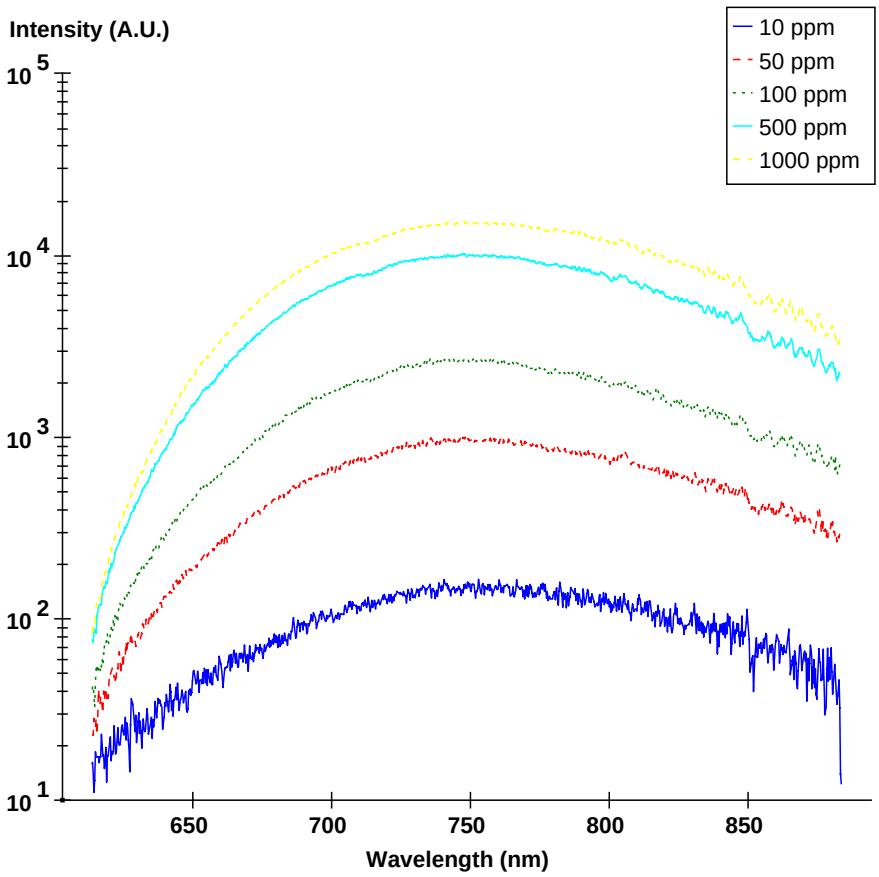

Figure 4.34: *Fluorescence spectra of Ti:Al_2O_3 with a nominal Ti concentration of 10, 50, 100, 500 and 1000 ppm. The wavelength of the excitation light is 470 nm. The spectra prove that the quantity of light emitted by the crystal depends on Ti concentration.*

checking the concentrations indicated by the manufacturer and it also confirms that the method works well for finding unknown weak doping concentrations of other crystals by comparison with crystals of known concentrations. Contrary to the optical absorption method, fluorescence can be used below 10 ppm.

Until now, we have seen how crystals can be characterized using optical methods. The most important method for determining the light emission properties of each crystal is scintillation under X ray flux. In order to find the impurity concentration in each crystal, two optical methods can be used: absorption and fluorescence. Fluorescence has the advantage of being sensitive down to ppm level concentrations, but requires crystals of the same geometry for comparison. Optical absorption gives a response that can directely be normalized to the crystal length so it can be used for comparing crystals of different sizes and shapes. Nevertheless, the threshold of sensitivity at low concen-

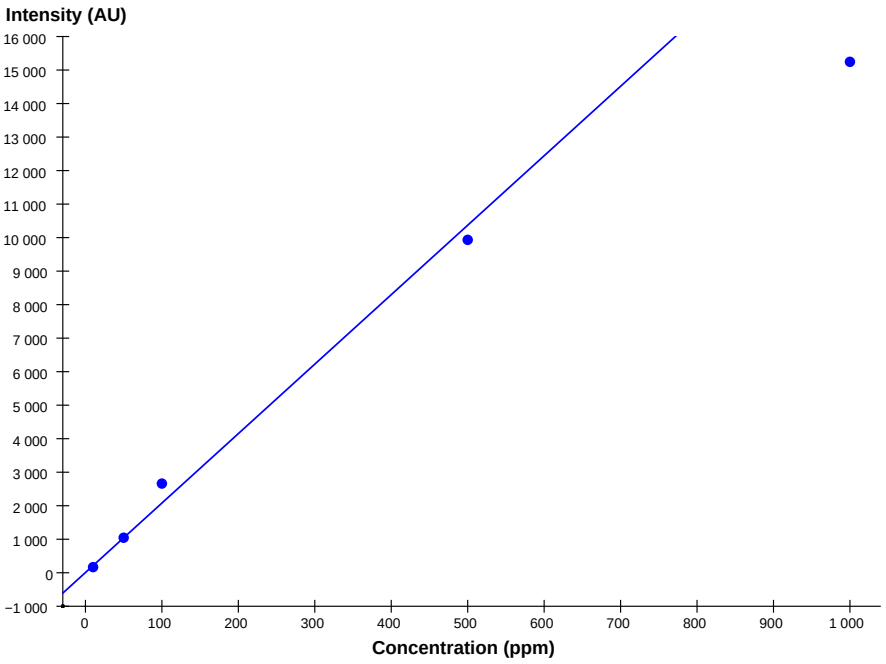

Figure 4.35: *Dependence of the fluorescence integrated light yield on the Ti concentration. There is a linear dependence between 10 and 500 ppm, while the 1000 ppm crystal appears to have less Ti than indicated by the manufacturer, confirming the results of the optical absorption tests.*

trations is about 100 times higher than for fluorescence. Both characterization methods have the advantage of being non-destructive and sensitive to the oxidation state of the crystal. Since sapphire is a material highly resistant to any chemical attack, it is very difficult to determine the impurity concentration by chemical methods. Commercially available methods that can work for this kind of materials are based on mass spectroscopy. During my thesis, I have verified the results that two of these methods can give on sapphire crystals: glow discharge mass spectrometry (GDMS) and laser ablation (LA).

4.7 Glow discharge and laser ablation mass spectrometry

The mass spectrometry is a method of finding the composition of a sample by measuring the mass-to-charge ratio of ions. The ions are removed from the sample using various techniques, then they are accelerated by an electromagnetic field, separated according to their mass before arriving on a detector. The concentration of each compound can be found thanks to the mass spectrum.

Glow discharge (GDMS) is a method of atomization of a solid sample by sputtering it in a low-pressure plasma. This way, the sputtered sample can be analysed by mass spectrometry. The plasma is contained in a discharge cell made from pure Tantalum, in order to avoid any contamination of the sample with elements from the cell. The discharge gas is high purity argon, helium, neon or krypton. The pressure within the cell is approximately 1 torr. The glow discharge is created by a potential of 1-2 kV applied between the anode (the cell body) and the cathode (the sample). This method does not suffer from the extreme matrix dependence of most sputtering techniques since most of the sample is atomized independently of the elements contained. The limit of detection for Cr and Ti in sapphire samples is 0.05 ppm and the error bars are +/- 20%. The method is applied to very small samples, typically of the order of 1 mm^3. Therefore, the result is reliable for a bigger crystal only if the entire crystal is homogenous and has the same concentration as the analysed fragment. The method is completely destructive for the analysed sample and is not sensitive to the oxidation state of the impurity.

Laser ablation (LA) is the process of removing material from a sample by irradiating it with a laser beam. The method depends on the matrix, so a previous callibration is necessary. The crystals tested with this method were up to 20 x 20 x 20 mm^3. LA is less distructive than GDMS in the sense that not the entire crystal has to be sputtered. Nevertheless, holes with a diameter of a few tens of micron are created on the surface. Testing crystal homogeneity is also easier with this method, as several holes can be made on different spots on the crystal surface. Like GDMS, the method is not sensitive to the oxidation state of the crystal.

The GDMS tests have been performed by the French company *Shiva Technology* and LA by the Mineralogy Department of the University of Würzburg. The first step in checking if these methods work well for analysing sapphire crystals is to check if results on fragments of the same crystal are the same when tested by GDMS or LA. One example is shown in Table 4.3, where three nominally pure sapphire crystals have been analysed using the two methods.

Crystal	[Cr] LA (ppm)	[Cr] GDMS (ppm)	[Ti] LA (ppm)	[Ti] GDMS (ppm)
MPP 2.2	3.09 - 3.86	0.8	6.85 - 19.2	0.69
IPNL 1.2	1.82 - 2.57	0.34	1.11 - 1.79	1.11
IAS 5.1	0.27 - 0.44	0.22	5.11 - 6.98	5.8

Table 4.3: *Nominally pure sapphire crystals analysed by LA and GDMS.*

LA has been done by measuring the Cr and Ti concentration in five different points, the table shows the range obtained for each of the two elements. We can see that while results are very similar for IAS 5.1 and for the Ti concentration in IPNL 1.2, they are

considerably different for the Ti concentration in MPP 2.2. Nevertheless, LA indicates a factor of 3 between Ti concentrations in different points, which means that the different results obtained may be caused by inhomogeneities in the sample. Therefore, the overall result is encouraging.

Taking into account that LA gives more information on the homogeneity of the sample and that it is less destructive than GDMS, I have decided to have the five Ti:Al_2O_3 crystals with nominal Ti concentrations of 10, 50, 100, 500 and 1000 ppm analysed by this method. Results are shown in Table 4.4.

Crystal	[Ti] (ppm)	[Cr] (ppm)
ISC 1000	679 - 766	$<$0.5 - 0.8
ISC 500	437 - 508	0.7 - 1.9
ISC 100	78 - 103	$<$0.5
ISC 50	24 - 36	$<$0.5 - 1.2
ISC 10	14 - 17	1.5 - 5.3

Table 4.4: *LA tests performed on Ti:Al_2O_3 with nominal Ti concentrations of 10, 50, 100, 500 and 1000 ppm. Concentrations measured by LA agree with the ones indicated by the manufacturer for most of the crystals.*

As the optical absorption and fluorescence tests indicate, the crystal with a nominal concentration of 1000 ppm appears to have less Ti. Tests also indicate a lower Ti concentration than the nominal one for the 50 ppm crystal. Nevertheless, there is a good agreement between the measured concentrations and the values indicated by the manufacturer for most of the crystals. Another interesting information is the very low Cr concentration in the five samples. This is in good agreement with the fact that no Cr line is visible in the scintillation spectra under X ray radiation.

In this chapter, I have presented several methods of characterizing scintillating crystals: light emission under X ray excitation, thermoluminescence, fluorescence, absorption, laser ablation and glow discharge mass spectrometry. During my thesis, I have used these methods in order to understand the light emission properties of sapphire crystals and define optimum growth conditions for obtaining good low temperature scintillators. The conclusion was that for low Ti concentrations, the precision of the concentration is not mandatory, which is an encouraging result for large scale reproducible manufacturing of sapphire cryogenic detectors. The spectroscopic characterization can be performed down to a temperature of 4 K. In the next chapter, we will see the behaviour of sapphire crystals at the working temperature of a cryogenic heat-scintillation detector, 20 mK.

Chapter 5

Sea Level Study of a Sapphire Heat-Scintillation Detector

Abstract

Un cristal de saphir a été testé à l'Institut Max Planck de Munich en tant que détecteur scintillation-chaleur. Des calibrations gamma et neutron ont testé le comportement du détecteur dans un montage de type CRESST. Les résultats montrent que le saphir pourrait être intégré comme détecteur dans l'expérience de recherche directe de matière noire CRESST.

5.1 A heat-scintillation detector

In the previous chapter it has been shown how scintillating crystals can be characterized at room temperature and down to 4 K using optical methods. In this kind of setup an optical detector is sensitive to the number of photons emitted by the crystals under certain sources of excitation. However, this kind of method can no longer be used at temperatures of the order of 20 mK, which are typical for dark matter searches. At very low temperatures, the light detector is usually a bolometer, sensitive to the energy of the incoming photons; the absorption of the scintillation light increasing its temperature.

During my thesis, I have participated in the tests performed on a nominally pure sapphire crystal, in a CRESST-like setup at the Max Planck Institut für Physik in Munich (MPP). The purpose of the test was to measure the light yield (the fraction of energy of the interacting particle collected in the light detector) and to characterize the general behaviour of this crystal as a heat-scintillation detector. The functioning of a heat-scintillation detector in the CRESST setup is illustrated in Fig. 5.1.

A particle interacting with the target creates two signals: heat and scintillation. In the CRESST experiment, the elevation of temperature is measured with a tungsten superconducting phase transition thermometer consisting of a thin tungsten film evaporated on the surface of the crystal. The thermometers are stabilized in the transition from the normal to the superconducting phase where a small increase in temperature creates an important increase in the resistance of the film, which makes it a very sensi-

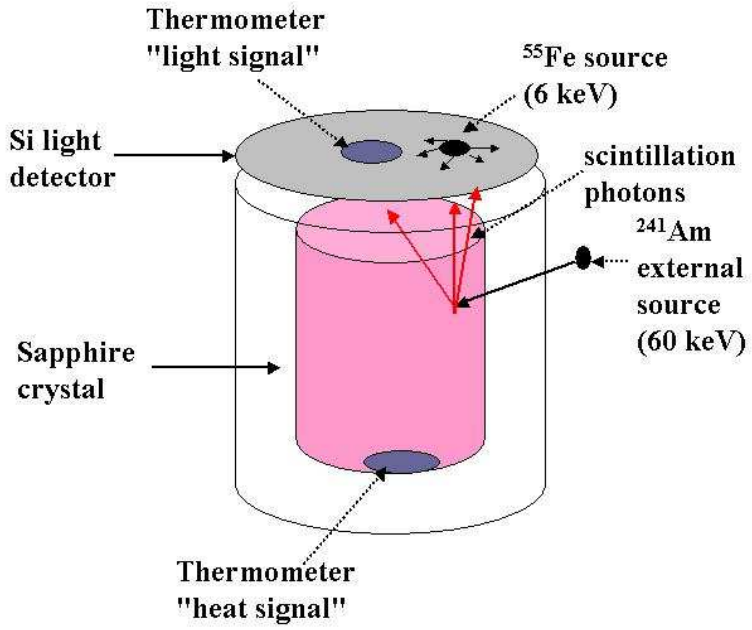

Figure 5.1: *Principle of a heat-scintilation detector in the CRESST setup. A particle interacting with the target creates two signals: heat, read with a tungsten superconducting thermometer and scintillation, detected with a silicon crystal. The signal coming from the silicon detector is also read with a tungsten thermometer. The light detector can be calibrated in energy with an* ^{55}*Fe gamma source and the heat signal with a* ^{241}*Am external gamma source.*

tive thermometer (Fig. 5.2) (Angloher 2002). The elevation of temperature induced by an interaction in the range of interest is much smaller than the width of the transition which insures that there is an approximately linear relation between the elevation of temperature and the increase in the film resistance. The rise in the thermometer resistance is measured via the current rise through a SQUID input coil. In order to keep the film at the desired point in the transition, it is equiped with a heater, regulated by an active feedback loop. The stability of the detector response is monitored by regularly injecting test pulses through the heater.

A silicon detector is used for reading the light signal. The detector is a 30 x 30 x 0.45 mm n-type silicon crystal with a natural oxide layer of about 200 å on each side. The thermal signal induced by the light absorption is also measured with a superconducting tungsten thermometer. The silicon light detector is shown in Fig. 5.3.

The light detector and the crystal are surrounded by a reflective aluminium foil in order to guarantee an efficient light collection.

The sapphire crystal used for this test was the nominally pure IAS15-A107. It is

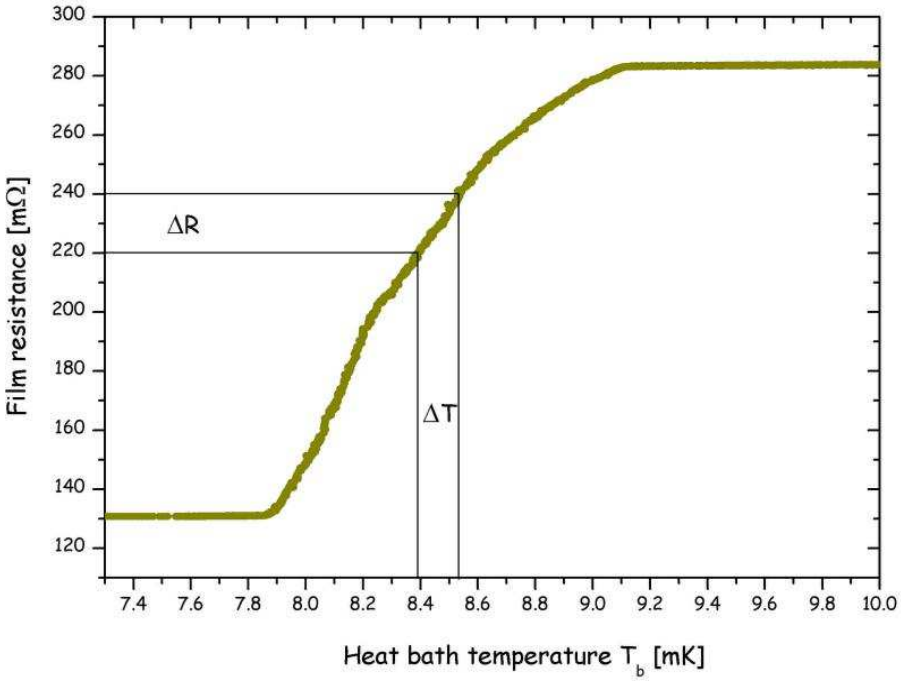

Figure 5.2: *Transition curve of a tungsten superconducting film. The working temperature is chosen so that the film can be stabilized between the normal and the superconducting state. This way, a small change in temperature results in an important change in the resistance of the film.*

a 50 g cylinder (h = 25 mm, ϕ = 25 mm), supplied by IAS and manufactured by the SOREM company. The crystal had been tested in Lyon at room temperature under X ray excitation, showing scintillation due to both $Cr^{3+}$and Ti^{3+}impurities (Fig. 5.4). It was read with the light detector BE10.

5.2 Calibration

The calibration in energy of the light detector was done using an internal ^{55}Fe X-ray gamma source (energy of 6 keV). Fig. 5.5 is showing the light signal plotted against the heat signal for the ^{55}Fe calibration.

The ^{55}Fe events in the light detector appear as light-only pulses with an energy around the value of 6 keV. Having the light detector calibrated in energy is useful in order to determine the light yield of the crystal. In order to do that, we need to determine the fraction of energy which is collected from a source with a given energy. For this test, we have used an external ^{241}Am gamma source (60 keV). The result is shown in Fig. 5.6.

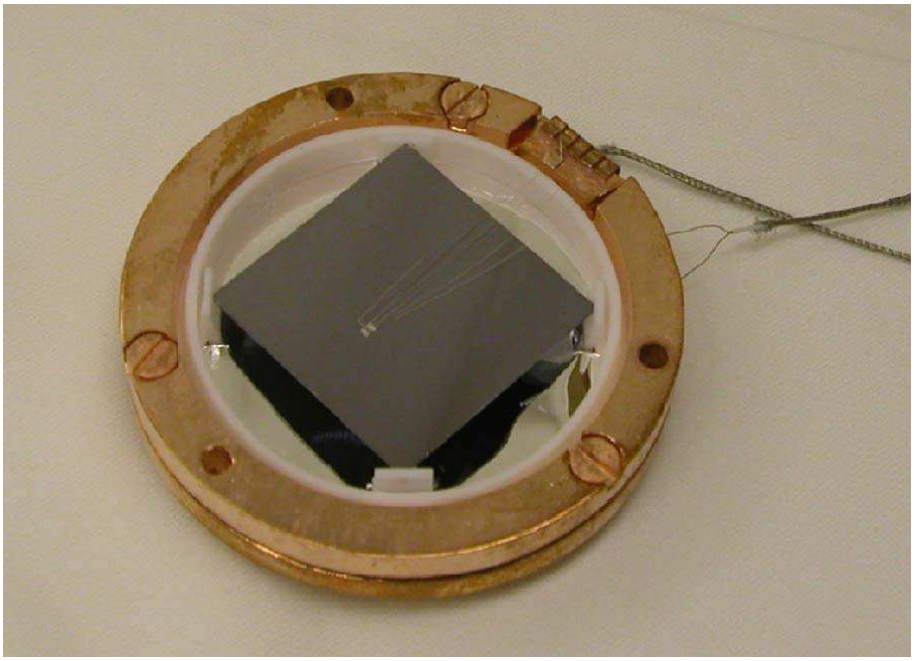

Figure 5.3: *Si detector used for reading the light signal coming from a scintillating crystal. The absorption of scintillation light raises the temperature of the detector, elevation which is measured with a tungsten superconducting film.*

The light yield obtained is of only 0.25%. This is four times lower than the typical light yield of the $CaWO_4$ crystals used by CRESST (Angloher 2005) and insufficient for a good quality heat-scintillation dark matter detector. Nevertheless, as shown in the previous chapter, other crystals tested at low temperature give much more encouraging results, with a light yield of up to 1.4%. Another aspect which is demonstrated by the two calibration spectra is the poor energy resolution of both the heat and the light channels. This is partly explained by the very extreme conditions in which the experiment took place, the detector being rather large for surface tests without any shielding (50 g, while crystals tested in this kind of setup usually have about 4 g), so the event rate was very high and the temperature of the films difficult to stabilize.

5.3 Detector response to neutrons

Even though the light yield of the crystal was low and the resolution poor, we have been able to test the response to an AmBe neutron source. The light versus heat signal is shown in Fig. 5.7.

Neutron due recoils from the AmBe source are visible and are separated from the gamma events down to an energy of about 50 keV. We can also plot the ratio between

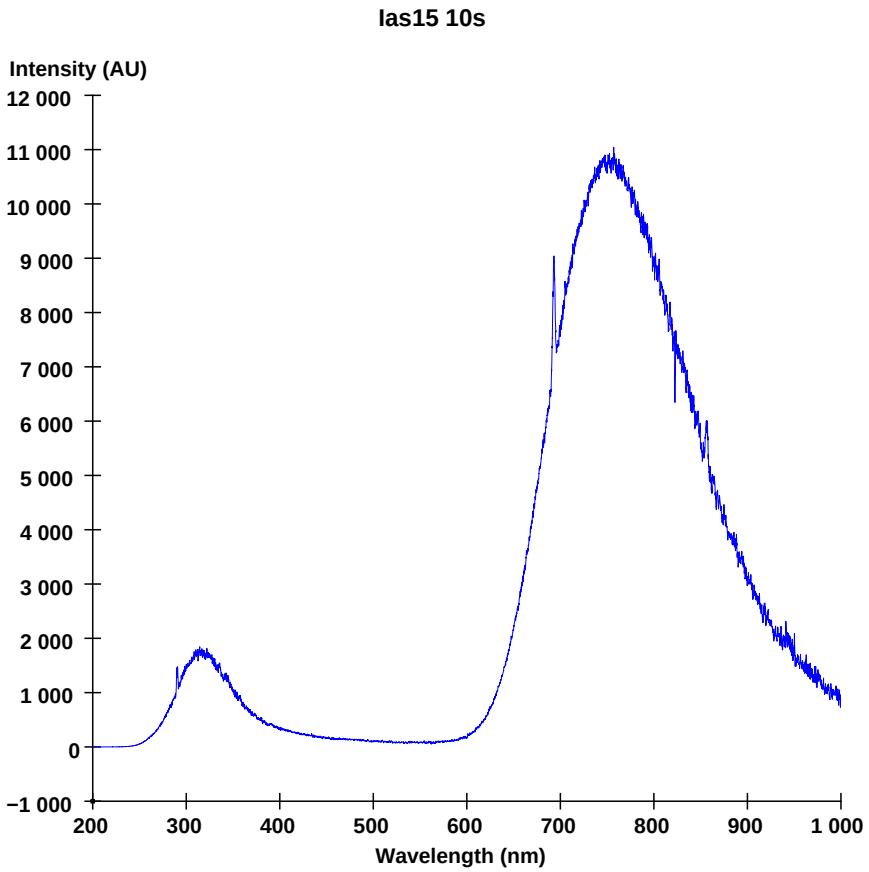

Figure 5.4: *Room temperature scintillation spectrum under X ray excitation of the sapphire crystal tested within the CRESST-like experimental setup. The spectrum proves that both Cr^{3+} and Ti^{3+} are present in the crystal lattice.*

the phonon and the light energy, that is the quenching value, as a function of the phonon energy (Fig. 5.8).

We can determine the ratio between the value of the quenching for gamma rays (which is one by definition) and the value of quenching for neutrons. This value is very important for characterizing the crystal, because a high ratio means a good separation between gammas and neutrons, but at the same time means that the light yield for neutron events is very low and that they may not be easy to distinguish from the background. For a good cryogenic detector, gamma events are well separated from neutrons and neutron events create enough light for the detection. For this crystal, this ratio is found to be about 10 at 100 keV. Tests previously performed by the ROSEBUD collaboration found a value of about 15 for another sapphire crystal (Coron 2004). Both values come from rough estimations which means that the two results are compatible.

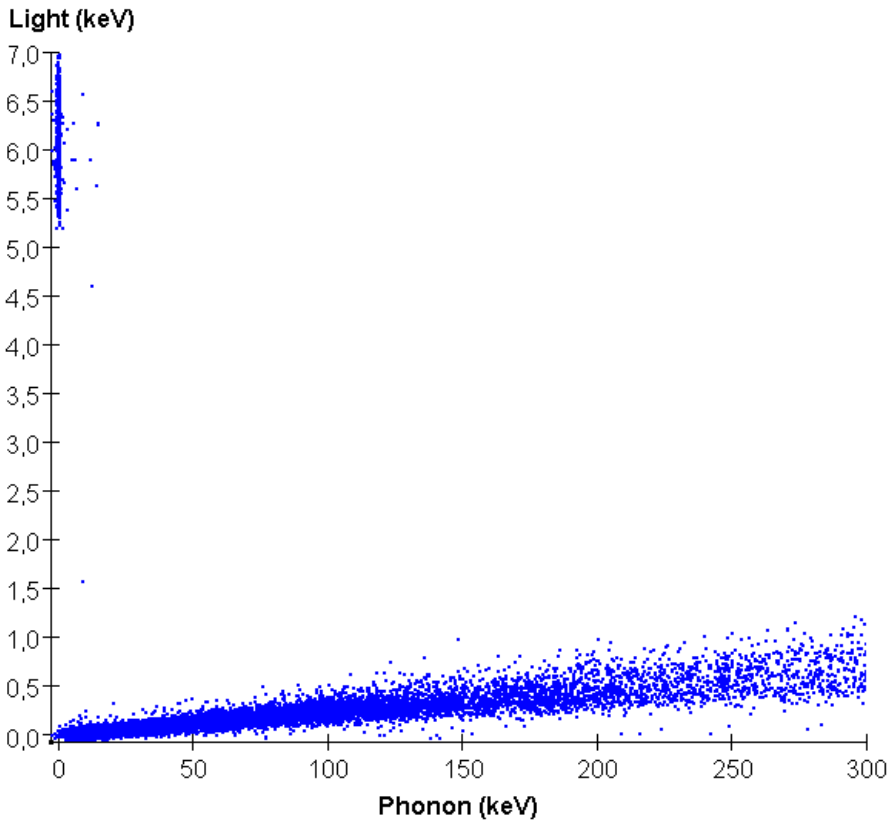

Figure 5.5: *Calibration of the light detector with an internal ^{55}Fe X-ray gamma source (6 keV).*

This ratio might also depend on the Ti concentration in a sapphire crystal, so an interesting future study would be to characterize this dependance.

In this chapter we have seen the results of cryogenic tests on a nominally pure sapphire crystal performed in a CRESST-like setup. The crystal has been randomly chosen. Concentration tests performed by laser ablation mass spectrometry on a sample coming from the same batch indicate a Ti concentration of 1-3 ppm and a Cr concentration of 0.5-1.5 ppm. These cryogenic tests have been performed before the systematic scintillation characterization under a X ray flux. Taking into account all data, we can now conclude that the Ti concentration was too low to guarantee good scintillation properties and future tests should concentrate on samples with a Ti concentration of at least 10 ppm, which is also easier to reproduce by the manufacturer. Even though the crystal had a light yield of only 0.25%, previous tests performed at both MPP (with light-only detectors) and IAS had shown much more encouraging results of light yields of up to 1.4%. The originality of the test presented here consists in the fact that it was the first time that a sapphire crystal was tested at MPP with the measure of both heat and scin-

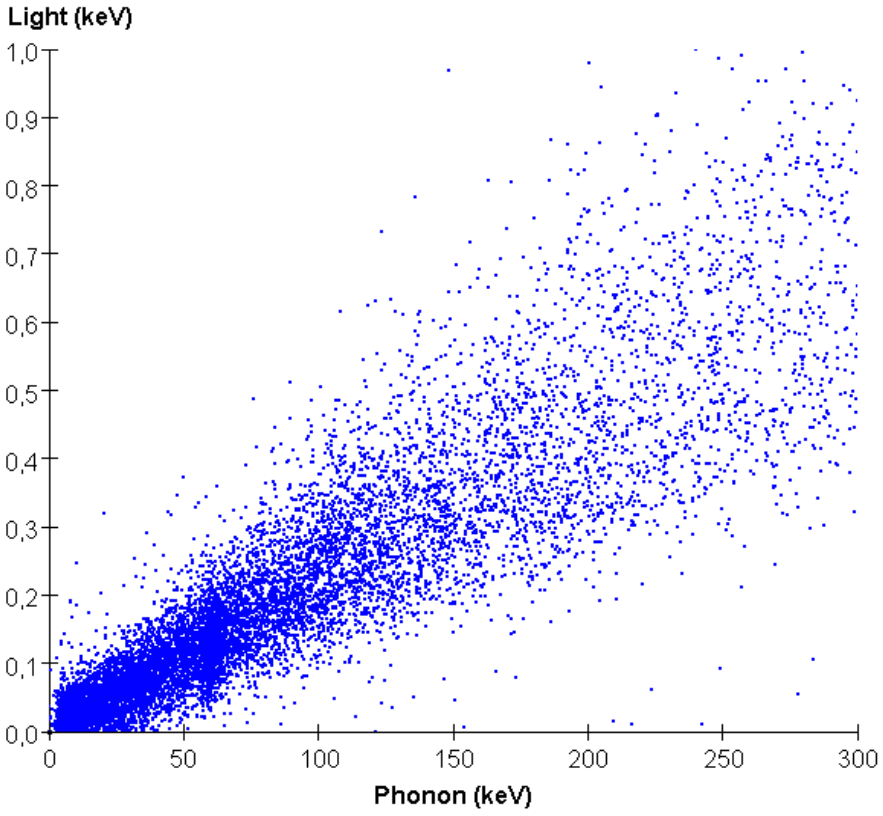

Figure 5.6: *Calibration of the detector with an external ^{241}Am gamma source (60 keV).*

tillation. Another important experimental challenge was testing a large crystal (50 g) at surface and without any shielding. Even with a poor resolution and a weak light yield, it has been possible to see neutron due recoils and to characterize the crystal. The results are encouraging for future tests done in similar experimental conditions.

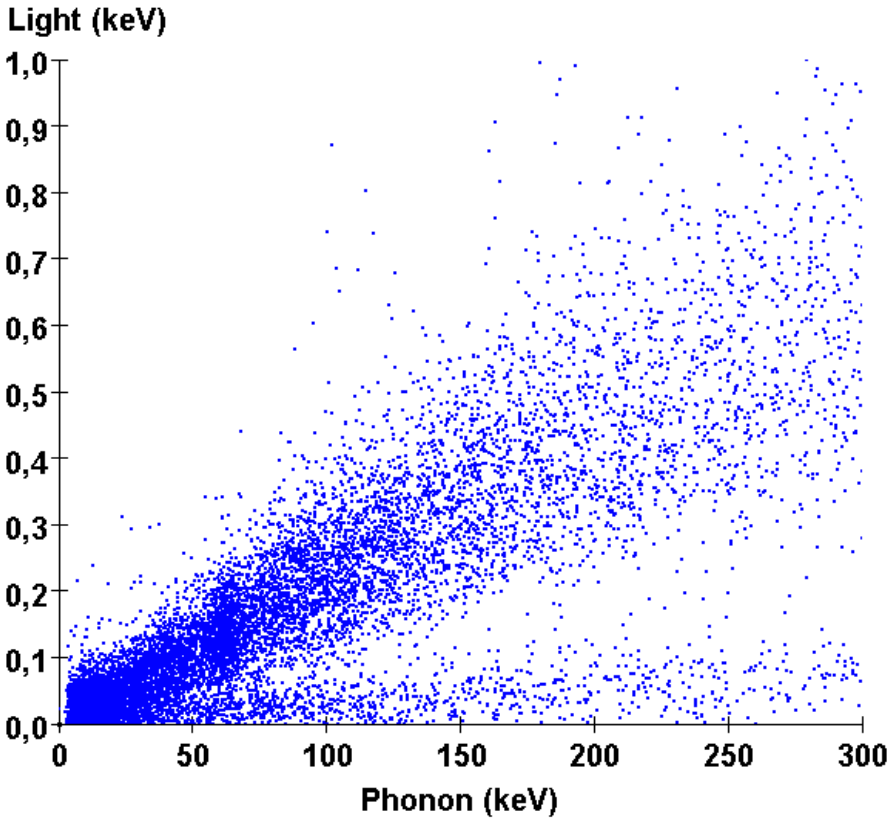

Figure 5.7: *Response of the sapphire detector to an AmBe neutron source. Neutron events are visible, even though the light yield is weak, and are separated from the gamma events down to an energy of about 50 keV.*

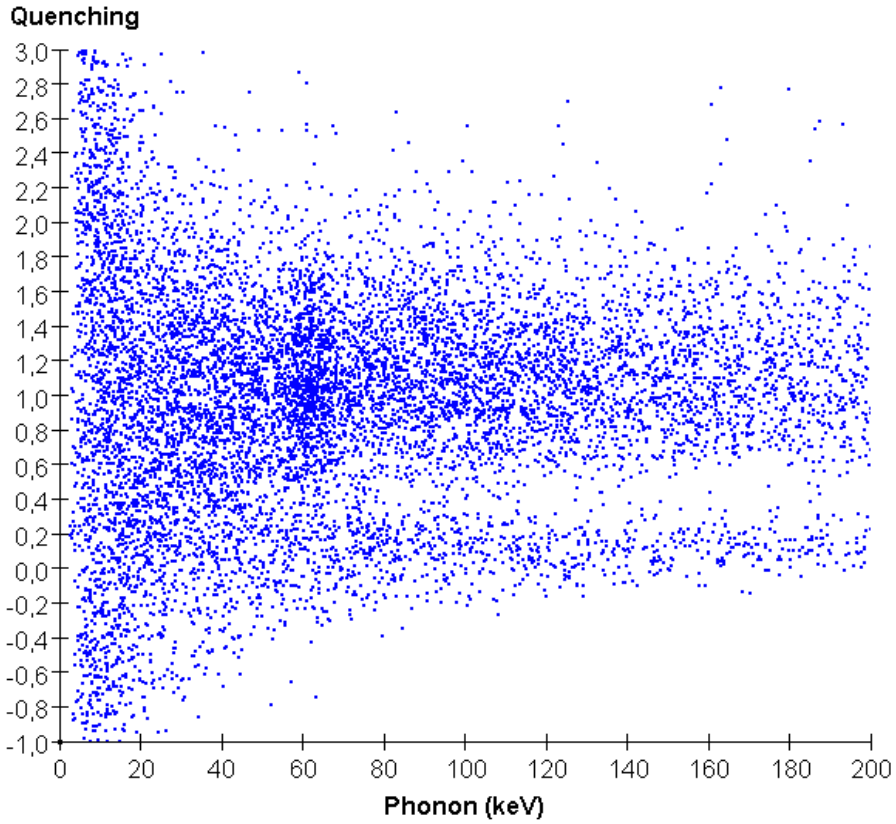

Figure 5.8: *Ratio between the phonon and the light energy (quenching) as a function of the phonon energy. The ratio between the value of the quenching for gamma rays and the one for neutrons is of about 10 at 100 keV for this crystal.*

Chapter 6

Study of a Sapphire Heat-Scintillation Detector in EDELWEISS II

Abstract

Un détecteur scintillation-chaleur en saphir a été intégré dans la première phase d'EDELWEISS II pour des tests de compatibilité. Les premiers résultats montrent que même si le détecteur a été conçu pour un environnement différent, il peut facilement être rendu compatible avec l'électronique et le système d'acquisition EDELWEISS. Cette conclusion est encourageante pour une future utilisation du saphir en tant que détecteur neutron.

6.1 A heat-scintillation detector in EDELWEISS II

In the previous chapters I have presented different approaches used in order to characterize the scintillation properties of sapphire crystals. In addition to this, some Al_2O_3 crystals have already been tested at low temperature within the ROSEBUD dark matter search and we know they behave as very efficient low temperature scintillators (Cebrian 1999). Nevertheless, the fact of having an efficient scintillator is not the guarantee that it will behave as an useful heat-scintillation detector within EDELWEISS II. Therefore, during my thesis, I have tested the compatibility between one of the heat-scintillation bolometers built and tested within ROSEBUD (IAS detector) with the EDELWEISS II setup. The long-term goal was to see if this type of detector could be used as in-situ neutron detector in the future.

The nominally pure sapphire crystal is a 50 g cylinder, h = 25 mm and ϕ = 25 mm, completely polished, manufactured by SOREM. The light yield of this crystal measured by IAS is 1.3% (Coron 2004). The light detector is made of germanium. It is a 195 mg disk, h = 75 μm and ϕ = 25 mm. The principle of the detector is shown in Fig. 6.1.

The heat signal of the sapphire crystal is measured with a Ge-NTD thermistor. The scintillation light is absorbed by the germanium detector, which raises its temperature. This increase in the temperature of the light detector is measured with a second Ge-NTD. The sapphire crystal and its light detector are kept in a copper holder with a silver sputtered cavity for an optimum light collection. The thermalization of the sapphire

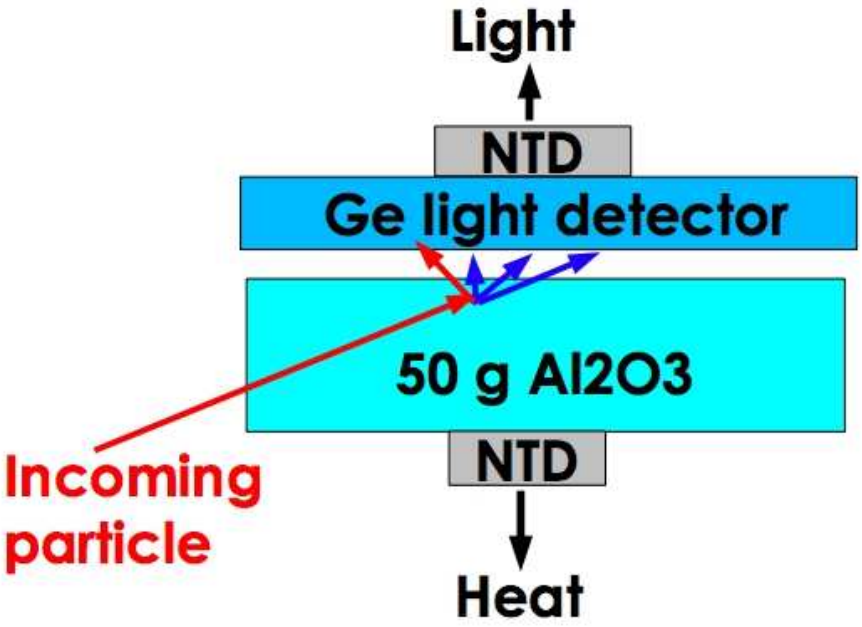

Figure 6.1: *Principle of a ROSEBUD heat-scintillation detector. The heat signal is measured with a Ge-NTD thermistor. Scintillation light is absorbed by a germanium detector which raises its temperature. This increase is measured with a second Ge-NTD thermistor.*

crystal is ensured by a thin sapphire thermal leak (6.8 x 0.64 x 0.89 mm^3) and that of the light detector by a germanium thermal leak (13.6 x 0.54 x 0.054 mm^3).

The short-term goal of the tests was to check whether a bolometer built for ROSEBUD could be made compatible with the EDELWEISS setup. There are several differences between the characteristics of the IAS detector and those of a germanium bolometer. The resistance of the IAS NTD is of the order of 100 MΩ at 20 mK, versus a resistance of only 10 MΩ for a Ge NTD. This difference comes from the fact that the ROSEBUD detectors have been designed in order to obtain very high sensitivities (the ratio between the number of nV of a pulse and the energy expressed in keV), while the EDELWEISS bolometers have been conceived for a large-scale experiment. The constraints of a large-scale experiment are different, especially from the point of view of the cable capacitance which is larger than for small-scale experiments (100-200 pF for EDELWEISS II) and which induces a larger RC factor. Indeed, within EDELWEISS, the biasing of the two NTDs is achieved by a current which is constant in absolute value and whose sign is inverted at a frequency of 1 kHz. The RC factor introduces a transient when the change from a positive to a negative current occurs. Another difference between the two systems is that the IAS detector is also very fast compared to the Ge NTD: its 90% fall time is of the order of 1 ms (2.4 ms for the sapphire and 3.3 ms for the germanium) versus

a fall time of the order of 100 ms or more for Ge. The reason is that the ROSEBUD detectors are often tested at the surface so they need fast time constants in order to avoid event pileup. The detector holder has been conceived for the ROSEBUD environment, while the Ge bolometers have been optimized for the EDELWEISS setup microphonics, so such a detector is more likely to suffer from microphonics. All Ge detectors have been optimized for the same working temperature between 15 and 20 mK. In order to evaluate the optimal temperature for the IAS detector, it is useful to have the possibility of heating the detector autonomously from the rest of the setup. The first step of the IAS commissioning was to evaluate the different parameters that can affect the compatibility of the detector with the setup. In order to obtain a good resolution, low baseline noise is needed, but also a good sensitivity. The value of the sensitivity depends on the temperature of the detector so it is important to know which is the temperature which insures the most convenient behaviour of the detector.

6.2 Working temperature

All Ge-NTD EDELWEISS thermistors have been optimized in order to work at roughly the same temperature. Since the IAS bolometer has been built for a different environment, we need the possibility to test it at different temperatures in order to find the optimum working point for a good compatibility with the EDELWEISS setup. Therefore, the crystal holder has been adjusted in order to allow the thermal decoupling as well as the autonomous heating of the detector. Fig. 6.2 shows the temperature regulation system: a 20kΩ resistance can be used for heating the copper plate holding the detector and a thermal decoupling with NbTi washers and stainless steel screws allows heating the plate without altering the temperature of the other detectors.

A voltage divider with a factor of 100 is used for biasing the 20kΩ resistance in order to avoid the over-heating of the setup as the biasing voltage ranges between -10 V and 10 V.

Since both the heat and light signal are measured using temperature dependant resistances, we can evaluate the temperature of the detector by measuring the biasing voltage as a function of the current intensity in the thermistor. As the detectors have already been completely characterized by IAS, we can compare the values obtained in the EDELWEISS setup with the values previously measured within ROSEBUD. Fig. 6.3 shows the voltage as a function of current intensity for the NTD reading the heat signal.

For each set of values, there are two regions: the first one where an increase in the current intensity leads to an increase in the voltage and the second one where the NTD is heated by the high value of current. In this region, the voltage saturates and the resistance decreases dramatically. In the first region of practically linear dependence

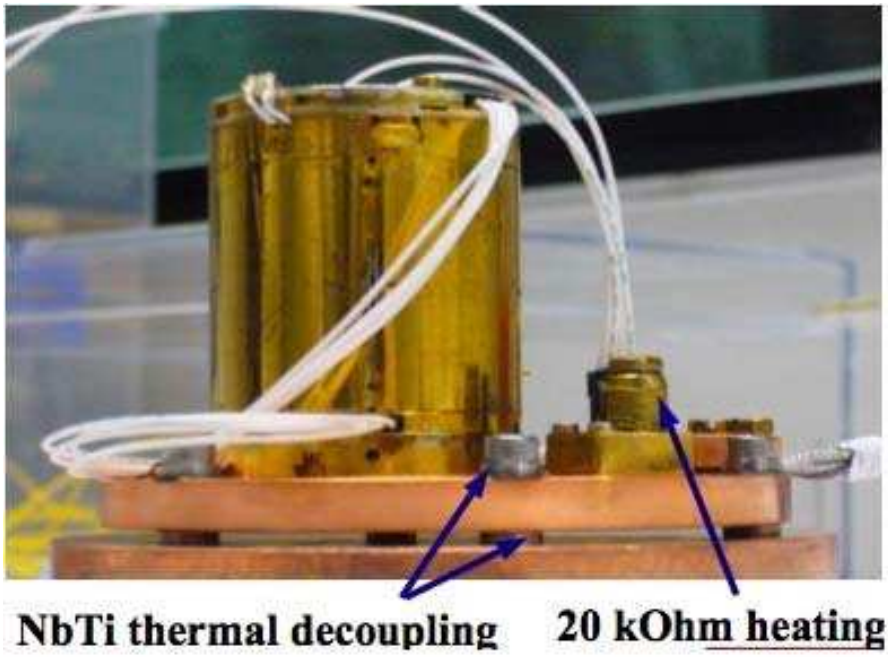

Figure 6.2: *Thermal decoupling of the plate holding the IAS detector using NbTi washers and stainless steel screws. This allows heating the detector with the 20kΩ resistance without altering the temperature of the other detectors.*

between the voltage and the current, the slope gives the resistance of the NTD which depends on the temperature of the detector. The resistance as a function of temperature for this NTD has been measured within ROSEBUD. When comparing our values with the ones measured within ROSEBUD, we obtain a temperature range between about 20 and 50 mK. We can see that the temperature of the detector is roughly constant during one week (from 4/12 to 11/12) and using a heating power of 0.8 nW does not produce a significant change in temperature compared to no heating. A heating power of 25.3 nW applied to the heater allows studying the characteristics of the detector at 50 mK, without affecting the rest of the setup. The values are also consistent within 5 mK with the temperature of the cryostat which was 21 mK during the entire week.

While the heat signal has a stable and consistent behaviour, this is not the case for the light detector, as shown in Fig. 6.4.

The temperature of the detector ranges between about 20 and 70 mK. We can see that for the same value of voltage applied to the heater, the temperature is not the same from one day to another. The coldest temperature was obtained on the 11/12, when the pulse tubes of the cryostat were off. This clearly shows that the pulse tubes can be a source of noise for the light detector, noise that heats the detector significantly. Unfortunately,

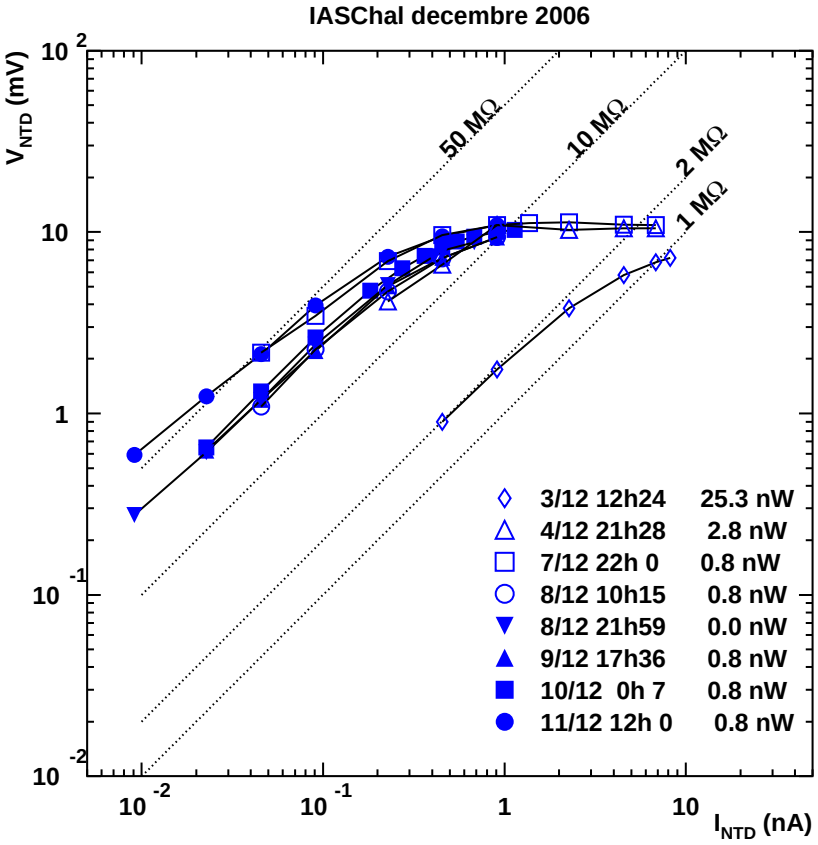

Figure 6.3: *Biasing voltage as a function of current intensity in the NTD reading the heat signal of the IAS bolometer. In the first region, current intensity is increasing with the increasing voltage, while in the second region the detector is heated by the biasing voltage, resulting in a saturation and a dramatic decrease of the NTD resistance. According to the tests performed by IAS, an asymptotic resistance of 50 MΩ corresponds to a temperature of about 20 mK, while an asymptotic resistance of 2 MΩ stands for a temperature of about 50 mK. The temperature of the cryostat was 21 mK during the entire week.*

this behaviour is not reproducible from one day to another, as turning off the pulse tubes on the 12/12 does not have the same effect as turning them off on the 11/12, the difference in the temperature of the light detector between the two tests being of about 10 mK, according to IAS measured characteristics. Another symptom of the problem is that there is a difference of up to 10 mK between the temperature of the light detector and the temperature of the heat detector measured simultaneously. There are several possible explanations for the extreme sensitivity of the light detector to the surrounding noise. The first one concerns the sensitivity of the detector, 9300 nV/keV (at 20 mK and

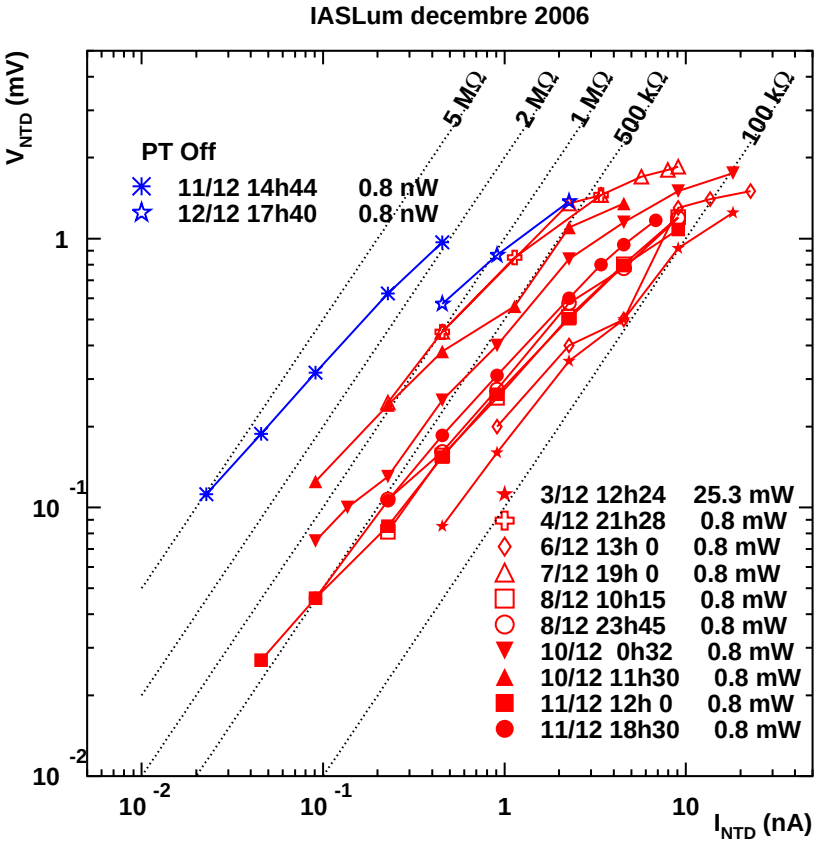

Figure 6.4: *Biasing voltage as a function of current intensity in the NTD reading the light signal of the IAS bolometer. According to the values measured by IAS, the temperature of the detector ranges between 20 and 70 mK, for the same value of voltage applied to the heater. Stopping the pulse tubes of the cryostat can significantly reduce the noise as seen on the 11/12, but this is not reproducible from one day to another if we compare the values of 11/12 and 12/12. All values have been taken for a cryostat temperature of 21 mK.*

a 0.57 nA biasing current) according to IAS, which is 10 times higher than the sensitivity of the heat detector, 970 nV/keV (at 20 mK and a 2.5 nA biasing current). Another reason may come from the size of the detector, which is very small and therefore easy to move by any vibration induced by the environment. Whatever the reason, the sensitivity of the detector to the noise is a drawback for photon detection, but has proved to be a useful tool for tracing possible sources of microphonics within the setup. It has been the first detector showing that the pulse tubes were an important source of noise, result confirmed later by the other detectors. The pulse tubes produce acoustic noise, but also vibrations and electric noise induced by the vibrations. Therefore, the pulse tubes have

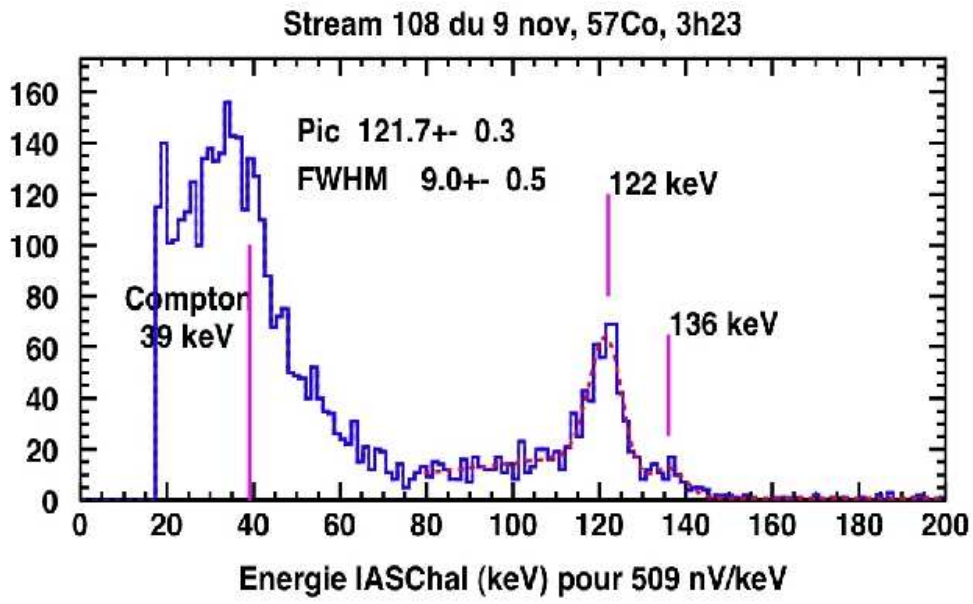

Figure 6.5: *Calibration of the IAS heat channel using a ^{57}Co gamma source. We can see the 122 keV peak with a resolution of 9 keV.*

been better isolated from the detectors in the present run and preliminary results show that this alteration has significantly reduced the overall noise. Because of the unstable working conditions, it has been difficult so far to determine the optimum working temperature. Having a thermal decoupling system and an autonomous heating is therefore useful since these tests can be resumed after the reduction of the microphonics when the detector will no longer be dominated by the noise.

6.3 Gamma calibration

We have seen in the previous section that the heat channel has a roughly stable and reproducible behaviour, while light is dominated by noise and especially by the presence of the pulse tubes of the cryostat. Another experimental challenge when testing the IAS bolometer is the fact that, as shown previously, the time constants of the pulses and the resistance of the NTDs are not the same as the ones of the germanium detectors. Therefore, we need to show that the detector can be read by the EDELWEISS II electronics giving reliable results.

Fig. 6.5 shows the calibration of the heat detector using a ^{57}Co gamma source.

The 122 keV peak is detected with a FWHM of 9 keV, which is compatible with the values found for the Ge detectors in the same conditions. There is also a hint of the sec-

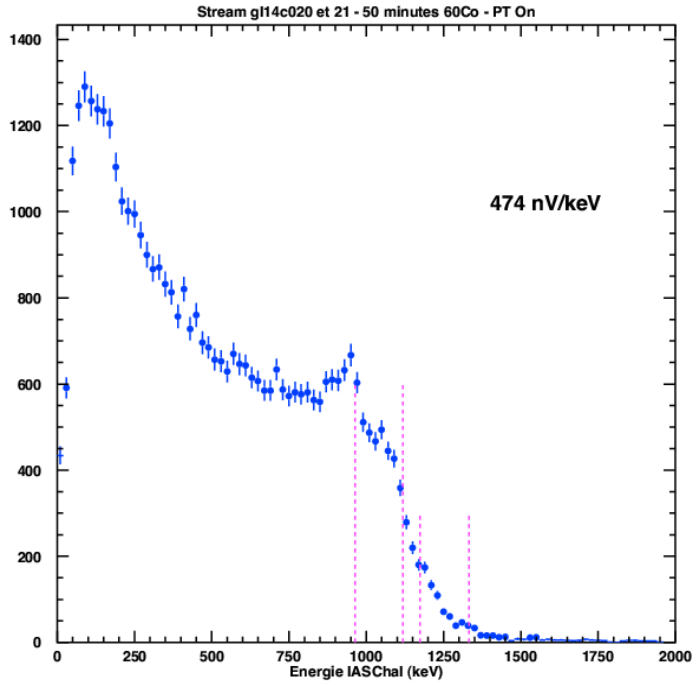

Figure 6.6: *Calibration of the IAS heat channel using a ^{60}Co gamma source. The energy of the source is too high to see the effect of the photoelectric peak interacting with the crystal, but the Compton edge can be used for the calibration.*

ond ^{57}Co peak at 136 keV and we can see the Compton edge at 39 keV. The importance of these results is twofold. First, they show that fast pulses can be read by the EDELWEISS II electronics and give consistent results. Another important feature is that the resolution of the heat signal of the IAS detector is of the same order of magnitude as the heat of the germanium detectors as long as the microphonics is the same.

^{57}Co is a low energy gamma source, ideal for the calibration of a light target, such as Al_2O_3 , because we can see the 122 keV photoelectric peak. Nevertheless, the low energy of ^{57}Co is a serious drawback when trying to chose the location of the sources on the cryostat, because low energy can easily be stopped by the important quantity of copper contained in the cryostat screens and detector holders. Therefore, such a calibration has to be carefully planned, only someone knowing the precise location of the detector in the cryostat can chose the location of the calibration sources and since the sources are conceived for low activities (about 10 kBq), 5 to 10 sources need to be used in order to have a reasonable event rate in the 50 g sapphire detector. These reasons make the ^{57}Co calibration inappropriate for quick tests checking the stability of the detector. A possible solution is to use a higher energy source, which does not produce a visible photoelectric peak in the crystal, but the Compton edge can be used for a reson-

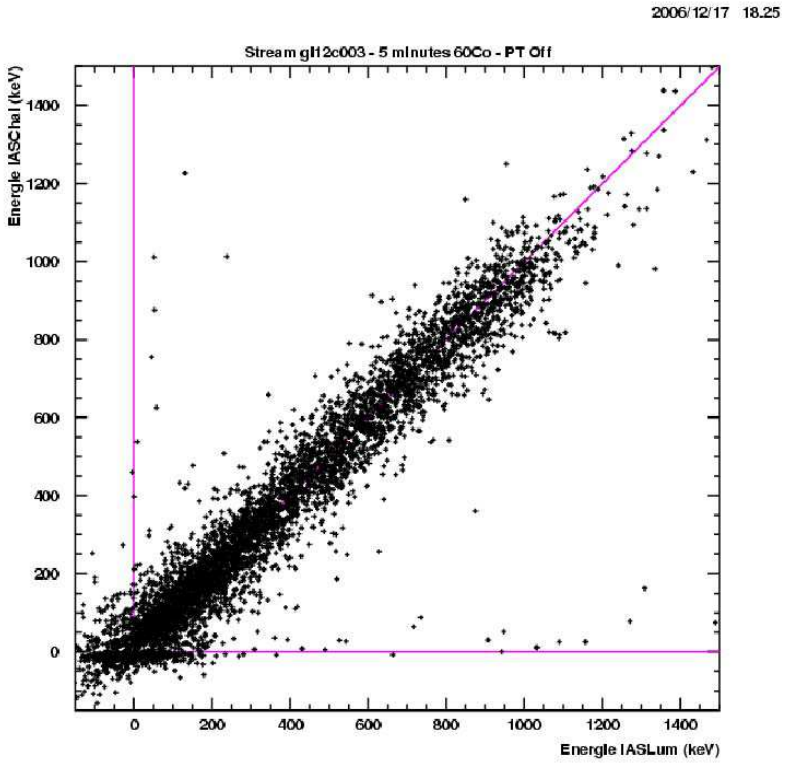

Figure 6.7: *Light and heat signal are correlated when the pulse tubes of the cryostat are turned off. A baseline resolution of 100 keV for the light signal leaves room for improvement.*

ably accurate calibration. Within EDELWEISS, ^{60}Co gamma sources (two photoelectric peaks, at 1173 and 1333 keV) are used twice a day for one hour in order to eliminate stray charges that are created in the germanium detectors. Fig. 6.6 shows the calibration of the heat signal using a ^{60}Co gamma source. We can see that the results are compatible with a Compton edge at 963 keV and a second one at 1119 keV.

We have seen in the previous section that the light channel is extremely sensitive to the noise and the only possibility to bring it to a base temperature of 20 mK is to operate with the pulse tubes of the cryostat turned off. This remains true when we try to see correlated event pulses on the heat and light channel. The only option before the present run to see anything coming from the light detector was to stop the pulse tubes. Fig. 6.7 shows the heat signal plotted against the light signal for a ^{60}Co calibration.

Events are correlated on the two channels, demonstrating that the light detector sees the incoming photons. The baseline resolution of 100 keV$_{ee}$ remains insufficient for this detector. The baseline resolution of the heat detector is of 8 keV before analysis and

can be reduced down to 4 keV after subtraction of the noise frequencies. This value is within the range of resolution of the germanium detectors.

6.4 Present status

After having understood that the pulse tubes of the cryostat were an important source of noise for all bolometers, the experimental setup has been altered in order to have a good isolation between the pulse tubes and the experimental volume. The preliminary results of the present run show that this isolation has been efficient for all detectors. The heat signal was previously affected by a 111 Hz oscillation which is no longer visible. The light signal has become measurable without turning off the pulse tubes and the baseline resolution has been considerably improved: from 100 keV with the pulse tubes off to less than 50 keV without stopping the pulse tubes. Both detectors are colder than in the previous runs.

Tests are still needed in order to completely characterize the performance of the IAS detector within the EDELWEISS setup. Nevertheless, the first questions concerning the compatibility of the detector with the setup have been answered: fast pulses can be read with EDELWEISS II electronics, the high resistance of the NTD thermistors is not incompatible with the acquisition system and the detector can be operated either at the same temperature as the others or at higher temperatures without any influence on the surrounding detectors. These results are encouraging for both EDELWEISS and future experiments like EURECA, using different targets and which are likely to encounter similar experimental challenges in the future.

Conclusion

This thesis presents different tests performed in order to characterize the properties of sapphire within a direct dark matter search. The future of dark matter search collaborations belongs to large-scale experiments using several targets. In this context, light crystals, complementary to the heavy targets already in use, can be valuable tools for confirming a future dark matter signal.

The spectroscopic characterization of nominally pure Al_2O_3 crystals with ppm level concentrations of Ti and Cr shows that all crystals emit light under X ray excitation. The tests performed at room temperature and down to 30 K prove that the presence of Ti in the crystal lattice has a very positive influence on the quantity of light produced by the crystal. Systematic tests of Ti:Al_2O_3 crystals with controlled Ti concentrations show that crystals containing 100 ppm of Ti have a maximum light yield at room temperature and crystals with 50 ppm are the most efficient scintillators at T = 45 K. The emission is stable within 30% between 10 and 500 ppm of Ti which means that in order to obtain efficient scintillators the precision of the Ti concentration is not mandatory within this range. Scintillation tests only give reliable results if we can check the Ti concentration in the crystal. This is of particular importance when the samples are purchased as nominally pure, i.e. without any deliberate doping. The experiments presented in this thesis show that optical absorption can be used for finding the Ti concentration in sapphire crystals down to 100 ppm at both room temperature and down to 10 K, while fluorescence is sensitive down to concentrations of the order of 1 ppm. There are also commercially available methods based on mass spectrometry that can be used for Al_2O_3 crystals. These methods are destructive and have no sensitivity to the oxidation state of the impurities, but can sometimes be complementary to the optical methods.

Once the scintillation properties of sapphire understood, it is important to check the feasibility of integrating a sapphire heat-scintillation detector in an existing experimental setup. Tests performed at Max Planck Institute in Munich show that such a detector

is compatible with the CRESST dark matter search setup. The nominally pure crystal has shown a 0.25% light yield, which is six times lower than the light yield found for different samples tested as light-only detectors. Nevertheless, a neutron calibration has been performed, proving that sapphire can work as heat-scintillation detector in the CRESST setup and future tests should focus on samples with a higher Ti concentration, of the order of 100 ppm.

It has also been checked whether a heat-scintillation sapphire detector could be integrated in the EDELWEISS setup. Tests have been performed during the first commissioning runs of EDELWEISS II. Although the detector had been conceived for a different environment, we have shown that its fast time constants and high resistance could be read by the EDELWEISS II electronics and acquisition system. The light detector being very sensitive to microphonics, it has been difficult to completely characterize it during the first runs. Microphonics noise has recently been considerably reduced, so the detector is expected to be fully operational in the near future.

Bibliography

Alcock, C. e. a.: 2000, *Astrophys. J* **542**, 281.

Alner, G.: 2007, *astro-ph/0701858v2* .

Alner, G. e. a.: 2005, *Astropart. Phys.* **23**, 444.

Angloher, G. e. a.: 2002, *Astropart. Phys.* **18**, 43.

Angloher, G. e. a.: 2005, *Astroparticle Physics* **23**, 325.

Baltz, E., Battaglia, M., Peskin, M. and Wizansky, T.: 2006, *Phys. Rev. D* **74**, 103521.

Barnabé-Heider, M. e. a.: 2005, *Phys. Lett. B* **624**, 186.

Beach, A. e. a.: 2001, *Phys. Rev. Lett.* **87**, 271101.

Benetti, P. e. a.: 2007, *astro-ph/0701286* .

Benoit, A. e. a.: 2006, *astro-ph/0607502* .

Bernabei, R. e. a.: 1998, *Phys. Lett. B* **424**, 195.

Bernabei, R. e. a.: 2000, *Phys. Lett. B* **480**, 23.

Birks, J.: 1964, The theory and practice of scintillation counting.

Blasse, G.: 1990, *Mat. Chem. and Phys.* **26**, 131.

Bottino, A.: 2005, *Phys. Rev. D* **72**, 083521.

Brownstein, J. and Moffat, J.: 2006, *Astrophys. J* **636**, 721–741.

Cebrian, S. e. a.: 1999, *Astropart. Phys.* **10**, 361.

Chabert, L.: 2004, Etude du bruit de fond neutron induit pas les muons dans l'expérience EDELWEISS II, thèse de doctorat à l'Université Lyon 1.

Chazal, V.: 1997, Etude de l'environment neutron au laboratoire souterrain de Modane, thèse de doctorat à l'Université Lyon 1.

Chazal, V. e. a.: 1998, *Astropart. Phys.* **9**, 163.

Clowe, D. e. a.: 2006, *astro-ph/0608407* .

Coron, N. e. a.: 2004, *NIM A* **520**, 159.

de Boer, W. e. a.: 2005, *Phys. Rev. Lett.* **95**, 209001.

Di Stefano, P. e. a.: 2001, *Astropart. Phys.* **14**, 329.

Dobrovinskaya, E., Lytvynov, L. and Pischik, V.: 2002, Sapphire and Other Corundum Crystals.

Dujardin, C. and Ledoux, G.: n.d., *Note interne* .

Fukuda, Y. e. a.: 1998, *Phys. Rev. Lett.* **81**, 1562.

Gaitskell, R. e. a.: n.d.
*http://dmtools.berkeley.edu/limitplots/

Grinberg, M. e. a.: 1993, *Phys. Rev. B* **48**, 5922.

Horns, D.: 2005, *Phys. Lett. B* **607**, 225–232.

Hunter, S. e. a.: 1997, *Astrophys. J.* **481**, 205.

Iorio, L.: 2006, *gr-qc/0608101v4* .

Juillard, A. e. a.: 2006, *Nucl. Instrum. Methods A* **559**, 393.

Kamionkowski, M. e. a.: 1996, *Phys. Rept.* **267**, 195.

Kraus, H. e. a.: 2006, *J. Phys.* **39**, 139–141.

Kudryavtsev, V.: 2004, *astro-ph/0406126* .

Lee, H. e. a.: 2006, *Phys. Lett. B* **633**, 201.

Lewin, J. and Smith, P.: 1996, *Astropart. Phys.* **6**, 87.

Lupei, A. e. a.: 1986, *Opt Commun.* **59**, 36.

Maiman, H.: 1960, *Nature* **187**, 493.

Maiman, T. e. a.: 1961, *Phys. Rev.* **123**, 1151.

Marleau, P.: 2005, *TAUP, Zaragoza, Spain* .

Martineau, O. e. a.: 2004, *Nucl. Instrum. Methods A* **530**, 426.

Mikhailik, V. e. a.: 2005, *NIM A* **546**, 523.

Morales, A.: 2002, *Nucl. Phys. B Proc. Suppl.* **110**, 39.

Moulton, P.: 1986, *J. Opt. Soc. Am. B* **3**, 125.

Navick, X.-F. e. a.: 2006, *Nucl. Instrum. Methods A* **559**, 483.

Nelson, D. and Sturge, M.: 1964, *Phys. Rev.* **137**, 1117.

Ostriker, J. e. a.: 1974, *Astrophys. J. Lett.* **193**, L1.

Peccei, R. and Quinn, H.: 1977, *Phys. Rev. Lett.* **38**, 1440.

Petricca, F. and De Marcillac, P.: n.d.

Pobell, F.: 1996, *Matter and Methods at Low Temperature* .

CDMS collaboration: 2006, *Phys. Rev. Lett.* **96**, 011302.

PVLAS collaboration: 2006, *Phys. Rev. Lett.* **96**, 110406.

Sanglard, V. e. a.: 2005, *Phys. Rev. D* **71**, 122002.

Shutt, T. e. a.: 2000, *Nucl. Instrum. Methods A* **444**, 340.

Tisserand, P. e. a.: 2007, *Astron. and Astroph.* **6017**.

Tremaine, S. and Gunn, J.: 1979, *Phys. Rev. Lett.* **42**, 407.

Vallayer, J.: 2001, *Opt. Mat.* **16**, 329.

Van Albada, T., Bahcall, J., Bregman, K. and Sanscisi, R.: 1985, *Ap. J.* **295**, 305.

Weinberg, D. e. a.: 1997, *Astrophys. J* **490**, 564.

Wong, W. e. a.: 1995, *Phys. Rev. B* **51**, 5682.

Yao, W.-M. e. a.: 2006, Review of Particle Physics, *Journal of Physics G* **33**, 1+.
*http://pdg.lbl.gov

Zwicky, F.: 1933, *F. Helv. Phys. Acta* **6**, 110.

NOM : LUCA (avec précision du nom de jeune fille, le cas échéant) Prénoms : Melisa	DATE de SOUTENANCE 20 juillet 2007

TITRE : Sapphire scintillation tests for cryogenic detectors in the EDELWEISS dark matter search

Numéro d'ordre : 114-2007

DIPLOME DE DOCT.	DOCTEUR-INGENIEUR	DOCTORAT D'ETAT	DOCTORAT DE 3e CYCLE	Spécialité : Physique des Particules
X	☐	☐	☐	

Cote B.I.U. – Lyon : T 50/210/19 / et bis	CLASSE :

RESUME :

Identifying the matter in the universe is one of the main challenges of modern cosmology and astrophysics. An important part of this matter seems to be made of non-baryonic particles. EDELWEISS is a direct dark matter search using cryogenic germanium bolometers in order to look for particles that interact very weakly with the ordinary matter, generically known as WIMPs. An important challenge for EDELWEISS is the radioactive background and one of the ways to identify it is to use a larger variety of target crystals. Sapphire is a light target which can be complementary to the germanium crystals already in use. Spectroscopic characterization studies have been performed using different sapphire samples in order to find the optimum doping concentration for good low temperature scintillation. Ti doped crystals with weak Ti concentrations have been used for systematic X ray excitation tests both at room temperature and down to 30 K. The tests have shown that the best Ti concentration for optimum room temperature scintillation is 100 ppm and 50 ppm at T = 45 K. All concentrations have been checked by optical absorption and fluorescence.

After having shown that sapphire had interesting characteristics for building heat-scintillation detectors, we have tested if using a sapphire detector was feasible within a dark matter search. During the first commissioning tests of EDELWEISS II, we have proved the compatibility between a sapphire heat-scintillation detector and the experimental setup.

MOTS-CLES : WIMP – dark matter – sapphire – scintillation – cryogenic – EDELWEISS – bolometer - detector

Laboratoire de recherche : Institut de Physique Nucléaire de Lyon

Directeurs de recherches : Martine Stern

Président du jury : C. Dujardin Composition du jury : P. Di Stefano – J. Jochum – J. Rich – C. Tao	93 pages